AD-A119 654 AIR FORCE INST OF TECH WRIGHT-PATTERSON AFB OH F/G 4/2
A COMPOSITE STUDY OF COMMA CLOUDS AND THEIR ASSOCIATION WITH SE--ETC(U)
1982 J P MILLARD
UNCLASSIFIED AFIT/CI/NR/82-57T NL

1 OF 2
ADA
19654




UNCLASS

SECURITY CLASSIFICATION OF THIS PAGE (When Data Entered)

AD A119654

REPORT DOCUMENTATION PAGE

READ INSTRUCTIONS BEFORE COMPLETING FORM

1. REPORT NUMBER AFIT/CI/NR/82-57T	2. GOVT ACCESSION NO. AD-A119 654
3. RECIPIENT'S CATALOG NUMBER	
4. TITLE (and Subtitle) A Composite Study of Comma Clouds and Their Association With Severe Weather Over The Great Plains	5. TYPE OF REPORT & PERIOD COVERED THESIS/DISSERTATION
	6. PERFORMING ORG. REPORT NUMBER
7. AUTHOR(s) James Peter Millard	8. CONTRACT OR GRANT NUMBER(s)
9. PERFORMING ORGANIZATION NAME AND ADDRESS AFIT STUDENT AT: University of Oklahoma	10. PROGRAM ELEMENT, PROJECT, TASK AREA & WORK UNIT NUMBERS
11. CONTROLLING OFFICE NAME AND ADDRESS AFIT/NR WPAFB OH 45433	12. REPORT DATE 1982
	13. NUMBER OF PAGES 119
14. MONITORING AGENCY NAME & ADDRESS (if different from Controlling Office)	15. SECURITY CLASS. (of this report) UNCLASS
	15a. DECLASSIFICATION DOWNGRADING SCHEDULE

16. DISTRIBUTION STATEMENT (of this Report)

APPROVED FOR PUBLIC RELEASE; DISTRIBUTION UNLIMITED

DTIC ELECTE SEP 28 1982 D

H

17. DISTRIBUTION STATEMENT (of the abstract entered in Block 20, if different from Report)

18. SUPPLEMENTARY NOTES

APPROVED FOR PUBLIC RELEASE: IAW AFR 190-17

16 SEPT 1982

Lynn E. Wolaver

LYNN E. WOLAVER
Dean for Research and Professional Development
AFIT, Wright-Patterson AFB OH

19. KEY WORDS (Continue on reverse side if necessary and identify by block number)

20. ABSTRACT (Continue on reverse side if necessary and identify by block number)

ATTACHED

82 ... 182

DTIC FILE COPY

DD FORM 1473 1 JAN 73 EDITION OF 1 NOV 65 IS OBSOLETE

UNCLASS

SECURITY CLASSIFICATION OF THIS PAGE (When Data Entered)

ABSTRACT

Thirty-five comma cloud systems which existed over the Great Plains during the 1980 and 1981 spring seasons (March through June) are analyzed using visible and infrared satellite imagery, rawinsonde data and gridded data sets. Each comma pattern is divided into eleven zones and the soundings from similar zones are then averaged together. Composite kinematic and thermodynamic quantities are examined on isobaric and relative-flow isentropic surfaces. Severe weather is also stratified by zone. Eighty percent of the severe events are found to have occurred in the comma tail (zones C, D and E).

A case study of one particular comma cloud system (March 21-22, 1981) is examined separately. This case was characterized by rapid convective cloud growth which developed in situ within the dry intrusion. Development occurred along a dryline where surface convergence was strong and where cold air advection aloft increased the potential instability. Synoptic-scale vertical motions are calculated and found to be upward in the northern portion of the dry intrusion. Comparisons are made to the composite comma cloud.

PRECEDING PAGE BLANK-NOT FILMED

AFIT/CI/NR/82-57T

AFIT RESEARCH ASSESSMENT

The purpose of this questionnaire is to ascertain the value and/or contribution of research accomplished by students or faculty of the Air Force Institute of Technology (ATC). It would be greatly appreciated if you would complete the following questionnaire and return it to:

AFIT/NR
Wright-Patterson AFB OH 45433

RESEARCH TITLE: A Composite Study of Comma Clouds and Their Association With Severe Weather Over The Great Plains

AUTHOR: James Peter Millard

RESEARCH ASSESSMENT QUESTIONS:

1. Did this research contribute to a current Air Force project?

( ) a. YES ( ) b. NO

2. Do you believe this research topic is significant enough that it would have been researched (or contracted) by your organization or another agency if AFIT had not?

( ) a. YES ( ) b. NO

3. The benefits of AFIT research can often be expressed by the equivalent value that your agency achieved/received by virtue of AFIT performing the research. Can you estimate what this research would have cost if it had been accomplished under contract or if it had been done in-house in terms of manpower and/or dollars?

( ) a. MAN-YEARS ________ ( ) b. $________

4. Often it is not possible to attach equivalent dollar values to research, although the results of the research may, in fact, be important. Whether or not you were able to establish an equivalent value for this research (3. above), what is your estimate of its significance?

( ) a. HIGHLY SIGNIFICANT ( ) b. SIGNIFICANT ( ) c. SLIGHTLY SIGNIFICANT ( ) d. OF NO SIGNIFICANCE

5. AFIT welcomes any further comments you may have on the above questions, or any additional details concerning the current application, future potential, or other value of this research. Please use the bottom part of this questionnaire for your statement(s).

NAME GRADE POSITION

ORGANIZATION LOCATION

STATEMENT(s):

FOLD DOWN ON OUTSIDE - SEAL WITH TAPE

AFIT/NR
WRIGHT-PATTERSON AFB OH 45433

OFFICIAL BUSINESS
PENALTY FOR PRIVATE USE, $300

NO POSTAGE
NECESSARY
IF MAILED
IN THE
UNITED STATES

BUSINESS REPLY MAIL
FIRST CLASS PERMIT NO. 73236 WASHINGTON D.C.

POSTAGE WILL BE PAID BY ADDRESSEE

AFIT/ DAA
Wright-Patterson AFB OH 45433

FOLD IN

THE UNIVERSITY OF OKLAHOMA

GRADUATE COLLEGE

A COMPOSITE STUDY OF COMMA CLOUDS AND THEIR ASSOCIATION WITH SEVERE WEATHER OVER THE GREAT PLAINS

A THESIS

SUBMITTED TO THE GRADUATE FACULTY

in partial fulfillment of the requirements for the

degree of

MASTER OF SCIENCE IN METEOROLOGY

BY

JAMES PETER MILLARD

Norman, Oklahoma

1982

A COMPOSITE STUDY OF COMMA CLOUDS AND THEIR

ASSOCIATION WITH SEVERE WEATHER OVER THE

GREAT PLAINS

APPROVED BY:

____

____

____

ABSTRACT

Thirty-five comma cloud systems which existed over the Great Plains during the 1980 and 1981 spring seasons (March through June) are analyzed using visible and infrared satellite imagery, rawinsonde data and gridded data sets. Each comma pattern is divided into eleven zones and the soundings from similar zones are then averaged together. Composite kinematic and thermodynamic quantities are examined on isobaric and relative-flow isentropic surfaces. Severe weather is also stratified by zone. Eighty percent of the severe events are found to have occurred in the comma tail (zones C, D and E).

A case study of one particular comma cloud system (March 21-22, 1981) is examined separately. This case was characterized by rapid convective cloud growth which developed *in situ* within the dry intrusion. Development occurred along a dry line where surface convergence was strong and where cold air advection aloft increased the potential instability. Synoptic-scale vertical motions are calculated and found to be upward in the northern portion of the dry intrusion. Comparisons are made to the composite comma cloud.

ACKNOWLEDGEMENTS

It is indeed a pleasure to thank the members of the thesis committee, Drs. F. H. Carr, H. B. Bluestein, and J. F. Kimpel, for their many helpful suggestions concerning this research. Special thanks go to Dr. John McGinley of NSSL for discussions concerning the relationship of severe weather to the comma cloud pattern. Mr. Paul Mulder of the Data Support Section at NCAR prepared the data tapes used in this research. The NWSFO at Oklahoma City kindly provided the satellite photographs. Neal Shores helped produce the maps and cross-sections used in the case study. Teri Cassil drafted many of the figures.

Support for this research was provided by NSF Grant ATM-8019430. The author's graduate studies have been funded by the Air Force Institute of Technology.

TABLE OF CONTENTS

	Page
ABSTRACT	iii
ACKNOWLEDGEMENTS	iv
LIST OF SYMBOLS	vii
LIST OF TABLES	ix
LIST OF ILLUSTRATIONS	x
Chapter	
I. INTRODUCTION	1
Background	1
Comma Clouds	3
Compositing	4
II. THE COMPOSITE COMMA CLOUD	7
Compositing Technique	7
Thermodynamic Diagrams	10
Isobaric Analyses	25
Isentropic Analyses	36
Climatological Means	42
Richardson Numbers	44
Severe Weather Activity	53
Other Composites	58
III. CASE STUDY: 21-22 MARCH 1981	60
Background	60
Surface Analysis	68
Temperature and Mositure Profiles	73
Vertical Motions	85
Richardson Numbers	100
Forecasting Dry Slot Convection	102

	Page
IV. SUMMARY AND SUGGESTIONS FOR FURTHER RESEARCH..	105
APPENDICES..	109
Appendix 1...............................	110
Appendix 2...............................	112
REFERENCES..	116

LIST OF SYMBOLS

c_p	specific heat of air at constant pressure
f	coriolis parameter
f_o	coriolis parameter at 37.5° N
g	acceleration due to gravity
h	moist static energy
L	latent heat of condensation
p	pressure
q	specific humidity
q_s	saturation specific humidity
R	gas constant for dry air
Ri	Richardson number
T	temperature
T_v	virtual temperature
u	east-west component of wind velocity
v	north-south component of wind velocity
$\lvert \overline{V} \rvert$	wind speed
z	height above sea level
α	specific volume
Γ	lapse rate
Θ	potential temperature
Θ_E	equivalent potential temperature

Θ_V	virtual potential temperature
Θ_W	wet-bulb potential temperature
ρ	density
σ	static stability
Ψ	stream function
ω	vertical velocity in pressure coordinates
$\frac{\partial}{\partial a}$	partial derivative with respect to a
J (a,b)	Jacobian operator
∇ (a)	gradient operator
∇^2(a)	laplacian operator

LIST OF TABLES

Table		Page
1.	Departure from Climatological Mean Values......	43
2.	Number of Severe Weather Events Occurring in Each Zone......................................	54
3.	Severe Weather Threat (SWEAT) Index............	57
4.	Inversion Layer Quantities.....................	115

LIST OF ILLUSTRATIONS

Figure		Page
1.	Location of zones relative to the comma cloud pattern	8
2.	Skew-T log-p diagram for zone 1	11
3.	Skew-T log-p diagram for zone 2	11
4.	Skew-T log-p diagram for zone 3	12
5.	Skew-T log-p diagram for zone 4	12
6.	Skew-T log-p diagram for zone 5	13
7.	Skew-T log-p diagram for zone 6	13
8.	Skew-T log-p diagram for zone A	14
9.	Skew-T log-p diagram for zone B	14
10.	Skew-T log-p diagram for zone C	15
11.	Skew-T log-p diagram for zone D	15
12.	Skew-T log-p diagram for zone E	16
13.	Equivalent potential temperature profiles for zones 5 and E. Units are °K	20
14.	Equivalent potential temperature profiles for zones 1 and C. Units are °K	21
15.	Moist static energy profiles for 0000 and 1200 GMT for zones 5 and E. Units are x 1000 Joules/Kg	23
16.	Moist static energy profiles for 0000 and 1200 GMT for zones 1+2 and C. Units are x 1000 Joules/Kg	24

Figure | Page

17. 850 mb. analysis. Values to the left of the station symbol are temperature and dew point depression in °C. Value to the right is height of the surface in meters. Winds are in knots.................................... 26

18. 700 mb. analysis. Values to the left of the station symbol are temperature and dew point depression in °C. Value to the right is height of the surface in meters. Winds are in knots.................................... 27

19. 500 mb. analysis. Values to the left of the station symbol are temperature and dew point depression in °C. Value to the right is height of the surface in meters. Winds are in knots.................................... 28

20. 400 mb. analysis. Values to the left of the station symbol are temperature and dew point depression in °C. Value to the right is height of the surface in meters. Winds are in knots.................................... 29

21. 300 mb. analysis. Values to the left of the station symbol are temperature and dew point depression in °C. Value to the right is height of the surface in meters. Winds are in knots.................................... 30

22. 250 mb. analysis. Values to the left of the station symbol are temperature and dew point depression in °C. Value to the right is height of the surface in meters. Winds are in knots.................................... 31

23. 200 mb. analysis. Values to the left of the station symbol are temperature and dew point depression in °C. Value to the right is height of the surface in meters. Winds are in knots.................................... 32

24. 150 mb. analysis. Values to the left of the station symbol are temperature and dew point depression in °C. Value to the right is height of the surface in meters. Winds are in knots.................................... 33

Figure Page

25. 100 mb. analysis. Values to the left of the station symbol are temperature and dew point depression in °C. Value to the right is height of the surface in meters. Winds are in knots 34

26. 297 K relative-wind isentropic surface. Value to the right of the station symbol is pressure, in millibars for this surface. Winds are in knots 38

27. 307 K relative-wind isentropic surface. Value to the right of the station symbol is pressure, in millibars for this surface. Winds are in knots 39

28. 317 K relative-wind isentropic surface. Value to the right of the station symbol is pressure, in millibars for this surface. Winds are in knots 40

29. Natural logarithm of the gradient Richardson number versus pressure for zones 1+2, B and C.. 46

30. Natural logarithm of the gradient Richardson number versus pressure for zones 5 and E....... 47

31. Static stability profiles for zones 1+2, B and C. Units are $m^2 sec/mb^2$........ 49

32. Static stability profiles for zones 5 and E at 0000 GMT and 1200 GMT. Units are $m^2 sec/mb^2$.... 50

33. Composite wind speeds, in knots, for zones 1-6. 51

34. Composite wind speeds, in knots, for zones A-E. 52

35. 1000 and 500 mb height fields for 1200 GMT March 21, 1981. Values of the 1000 mb surface are in meters; values of the 500 mb surface are in decameters........ 62

36. 500 mb temperature field for 1200 GMT March 21, 1981. Temperatures are in degrees Celsius..... 63

37. 1902 GMT March 21, 1981 GOES-East visible imagery........ 64

Figure		Page

38. 2000 GMT March 21, 1981 GOES-East infrared imagery.. 65

39. 2200 GMT March 21, 1981 GOES-East visible imagery.. 66

40. 2330 GMT March 21, 1981 GOES-East visible imagery.. 67

41. 1000 and 500 mb height fields for 0000 GMT March 22, 1981. Values of the 1000 mb surface are in meters; values of the 500 mb surface are in decameters.................................. 69

42. 500 mb temperature field for 0000 GMT March 22, 1981. Temperatures are in degrees Celsius..... 70

43. NMC surface analysis for 2100 GMT March 21, 1981.. 71

44. Re-analysis of the surface data for 2100 GMT March 21, 1981................................. 72

45. Skew-T log-p diagram for Oklahoma City, Oklahoma (zone A) at 0000 GMT March 22, 1981... 74

46. Skew-T log-p diagram for Monett, Missouri (zone 1) at 0000 GMT March 22, 1981............ 75

47. Skew-T log-p diagram for Little Rock, Arkansas (zone C) at 0000 GMT March 22, 1981............ 76

48. Temperature profile for Oklahoma City, Oklahoma at 1200 GMT March 21, 1981. Surface temperatures and assumed lapse rates at Tulsa, Oklahoma are superimposed for 1500, 1800 and 2100 GMT.. 78

49. Skew-T log-p diagram for Stephensville, Texas (zone 4) at 0000 GMT March 22, 1981............ 79

50. Skew-T log-p diagram for Longview, Texas (zone 3) at 0000 GMT March 22, 1981............ 81

51. Skew-T log-p diagram for Lake Charles, Louisiana (zone D) at 0000 GMT March 22, 1981.. 82

Figure		Page
52.	Relative humidity cross-section between Amarillo, Texas and Lake Charles Louisiana at 0000 GMT March 22, 1981........................	83
53.	Relative humidity cross-section between Del Rio, Texas and Salem, Illinois at 0000 GMT March 22, 1981..	84
54.	600 mb quasi-geostrophic vertical motions for 1200 GMT March 21, 1981. Units are x 10^{-5} mb/sec..	87
55.	600 mb quasi-geostrophic vertical motions for 0000 GMT March 22, 1981. Units are x 10^{-5} mb/sec..	88
56.	Component of the vertical motion in Figure 54 which is due to differential vorticity advection (F1)......................................	90
57.	Component of the vertical motion in Figure 54 which is due to thermal advection (F2).........	91
58.	Component of the vertical motion in Figure 55 which is due to differential vorticity advection (F1)......................................	92
59.	Component of the vertical motion in Figure 55 which is due to thermal advection (F2).........	93
60.	600 mb kinematic vertical motions for 1200 GMT March 21, 1981. Units are x 10^{-5} mb/sec.......	94
61.	600 mb kinematic vertical motions for 0000 GMT March 22, 1981. Units are x 10^{-5} mb/sec.......	95
62.	300 K isentropic surface analysis for 0000 GMT March 22, 1981. Value to the right of the station symbol is pressure, in millibars, for this surface. Winds are in knots.............	97
63.	310 K isentropic surface analysis for 0000 GMT March 22, 1981. Value to the right of the station symbol is pressure, in millibars, for this surface. Winds are in knots.............	98

Figure Page

64. 320 K isentropic surface analysis for 0000 GMT March 22, 1981. Value to the right of the station symbol is pressure, in millibars, for this surface. Winds are in knots............. 99

65. Natural logarithm of the gradient Richardson number versus pressure for Del Rio, Texas (zone 5) and Victoria, Texas (zone E) at 0000 GMT March 22, 1981............................ 101

A COMPOSITE STUDY OF COMMA CLOUDS AND THEIR ASSOCIATION WITH SEVERE WEATHER OVER THE GREAT PLAINS

CHAPTER I

INTRODUCTION

1.1 Background

When the first satellite photographs of the earth appeared in the early 1960's, it was apparent that cloud patterns associated with mid-latitude cyclones evolve through a number of identifiable stages. Cyclones at the same phase in their development were seen to have similar cloud patterns. Furthermore, these patterns agreed remarkably well with the classical models of clouds and weather associated with wave cyclone life cycles (e.g., Bergeron, 1951).

The evolution of satellite-observed cloud patterns accompanying cyclogenesis was first conceptually modeled by Boucher and Newcomb (1962). Their model consisted of five phases from "open, frontal wave" to "filling cyclone," and formed the basis for later models. They attributed the

clear area behind the cold frontal cloud band to strong subsidence. Leese (1962) proposed that the clear region is not formed by active, on-going subsidence, but by the horizontal advection of dry air which only has a prior history of subsidence. Further interpretations made by other researchers, and summarized by Widger (1964), supported and elaborated on the model of Boucher and Newcomb.

The early observations were later explained in terms of atmospheric dynamics by several authors. Barr et al. (1966) used a ten-level quasi-geostrophic model to explore the usefulness of satellite imagery for determining the vertical motions in a cyclone. They found that the pattern of rising motion resembles the cloud pattern in the early phase of the storm, but that horizontal motions soon become just as important in determining the evolution of the cloud pattern. McClain and Brodrick (1967) and Widger et al. (1967) modeled cyclone development and cloud patterns in terms of changes in vorticity and thermal structure. Weldon (1976, 1979) has observed the importance of deformation of the winds relative to the moving system as being important for the evolution of the comma-shaped cloud. Carlson (1980) used relative-flow isentropic analysis to depict the three-dimensional flow of air in the comma cloud. He described three major airstreams of differing origins which are present in the storm.

Satellite imagery has also been useful for forecasting

severe weather. Many of the observations and forecast rules relate mesoscale changes in cloud patterns to severe weather events, but synoptic-scale changes are important as well. Skidmore and Purdom (1973) have discussed many of these. McNulty (1978) examined upper tropospheric wind maxima and their associated divergence fields in terms of severe weather occurrences. Miller and McGinley (1978) show that certain regions within the synoptic-scale cloud patterns are more favorable than others for the development of severe weather.

1.2 Comma Clouds

The term "comma cloud" has been used by different authors to describe somewhat different phenomena, and, as used in this study, "comma cloud" differs from its earliest definition. Widger et al. (1967) ascribe the term, "comma-shaped pattern," to clouds associated with a vorticity maximum moving in northwesterly flow around an old cyclone. They differentiate between this and the "hook-shaped" pattern associated with the initial stage of frontal-wave cyclogenesis. Anderson et al. (1969) also use "comma-shaped cloud" to mean the pattern associated with cyclone development within the cold air, behind the major cold frontal band, and separated from an older, occluded cyclone. The cloud formation associated with the larger, synoptic-scale system has generally been referred to as a "vortex cloud pattern" (Barr et al. 1962; Widger, 1964). Reed (1979) and Mullen (1979) have

also referred to the cloud formations associated with polar lows as comma clouds.

In recent years, however, "comma cloud" has come to include any vortical pattern of clouds, including that surrounding the synoptic-scale cyclone itself. Weldon (1979) used the terms "storm comma system" and "large storm comma" to describe synoptic-scale patterns. Miller and McGinley (1978) and Carlson (1980) have also used the term in this context. In this study, any comma-shaped cloud pattern which was of sufficient size to cover several rawinsonde sounding sites was a candidate for inclusion in the composite averaging scheme. Not all of these cloud patterns are of sufficient size to be synoptic-scale. Others are not associated with surface low pressure centers. In the mean, however, the composite averages represent synoptic-scale cyclonic circulations. The "composite comma cloud" referred to in this study is, therefore, related to the synoptic-scale cyclone itself and not the smaller cloud patterns sometimes seen in connection with regions of maximum cyclonic vorticity advection.

1.3 Compositing

While the compositing of storm systems has been useful in tropical meteorology, very few studies have been undertaken using composited data on mid-latitude systems. Fawcett and Saylor (1965) studied the distribution of clouds and weather associated with 21 cases of Colorado cyclogenesis.

Mullen (1979) composited the comma cloud patterns associated with 22 polar lows in the North Pacific. In tropical research, Williams and Gray (1973) and Ruprecht and Gray (1976) used composite upper-air soundings to investigate the structure of tropical cloud clusters. McBride (1981) has used the compositing approach to study tropical cyclogenesis. Since upper-air observations are sparse at low latitudes, few individual systems can be adequately analyzed. Compositing methods are advantageous in the tropics for constructing an "average" system for study. In mid-latitudes, over continents, the upper-air network provides better coverage of storms, and individual cases of cyclogenesis and cyclone structure have been quantitatively portrayed quite adequately. Still, the large variability in the kinematic and thermal structure of mid-latitude cyclones may make it more useful to study a composite system. The composite then serves as a reference against which individual storms may be compared.

While Miller and McGinley (1978) and Weldon (1979) have explained many of the qualitative aspects of comma cloud patterns, these authors have also suggested the need for quantitative studies in order to validate their findings and to identify new relationships which may be important. The purpose of this research is to calculate composite values of kinematic and thermodynamic parameters from different regions of the comma cloud, and to relate these to the location of severe weather. Chapter II examines the composite

comma cloud pattern. Analyses are presented on isobaric and relative-flow isentropic surfaces. Comparisons are made between different portions of the cloud pattern with emphasis on the differences between cloudy and cloud-free regions. Severe weather occurrences are also analyzed. Chapter III examines an individual comma cloud and a phenomena which has not been given much attention in the literature: the *in situ* growth of organized convection within the dry portion of the comma cloud. Certain features of this storm will be compared to the composite comma cloud.

CHAPTER II

THE COMPOSITE COMMA CLOUD

2.1 Compositing Technique

Thirty-five separate comma systems were found which formed or traversed over the central U.S. during the 1980 and 1981 spring seasons (March through June). These are the months when severe weather is most likely to occur, and also when the frequency of cyclogenesis is at a maximum (Whittaker and Horn, 1981). Only comma-shaped cloud patterns which existed at standard rawinsonde launch times (0000 and 1200 GMT) were chosen. Many systems maintained a comma shape for more than one sounding time; thus a total of sixty-eight data periods are included in the composite analysis.

Based on GOES visual and infrared (IR) imagery, each cloud pattern was divided into eleven zones, five of which (A-E) contained the cloudy portion and six of which (1-6) partitioned the dry intrusion (Fig. 1). The most representative sounding in each zone was then selected for composite averaging. Zones 1 and 2 were included only if the dry intrusion had penetrated north of the comma head. All

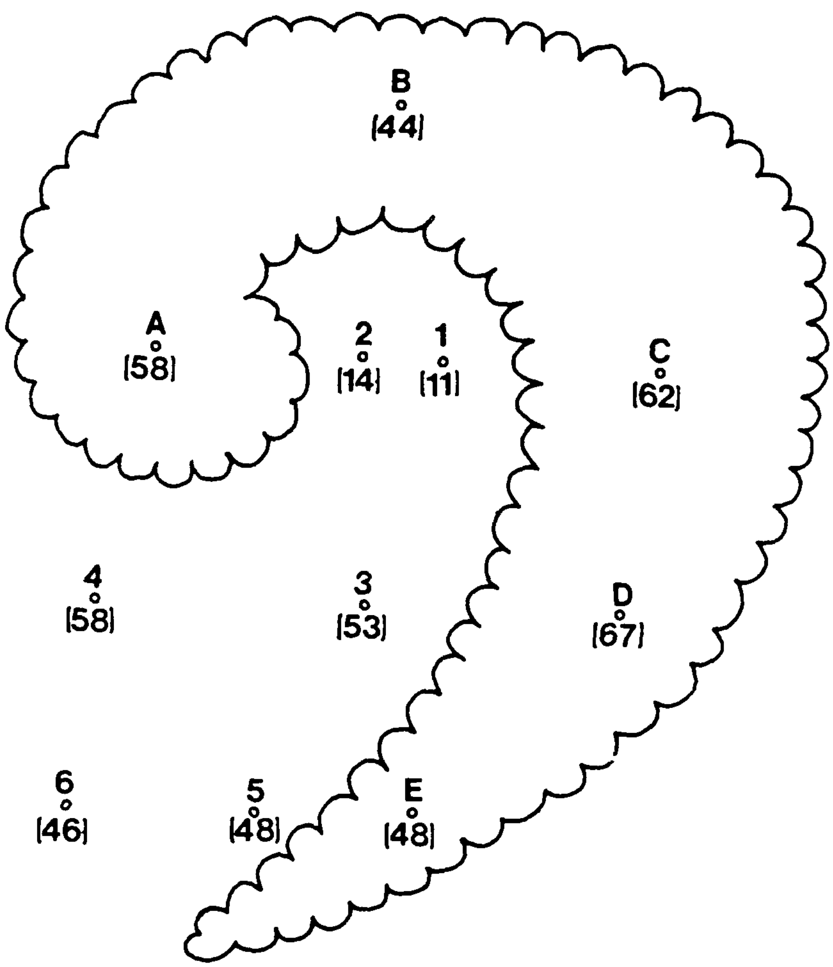

FIGURE 1: Location of zones relative to the comma cloud pattern.

soundings used in the composite for a given zone were taken within that zone and no attempt was made to include a sounding simply because it was the nearest one. Thus, there are unequal numbers of soundings in each zone. A comma cloud having only a very short tail portion, for example, may not have included a sounding for zone E. Appendix 1 lists the soundings used in each of the zones for each date and time period. There is a slight bias ($\approx$ 3:2) towards 1200 GMT soundings.

Sounding data for the two four-month periods were obtained from NMC data tapes. These included temperatures and dew point depressions at mandatory and significant reporting levels. Geopotential heights and vector winds are also reported at mandatory levels. Significant level wind data were also used for Richardson number calculations.

To produce the composite sounding for each zone, temperatures and dew point depressions from individual soundings were interpolated with respect to the logarithm of pressure between 1000 and 100 mb in 25 mb increments. The maximum dew point depression reported was 30° C, so that conditions in the dry zones may be even drier than the composite values indicate. Arithmetic means of the temperature and dew point depression were calculated every 25 mb from the soundings in each zone. Values of vapor pressure and saturation vapor pressure were derived using the method of Lowe (1977). Values of specific and relative humidity, virtual temperature and

virtual potential temperature are calculated at each level for which dew point depressions were available. Potential temperatures are calculated at all levels. Values of moist static energy, $h = gz + c_p T + Lq$ are calculated at mandatory levels for which q is known. Two static stability parameters are calculated:

$$S = \frac{-T_v}{\Theta_V} \frac{\partial \Theta_V}{\partial p} \qquad \text{and } \sigma = \frac{-\alpha}{\Theta} \frac{\partial \Theta}{\partial p}$$

Centered finite difference estimates of $\frac{\partial \Theta}{\partial p}$ and $\frac{\partial \Theta_V}{\partial p}$ are taken with Δp = 50 mb.

Winds at mandatory levels were averaged by decomposing each vector wind into u- and v- components. the magnitude of the composite vector wind is less than the mean wind speed because of the triangle inequality:

$$\left| \sum_{i=1}^{N} \overline{V}_i \right| \leq \sum_{i=1}^{N} |\overline{V}_i| \; .$$

The composite vector wind speeds in Figures 17-25 are, therefore, less than the mean wind speeds in Figures 33 and 34.

2.2 Thermodynamic Diagrams

Thermodynamic diagrams have been plotted for each of the zones (Figs. 2-12). The starting point is the first level to be representative of at least half of the total soundings possible in any zone. Composite soundings in zones 4 and 6, for example, start at 900 mb because most of the

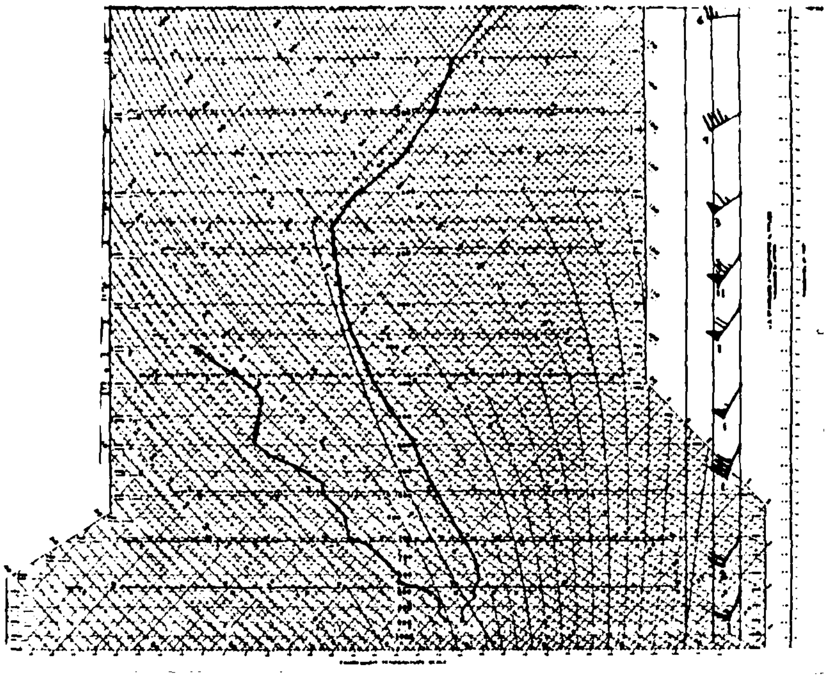

FIGURE 2: Skew-T log-p diagram for zone 1.

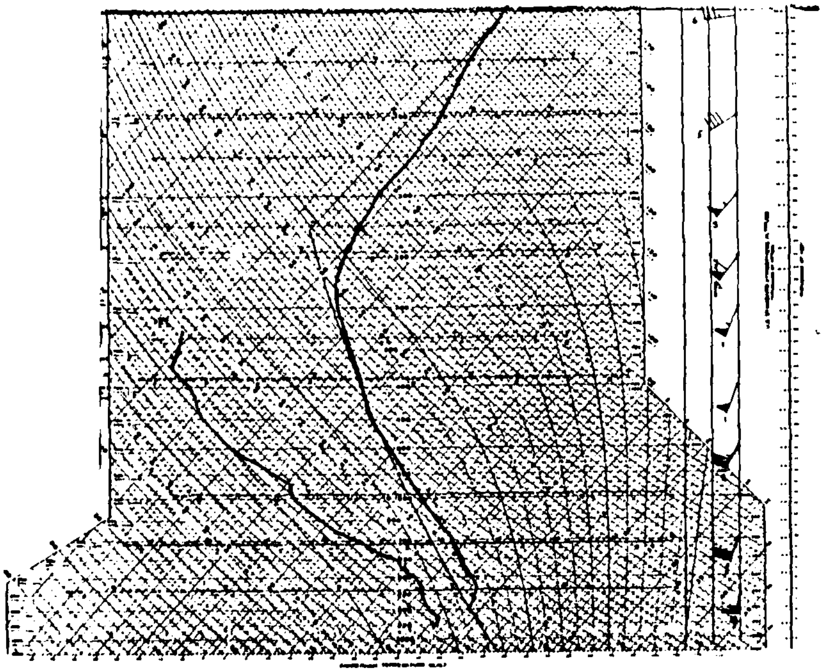

FIGURE 3: Skew-T log p diagram for zone 2.

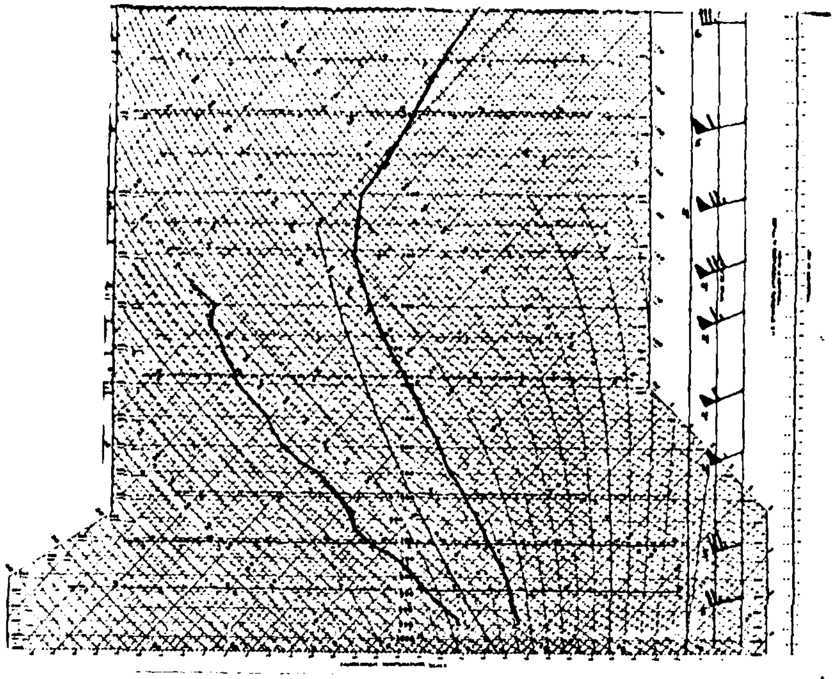

FIGURE 4: Skew-T log-p diagram for zone 3.

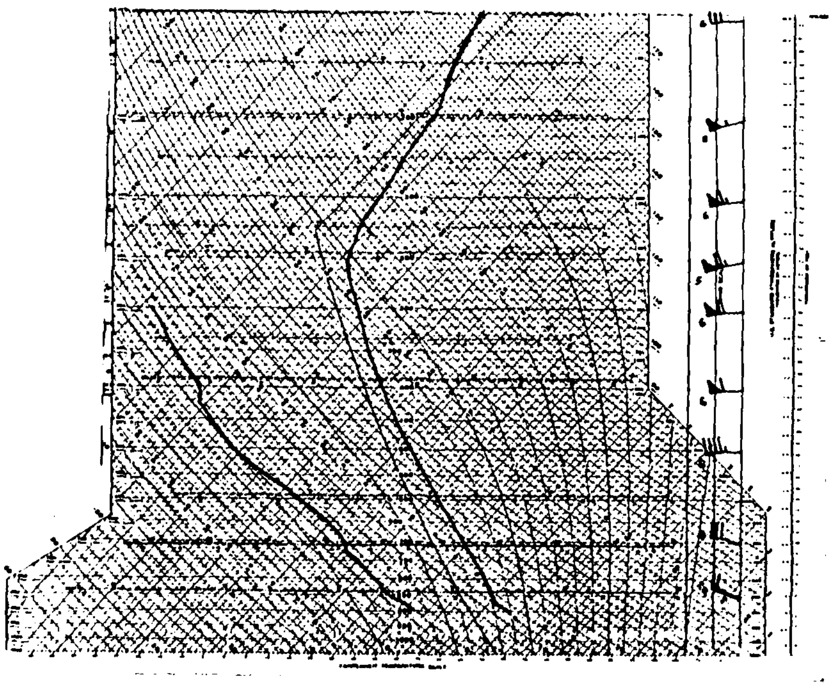

FIGURE 5: Skew-T log-p diagram for zone 4.

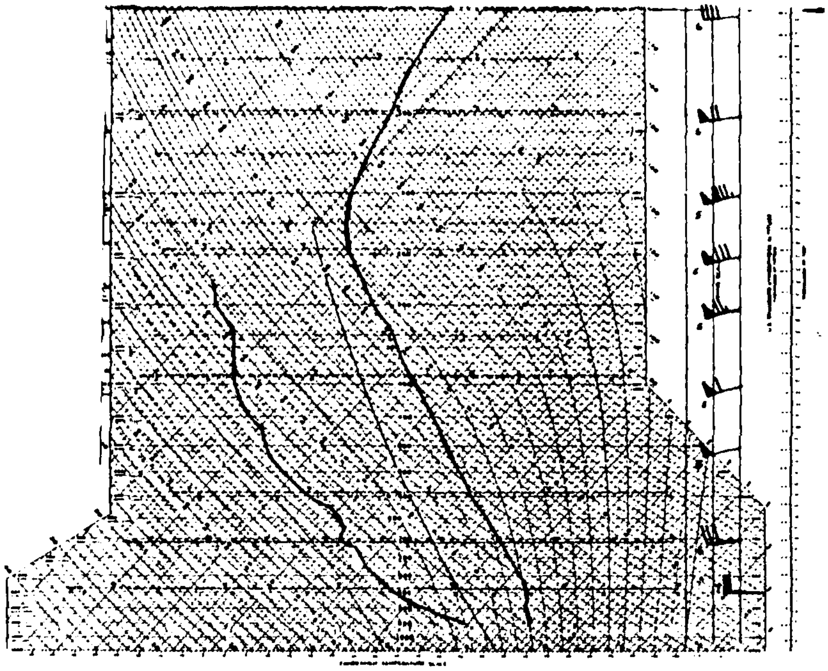

FIGURE 6: Skew-T log-p diagram for zone 5.

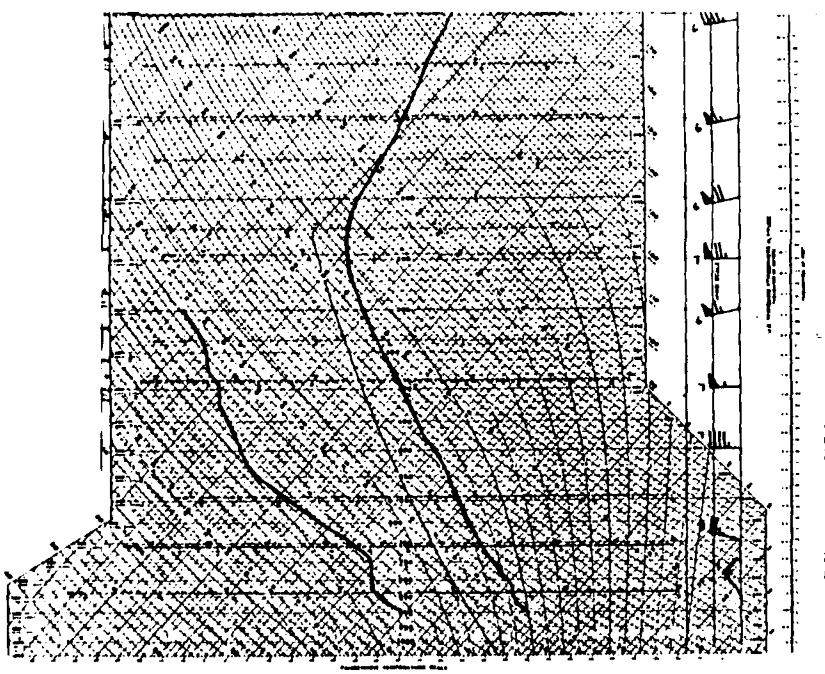

FIGURE 7: Skew-T log-p diagram for zone 6.

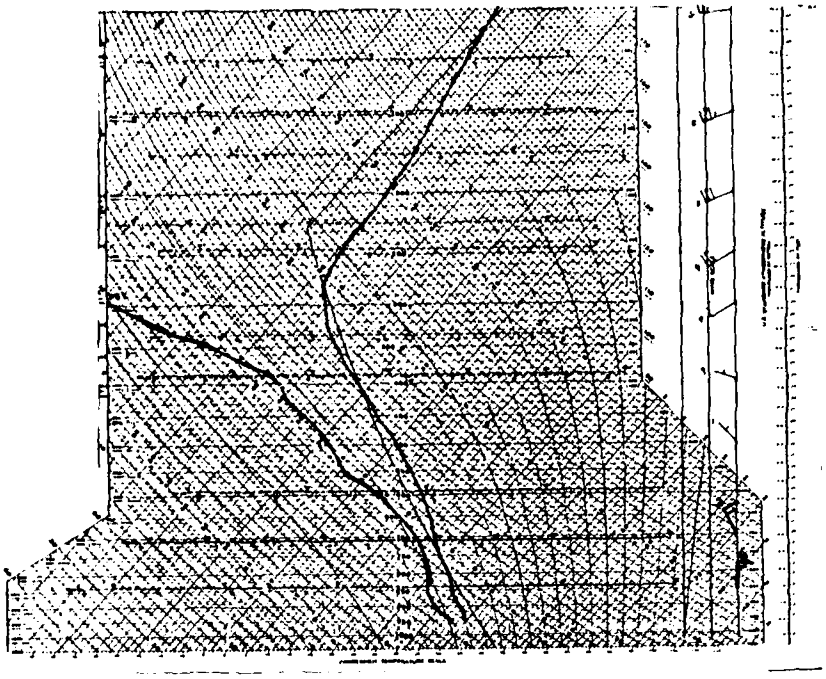

FIGURE 8: Skew-T log-p diagram for zone A.

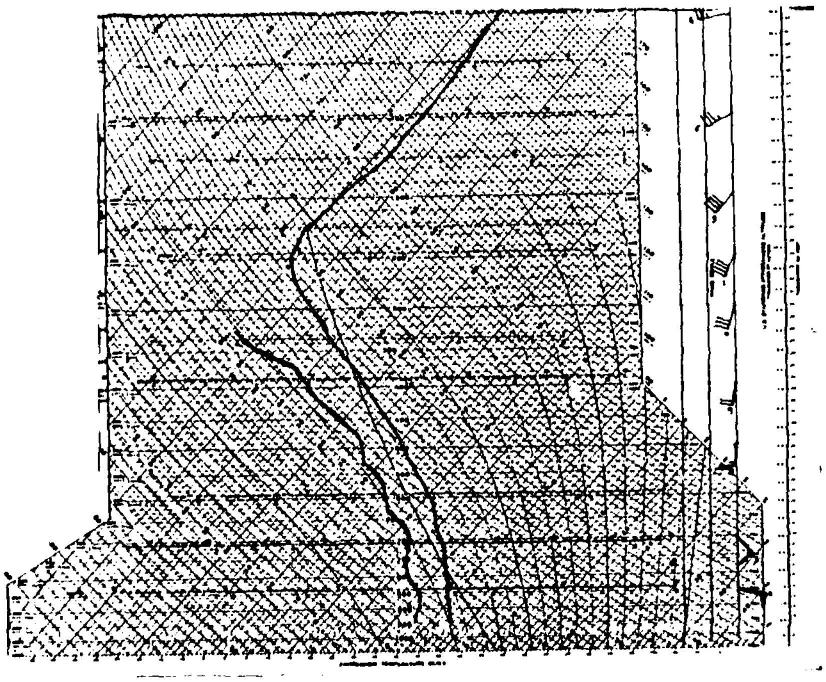

FIGURE 9: Skew-T log-p diagram for zone B.

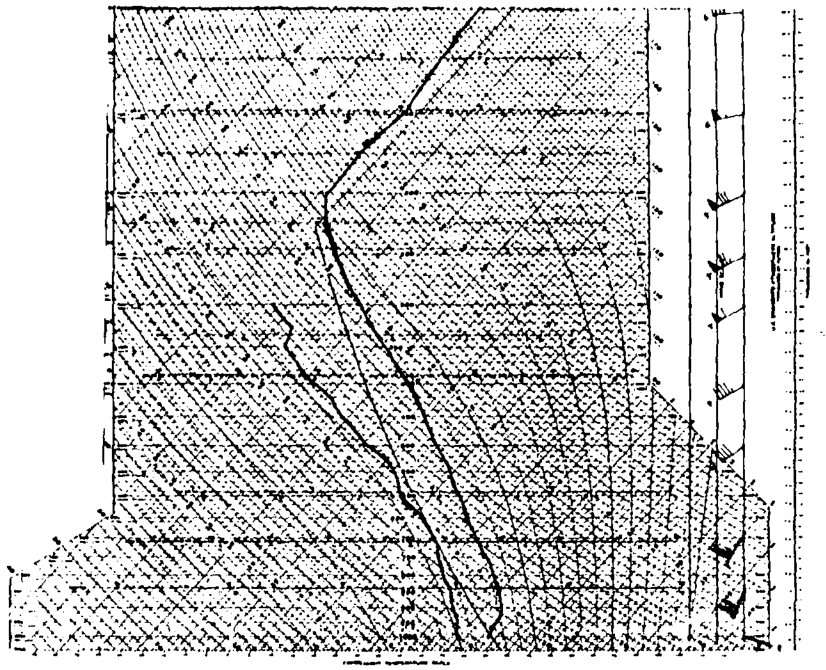

FIGURE 10: Skew-T log-p diagram for zone C.

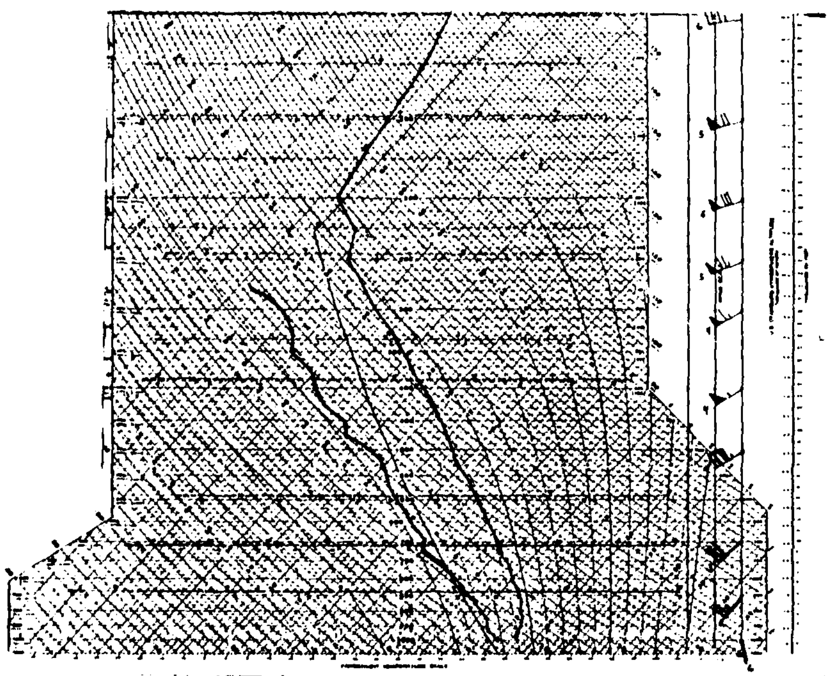

FIGURE 11: Skew-T log-p diagram for zone D.

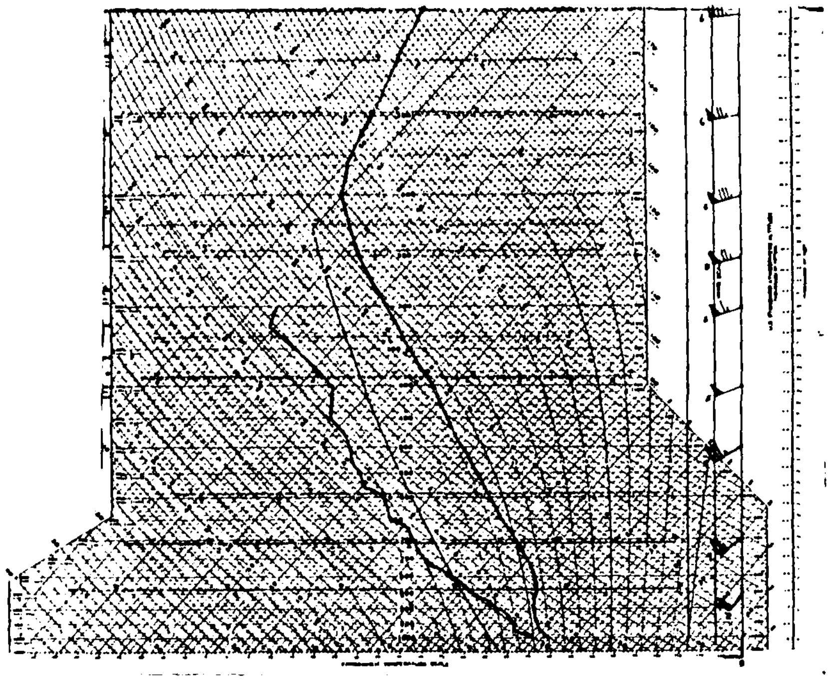

FIGURE 12: Skew-T log-p diagram for zone E.

individual soundings which make up those composites are from stations at high elevations. An examination of these soundings shows only weak stable layers without any pronounced inversions. The compositing method does not preserve the intensity of inversions since only the temperature and dew point at each pressure level are averaged, not their vertical derivatives. A more complete treatment of this problem and an examination of average lapse rates within and above inversion layers are presented in Appendix 2. Static stability values taken from the composite averages are underestimated within the low-level inversion layer.

Composite soundings taken from within the dry intrusion are notably drier than those in the cloudy zones and, except

for zones 1 and 2, lack any significant stable layers. Zone 1's sounding is characterized by an absolutely stable lapse rate from the surface to about 800 mb and, except in the lowest 1 km, is warmer than zone 2 to the west. There is slightly more moisture below 900 mb in zone 1 than in zone 2. These zones represent the northern end of the dry intrusion where dry air has been advected in from west of the upper-level trough axis. In these zones a nocturnal, low-level inversion is often present. The lowest 1-2 km remains cool and moist, and a low overcast cloud cover may be seen on the satellite pictures. Even though middle and upper level clearing has occurred, moist air remains at low levels. Usually, daytime surface heating warms the air in this layer sufficiently to eliminate the inversion by 0000 GMT. Generalties about zones 1 and 2 are made with some caution because of the fewer number of soundings taken in these zones.

Zones 3, 4, 5 and 6 represent the portion of the dry intrusion south of the comma head. The warmest air is in the eastern portion represented by zones 3 and 5, while the driest air lies to the west. The composite lapse rates in zones 4 and 6 are nearly dry adiabatic in the first few hundred meters above ground level. There is also a backing of the wind with height in zones 4 and 6 where cold air advection is the strongest. Slight backing of the wind also occurs in zone 5.

Zone A's sounding represents conditions within the

comma head. This is the mid-level circulation center of the cyclone, as indicated by the 3 m/sec wind at 400 mb. The surface low center lies farther east; winds back with height as colder air from the north enters at low levels. Averaged over the depth of the troposphere, the air here is colder than in any other zone except B. Below 600 mb the atmosphere is conditionally stable. Dew point depressions below this level are less than 5° C. For a composite sounding, this represents very moist air. Rapid drying occurs above 400 mb.

Zone B soundings are taken within the band of clouds north of the low center that connects the comma head and tail portions. Enhanced IR imagery often shows the coldest cloud tops are present in this zone, indicative of upward vertical motion and widespread precipitation. Fawcett and Saylor (1965) also found the maximum probability of precipitation was centered north of the surface low. The 300 mb temperature of -47° C is colder than in any other zone at that level and the upper level drying is not as intense as in zone A. Surface temperatures are also the coldest of any of the zones. This colder air is advected into zone A (cf. the "cold conveyor" of Carlson, 1980).

Zones C, D and E make up the tail portion of the comma pattern. They represent conditions in the warm sector ahead of the surface cold front. Winds veer with height in all three of these zones in response to the advection of warmer

air. The warmest temperature profile is in the southernmost portion; zone E. The greatest surface moisture is also in E, but the air dries out rapidly with height. Further north the lowest levels are not as moist, but the air is rising and this spreads the moisture over a deeper layer. For example, the 700 mb dew point depression is 13° C in zone E, but only 6° C at that level in zone C. Weldon (1979) points out that the cloud tops increase northward along the comma tail and the moisture profiles of these soundings support this.

Unlike potential temperature, which is conserved only for a dry adiabatic process, equivalent potential temperature is conserved for both dry and moist processes. This follows from the definition of equivalent potential temperature, the temperature a sample of air would have if all of its moisture were condensed out and then brought dry-adiabatically back to 1000 mb. A measure of the potential instability of that air sample is $-\frac{\partial \Theta_E}{\partial p}$. If $-\frac{\partial \Theta_E}{\partial p} < 0$ and the air is lifted, its Θ_E will be warmer than the Θ_E of the environment and it and it will be positively buoyant. Equivalent potential temperature profiles (Fig. 13) show zone E is potentially unstable to 650 mb. The potential instability, $-\frac{\partial \Theta_E}{\partial p}$, is -3.7×10^{-2}° C/mb between 950 and 700 mb in zone E, while only -1.9×10^{-2}° C/mb in zone 5. In the northern portion of the comma cloud, the situation is reversed (Fig. 14). Here the greater potential instability is in the dry air.

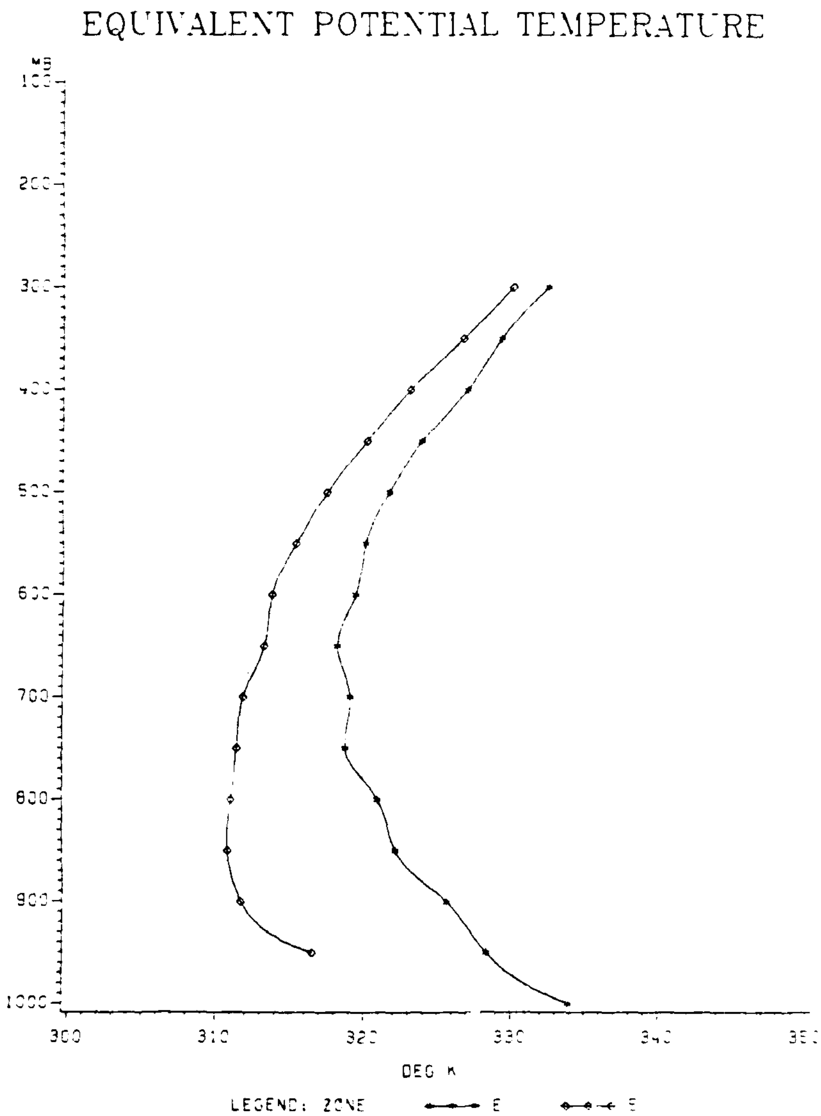

FIGURE 13: Equivalent potential temperature profiles for zones 5 and E. Units are °K.

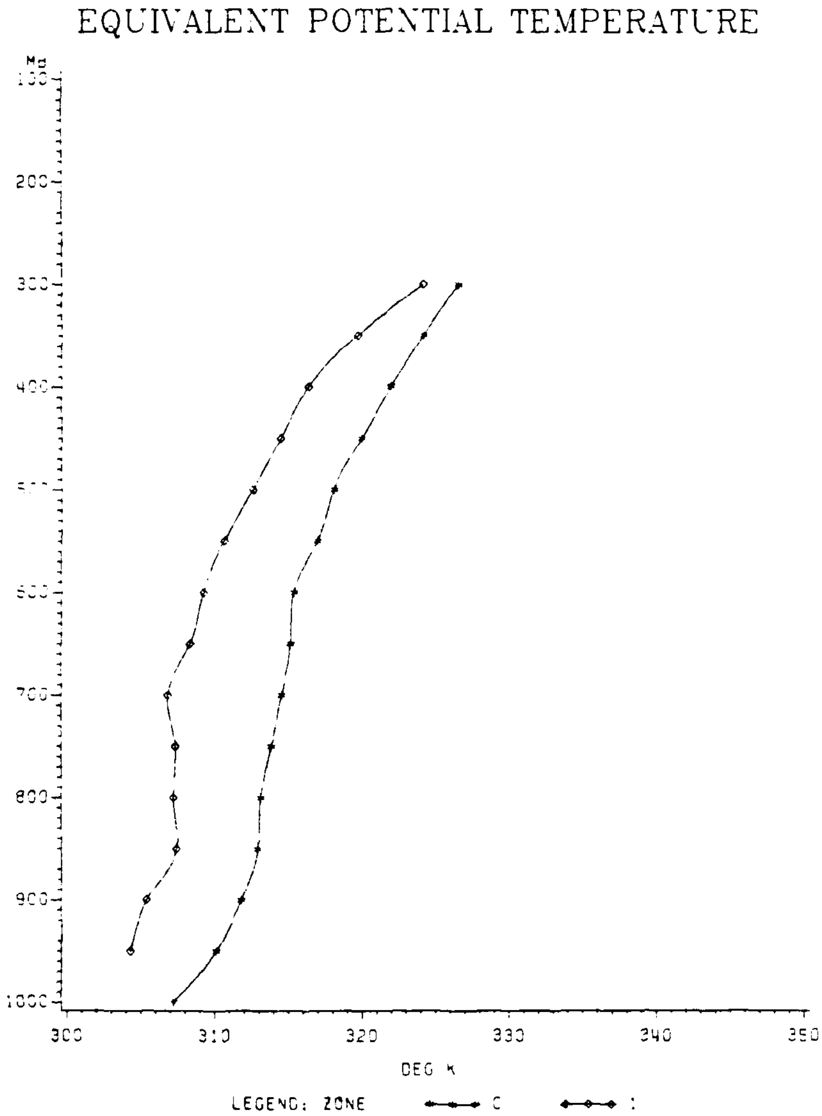

FIGURE 14: Equivalent potential temperature profiles for zones 1 and C. Units are °K.

In zone C, $-\frac{\partial \Theta_E}{\partial p} < 0$ at all levels, but equals -4.0×10^{-3}° C/mb between 850 and 700 mb in zone 1. Note also that the equivalent potential temperature difference is much larger across the cloud edge at the southern end of the comma tail. Comparing zones 5 and E, there is an 11° C difference at 950 mb. This represents the difference in equivalent potential temperature across the cold front or dry line which is normally present between these two zones.

Diurnal differences in moist static energy are shown in Figures 15 and 16. This quantity is also conservative with respect to dry and moist adiabatic processes, so that a decrease with height represents potential instability just as a decrease in equivalent potential temperature with height does (Kreitzberg and Brown, 1970). Figure 15 shows that the difference in moist static energy between zones 5 and E is much larger than the diurnal changes in that quantity. Even though there is greater warming in the dry air at low levels during the day, there still remains a large gradient in moist static energy across the cloud edge. There is no potential instability in the dry air at 1200 GMT. However, zone E is potentially unstable to 700 mb at both the morning and afternoon sounding times. The relatively few severe weather events which did occur during the morning hours were more frequently found in the southern portion of the comma tail than anywhere else. $-\frac{\partial h}{\partial p}$ is -36 J kg^{-1} mb^{-1} in zone E compared to -12 J kg^{-1} mb^{-1} in zone 5, at 0000 GMT. Figure 16

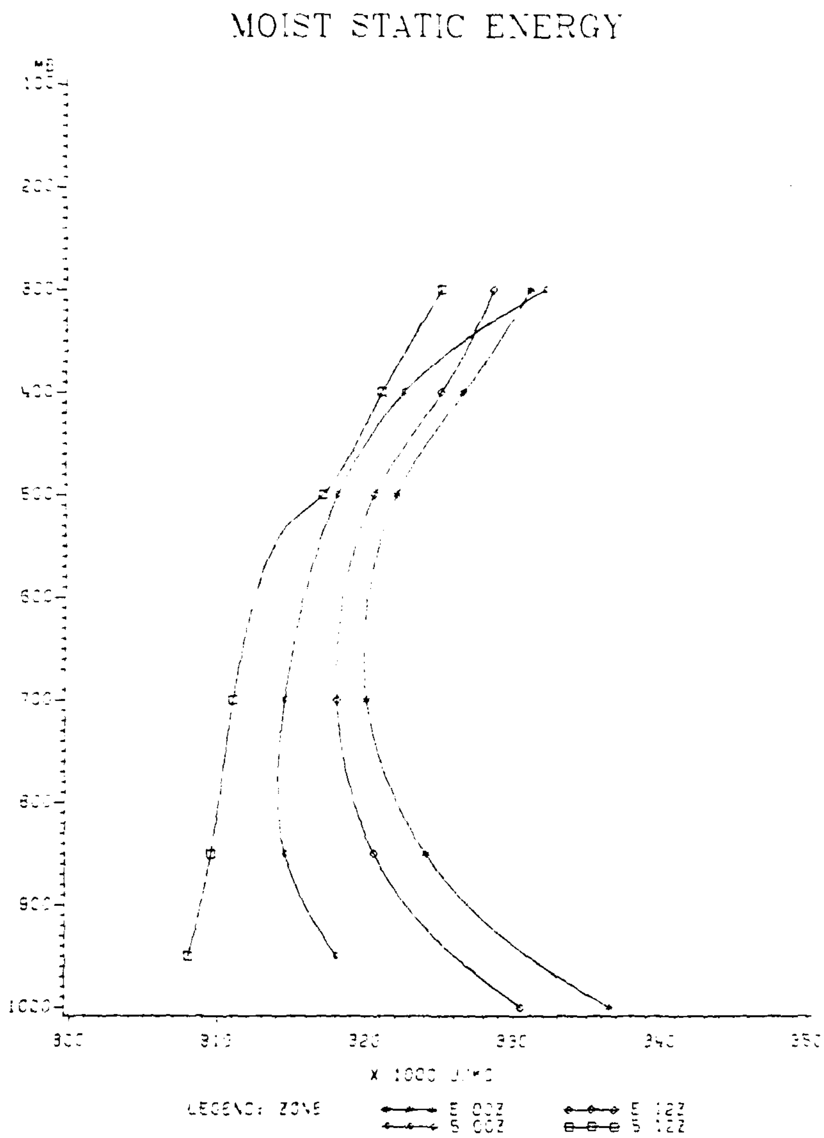

FIGURE 15: Moist static energy profiles for 0000 and 1200 GMT for zones 5 and E. Units are x 1000 Joules/kg.

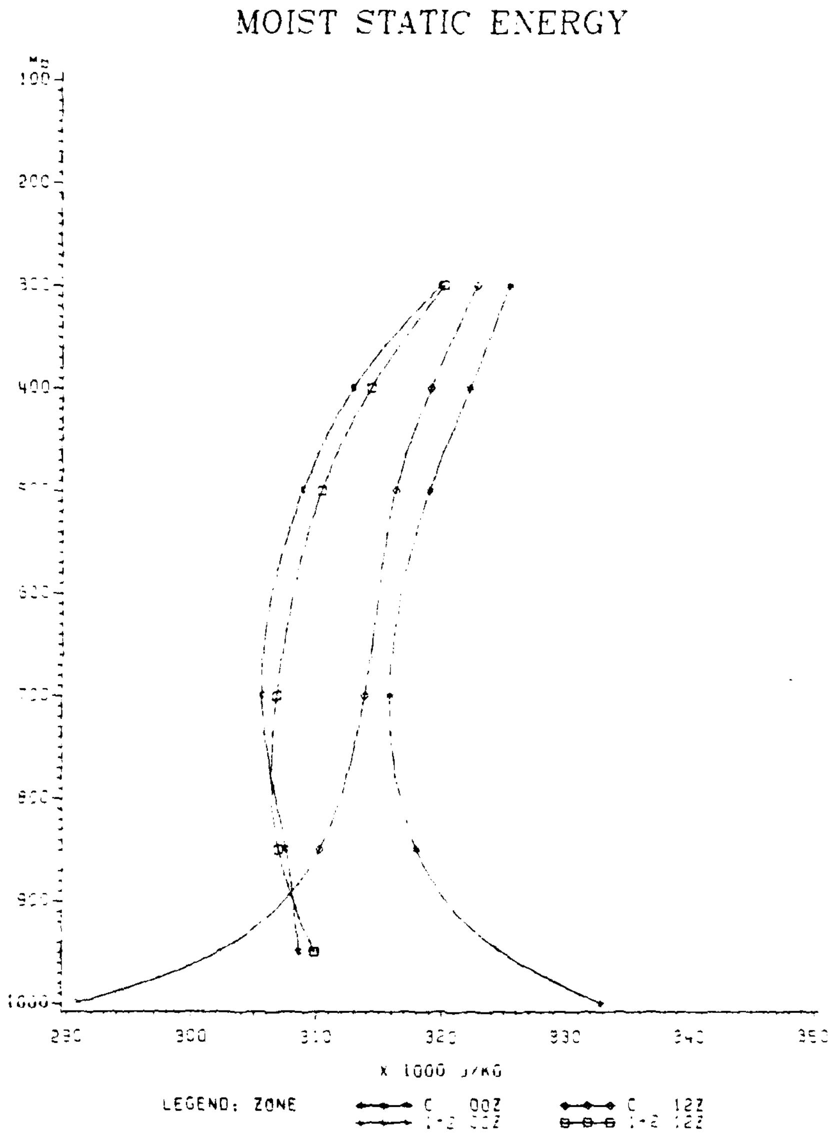

FIGURE 16: Moist static energy profiles for 0000 and 1200 GMT for zones 1+2 and C. Units are x 1000 Joules/kg.

shows differences between zones 1 and 2 (averaged together), and zone C. In both of these zones, $-\frac{\partial h}{\partial p} > 0$ in the morning. Potential instability increases during the day, but the magnitude of the afternoon difference in $-\frac{\partial h}{\partial p}$ between these two zones is much smaller than it is further south.

2.3 Isobaric Analyses

Composite averages at standard pressure levels are shown in Figures 17 to 25. The 1000 mb surface is not shown because it is below ground in most zones. A closed circulation is centered between zones A and 2 at 850 and 700 mb. Although the circulation center appears to tilt back towards zone A at higher levels, the heights in zone 2 are lower than in zone A at all levels. This is a consequence of the compositing. In those cases where zone 2 has been included, the systems are at maximum intensity and heights of the pressure surfaces should be near their lowest values. There are many more observations of zone A than zone 2, however, and the composite zone A includes many weaker systems. This moderates the height values in zone A while zone 2 represents only strong, fully occluded systems. The low center does exhibit a tilt with height back toward zone A in a composite of only those comma cloud cases which occurred in March.

Above 850 mb, the maximum winds are in the dry air behind the western edge of the comma tail. The maximum ranges from 28 m/sec at 500 mb to 43 m/sec at 200 mb. Weldon

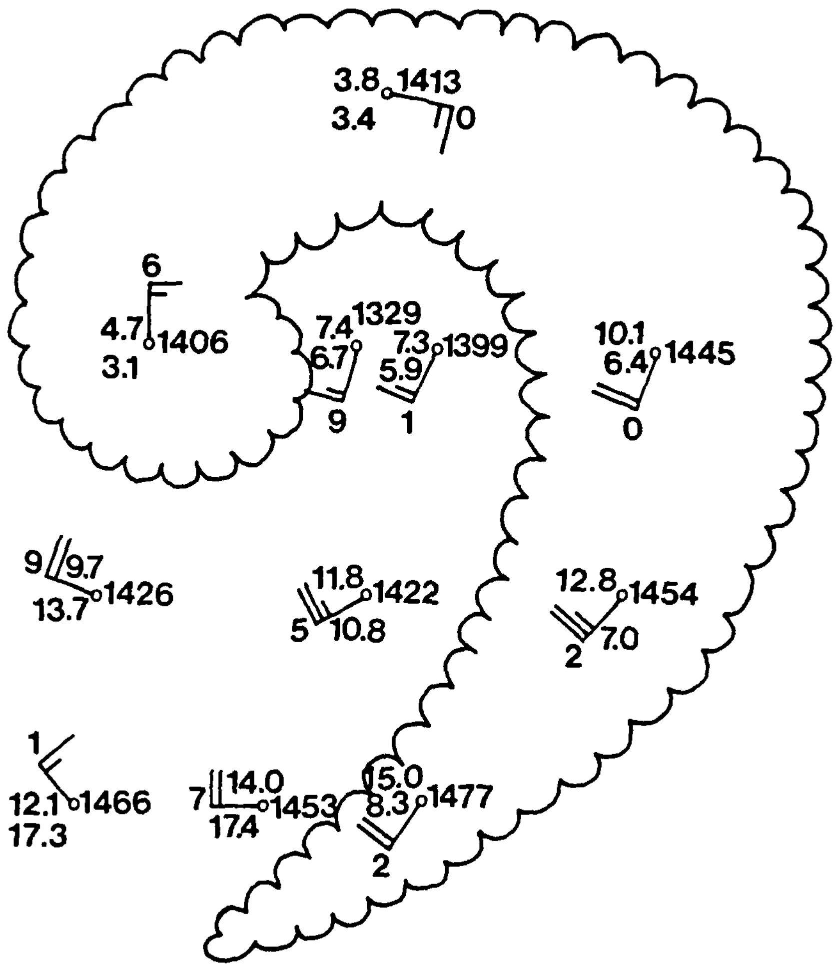

FIGURE 17: 850 mb analysis. Values to the left of the station symbol are temperature and dew point depression in °C. Value to the right is height of the surface in meters. Winds are in knots.

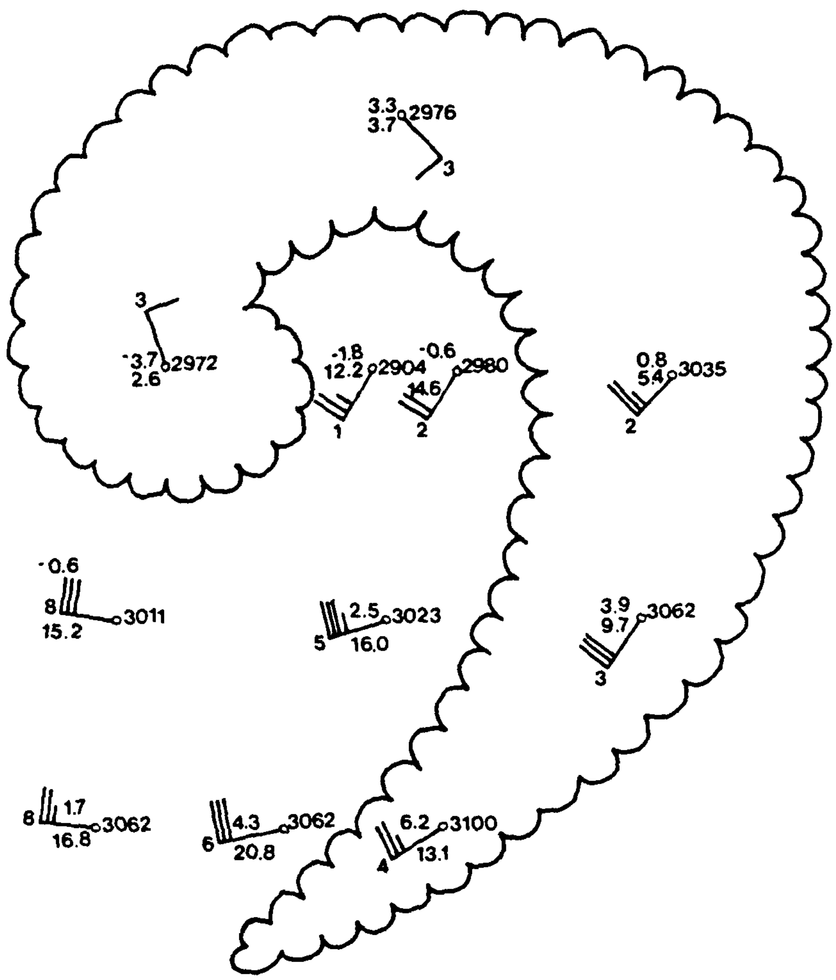

FIGURE 18: 700 mb analysis. Values to the left of the station symbol are temperature and dew point depression in °C. Value to the right is height of the surface in meters. Winds are in knots.

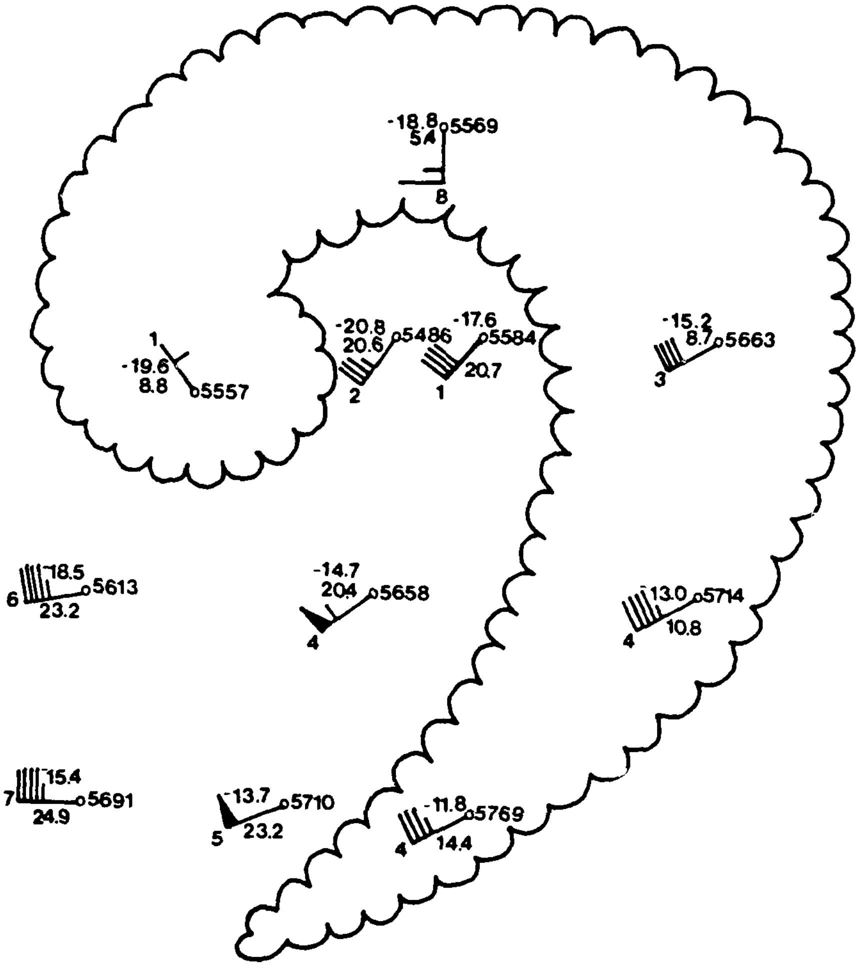

FIGURE 19: 500 mb analysis. Values to the left of the station symbol are temperature and dew point depression in °C. Value to the right is height of the surface in meters. Winds are in knots.

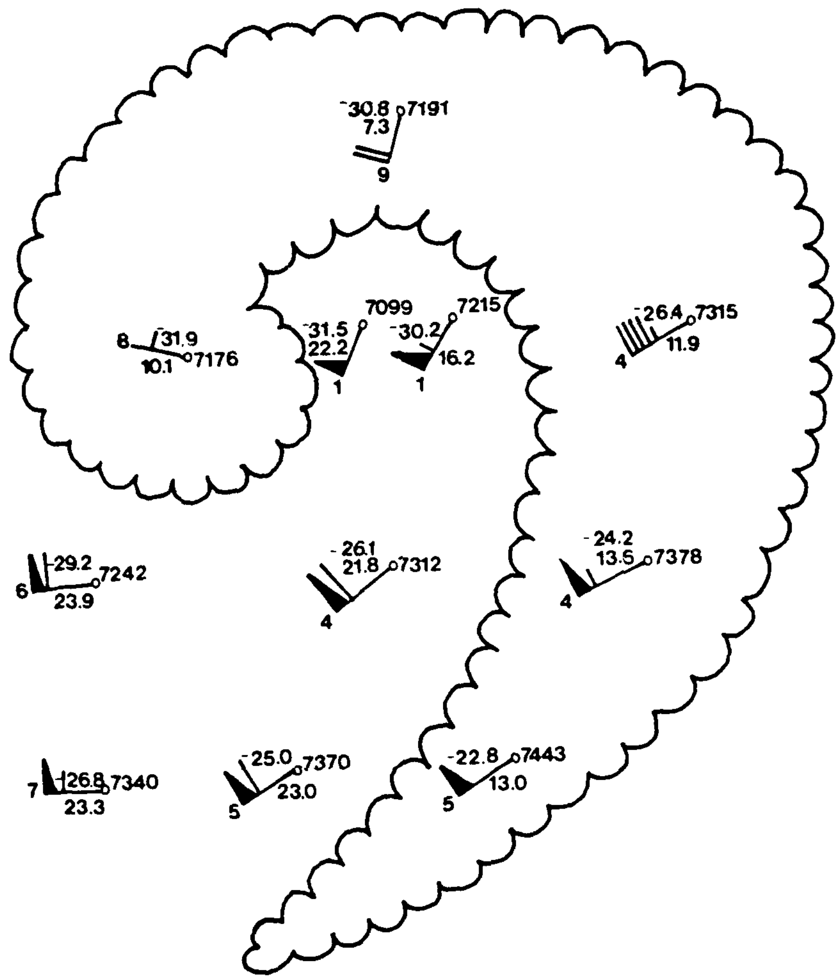

FIGURE 20: 400 mb analysis. Values to the left of the station symbol are temperature and dew point depression in °C. Value to the right is height of the surface in meters. Winds are in knots.

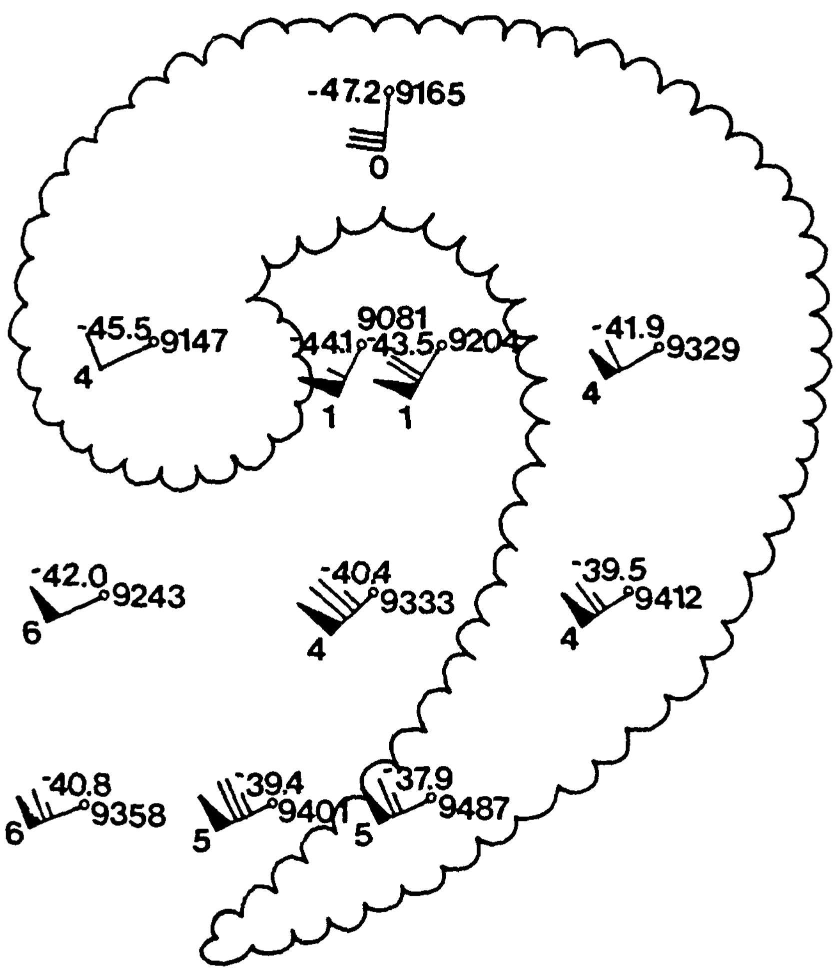

FIGURE 21: 300 mb analysis. Values to the left of the station symbol are temperature and dew point depression in °C. Value to the right is height of the surface in meters. Winds are in knots.

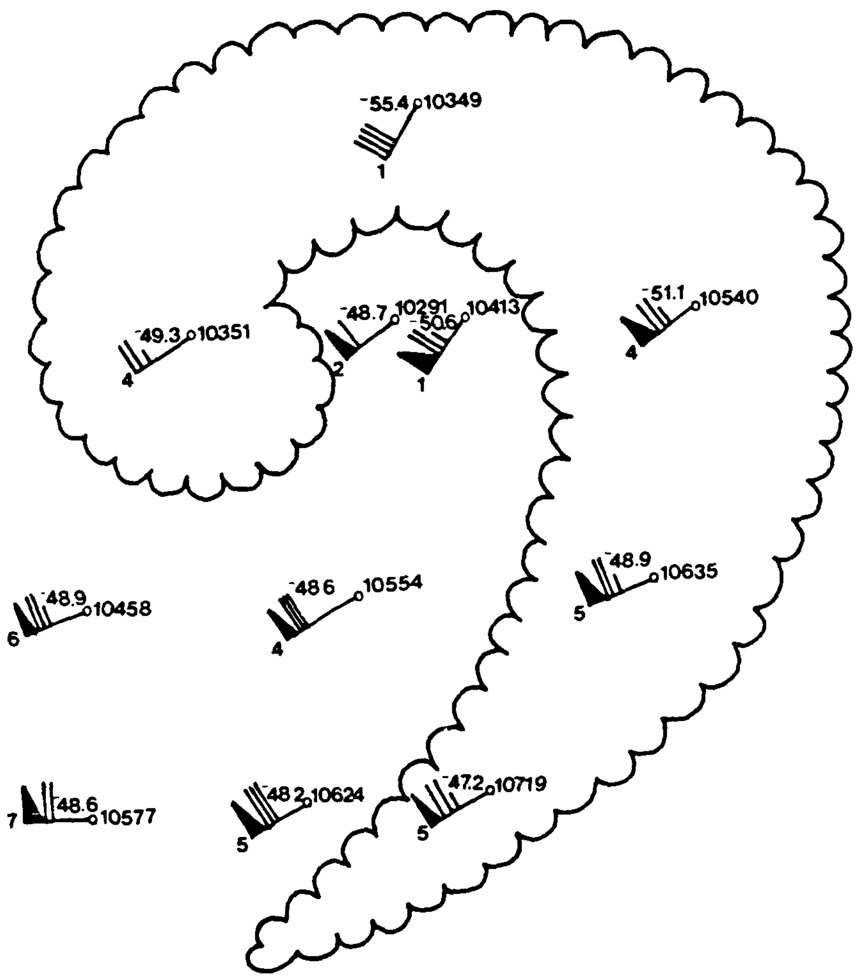

FIGURE 22: 250 mb analysis. Values to the left of the station symbol are temperature and dew point depression in °C. Value to the right is height of the surface in meters. Winds are in knots.

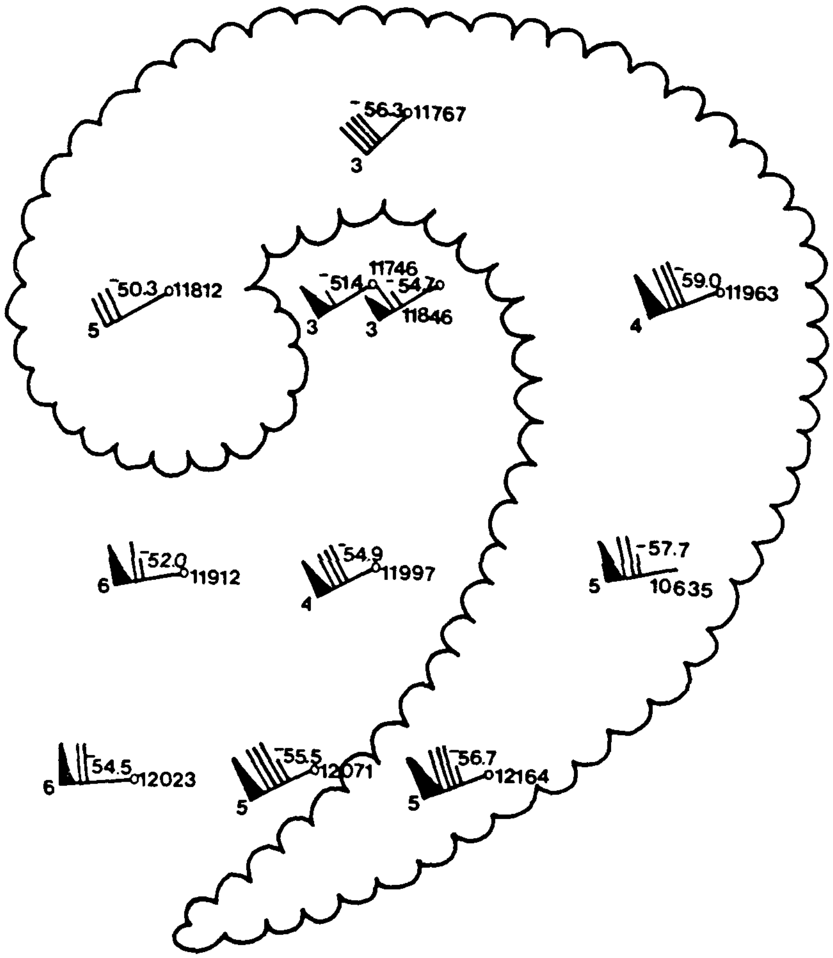

FIGURE 23: 200 mb analysis. Values to the left of the station symbol are temperature and dew point depression in °C. Value to the right is height of the surface in meters. Winds are in knots.

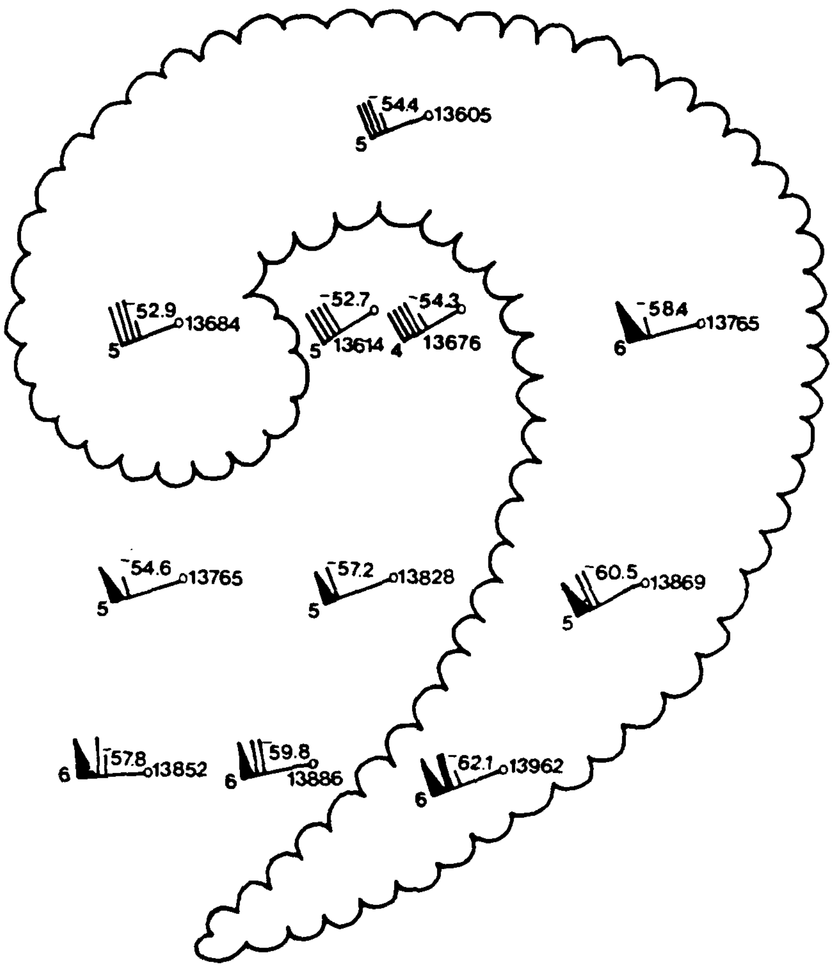

FIGURE 24: 150 mb analysis. Values to the left of the station symbol are temperature and dew point depression in °C. Value to the right is height of the surface in meters. Winds are in knots.

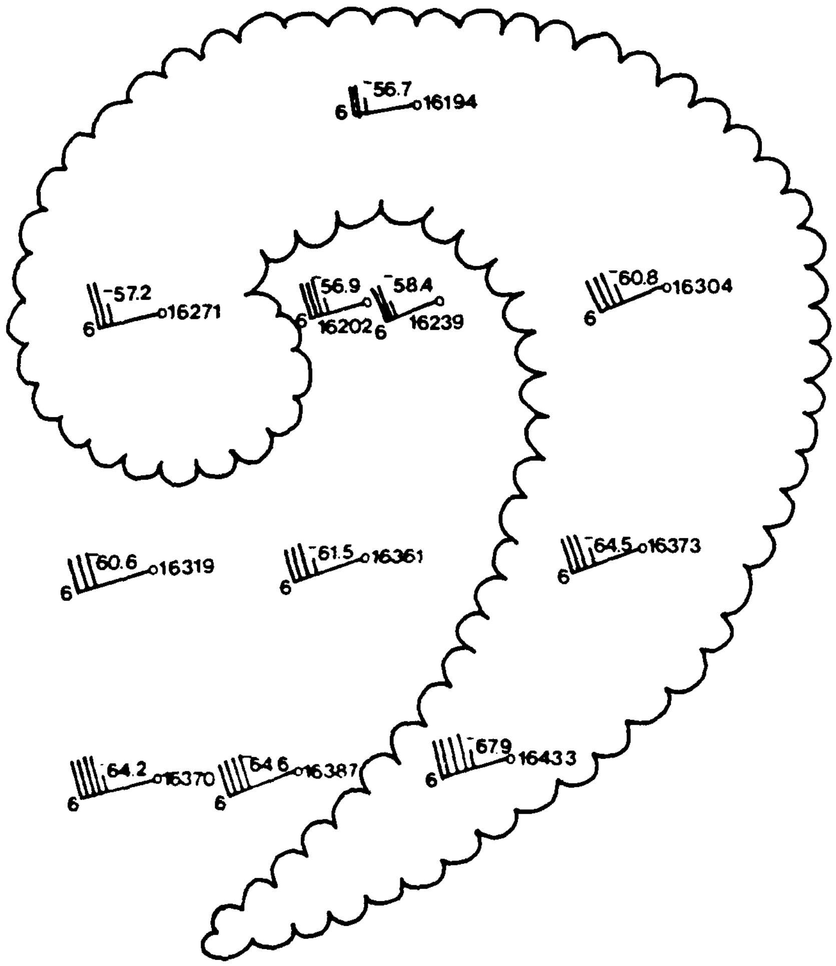

FIGURE 25: 100 mb analysis. Values to the left of the station symbol are temperature and dew point depression in °C. Value to the right is height of the surface in meters. Winds are in knots.

(1979) relates the horizontal wind shear produced by this speed maximum to the eastward progression of the cloud edge relative to the rest of the comma (i.e., the widening of the dry intrusion). The shape of the dry intrusion is related to the position and orientation of this speed maximum. Miller and McGinley (1978) have observed the position of the speed maximum to be related to where severe weather occurs along the comma tail.

Although difficult to resolve with so few zones, there is some evidence of split flow at 400 and 300 mb; flow in zones 1 and D being stronger than in zone C at these levels. Diffluence in the middle and upper level wind patterns is favorable for the development of severe storms. Miller (1972) found the region of diffluence to be most pronounced at the 200 mb level. Miller and McGinley (1978) also locate the axis of diffluence in this same portion of the comma cloud and show that most of the severe weather occurs within the region of diffluence between the polar and subtropical jets.

While all of the zones in the tail of the comma are warmer than those in the dry intrusion, this difference is not large. Temperature differences across the cloud edge are less than 3° C at 850, 700 and 500 mb. This difference is not much larger than the climatological difference which ordinarily exists between these zones (see section 2.5). There are large differences in moisture between the clear and cloudy zones, especially above 850 mb. There is also a

reversal in the pattern of warmest temperatures in the comma tail at about 250 mb indicating higher tropopause heights in this region compared to the dry air zones.

2.4 Isentropic Analyses

Green et al. (1966) discuss the advantages of analysis on isentropic surfaces. One advantage is that the large-scale vertical motion, as well as horizontal flow components, are shown. Carlson (1980) uses relative-flow isentropic analysis to model the air flow through a comma cloud. By subtracting out the translation speed of the system, winds relative to the moving cloud pattern are shown. Where condensation is widespread, trajectories are more likely to be along surfaces of constant wet-bulb potential temperature. Carlson uses Θ-surfaces to depict trajectories in the dry air and Θ_w- surfaces in the cloud region. This leads to large discontinuities at the cloud boundaries. In this study, analysis is performed over the entire system on constant dry-bulb potential temperature surfaces. In the composite mean, the comma cloud system is largely unsaturated so that the assumption that the airflow is adiabatic is reasonable. Saturated conditions are most likely in zones A and B, especially at low levels, as shown by the composite soundings. In any one storm, the motions represented in Figures 26-28. are least likely to occur in these zones; but, the underlying assumption that the air motions are adiabatic should

be valid over the remainder of the system. The resultant flow patterns do not differ from Carlson's model, even though θ rather than θ_w is used in the cloudy region.

Composite wind components were interpolated to produce a vector wind representative of the pressure level in each zone shown on each of the three analyses (Figs. 26-28). An average translation vector of 255° at 8.7 m/sec was then subtracted from each wind vector to show the air flow relative to the moving pattern. This estimate of the composite translation speed was obtained by averaging movements of closed low centers at three levels. Six-hourly positions of surface lows were obtained from the NOAA Daily Weather Map Series. 700 and 500 mb movements were obtained from successive NMC upper-air charts whenever these were available.

The relative-flow analyses presented here, unlike Carlson's model, provide a quantitative measure of wind speeds in the cyclone. This information is important because it defines regions of convergence and deformation. From time-lapse movies, Weldon (1979) observed that cloud motions within the dry air were slower than the eastward translation of the cloud boundary. He concluded that the distinct edge must therefore represent a zone of high-level convergence. The 317 K isentropic surface in Figure 28 shows that relative wind speeds in zones 3 and 5 are indeed faster than those in the cloudy zones to the east so that speed convergence must occur along the cloud edge. Widger et al. (1967)

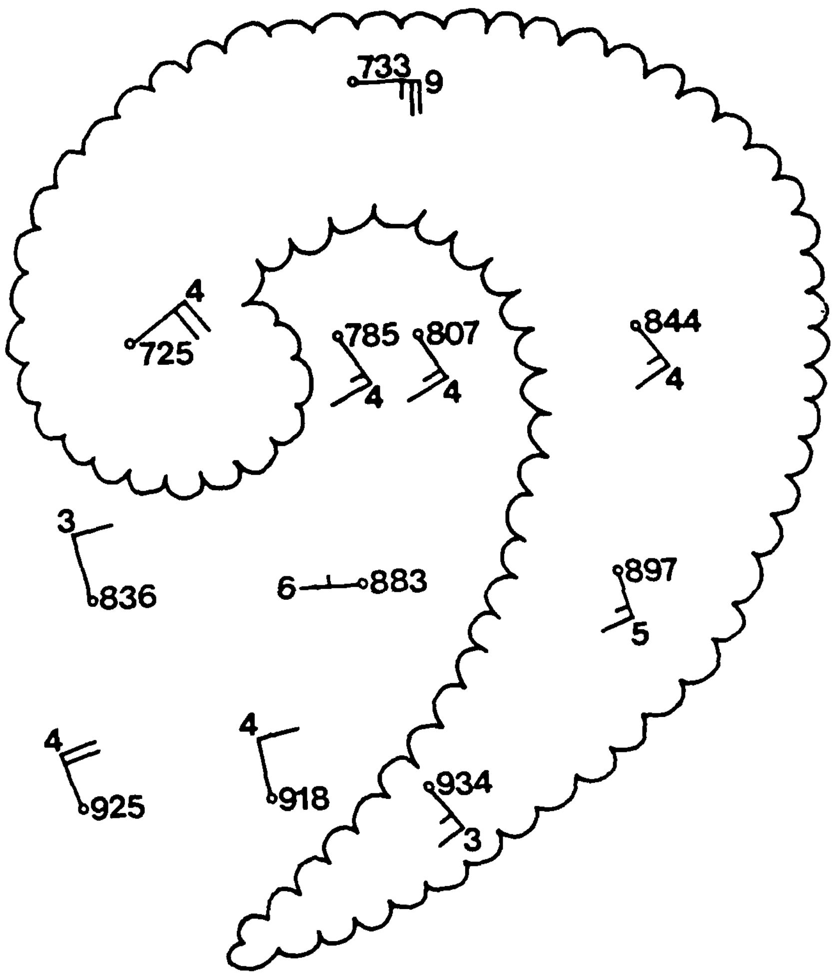

FIGURE 26: 297 K relative-wind isentropic surface. Value to the right of the station symbol is pressure, in millibars for this surface. Winds are in knots.

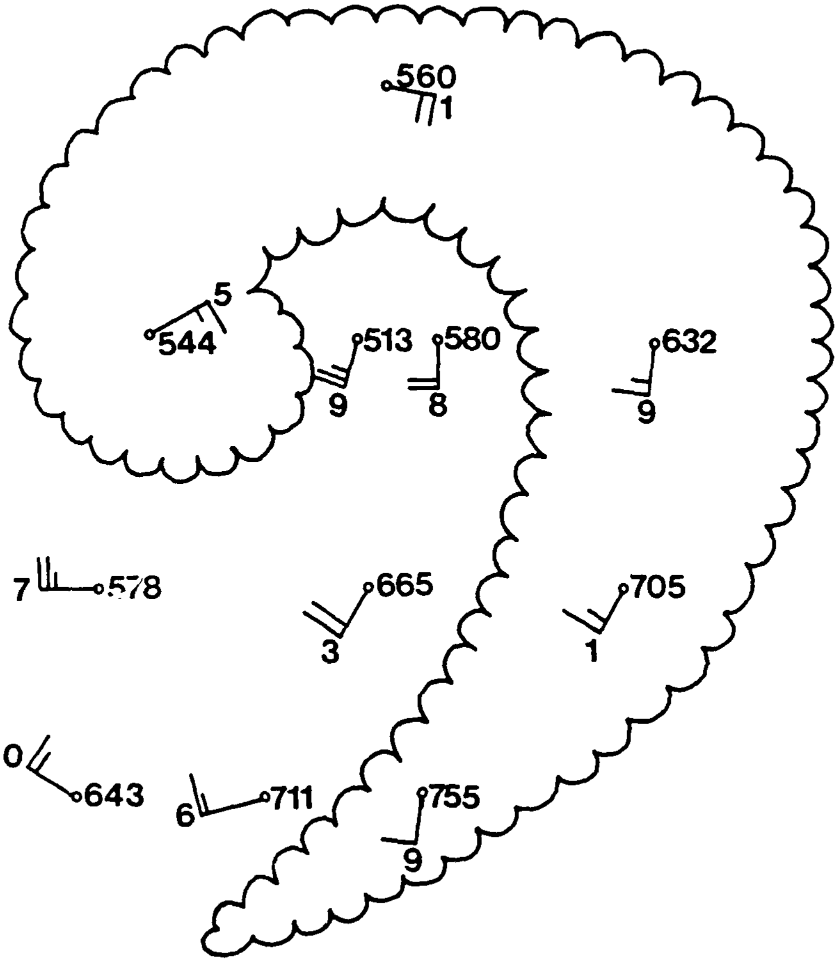

FIGURE 27: 307 K relative-wind isentropic surface. Value to the right of the station symbol is pressure, in millibars for this surface. Winds are in knots.

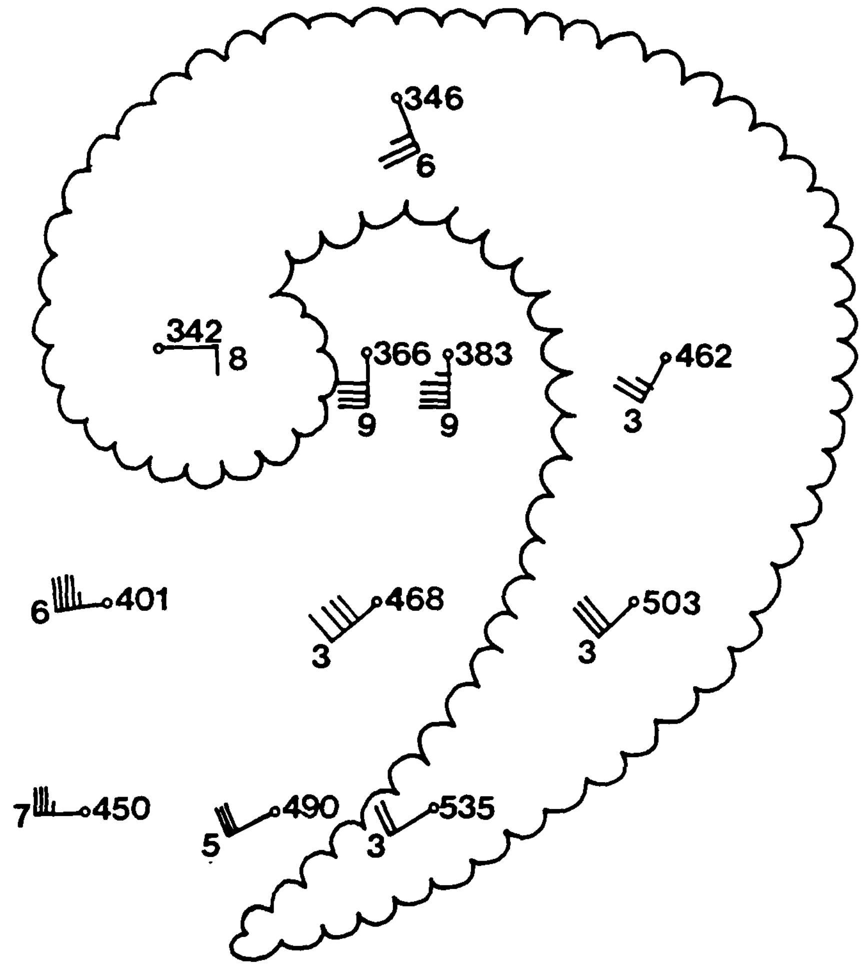

FIGURE 28: 317 K relative-wind isentropic surface. Value to the right of the station symbol is pressure, in millibars for this surface. Winds are in knots.

attributed the concave shape of the boundary to the fact that the air was undergoing the greatest descent and drying directly behind the middle portion of the cloud band. The 307 K isentropic analysis (Fig. 27) shows the air moving between zones 4 and 3 undergoes a mean descent of 87 mb, and that this subsidence is greater here than it is between zones 6 and 5 to the south. Nevertheless, the mere fact that the air is drier is probably too simple an argument. The concavity is more likely related to the stronger horizontal winds (Barr et al. 1966; Weldon, 1979) which are also in this region and the more rapid horizontal advection of the dry air eastward.

Another interesting aspect of the isentropic analyses is that all three surfaces show the subsidence region remains south of the comma head. Air moving north into zones 1 and 2 is ascending at all three levels. This would seem to confirm the findings of Leese (1962), and others, that the dry air advected northward and spiraling into the cyclone center is not subsiding, but remains dry and cloud-free. Carlson (1980, Fig. 10) also models rising motions within this portion of the dry intrusion. The relative winds in the dry air here are also much faster than the northward progression of the cloud boundary separating zones 1 and 2 from zone B. This portion of the cloud edge is also a region of speed convergence, relative to the moving cyclone, except that here the air is rising as it reaches the edge.

The 297 K isentropic surface (Fig. 26) shows relative flow which indicates deformation in the clear region behind the front, centered in zone 3. Weldon (1979, Fig. 45) also shows a deformation of the streamlines in this area. Deformation of winds at low levels is necessary for the maintenance of the strength of the cold front. This is because deformation acts to concentrate isotherms along the axis of dilatation, thus maintaining the strong thermal gradient (see Palmén and Newton, 1969; sect. 9.1).

2.5 Climatological Means

Climatological means for the 4-month period are obtained at 5° lat./long. grid points in the domain of the composite comma. Climatological data for the 1950-1964 period are taken from NCAR data tapes which have digitized the atlas of Crutcher and Meserve (1970). Values of temperature and dew point depression for 850 and 500 mb are then interpolated to the mean position of each zone. Differences between the composite and the climatological mean values are shown in Table 1.

At 850 mb, all zones except B are warmer than climatology, with the largest differences in the eastern half of the cloud pattern. The dew point depressions in the dry intrusion (zones 3-6) are 5-11° C drier than climatology. The comma cloud head is 1-2° C more moist than climatology. At 500 mb, all zones except C and D are colder than climatology,

with the largest differences in the western portion of the dry intrusion (zones 4 and 6). Dew point depressions in the dry zones are 11-14° C drier than climatology at that level.

TABLE 1

DEPARTURE FROM CLIMATOLOGICAL MEAN

	850 mb		500 mb	
Zone	T	(T-TD)	T	(T-TD)
1+2	+1.3	+1.0	-4.1	+11.4
3	+3.8	+5.1	-1.1	+10.7
4	+1.4	+7.9	-6.1	+13.6
5	+4.3	+11.3	-2.1	+12.4
6	+0.6	+10.8	-5.4	+14.4
A	+0.4	-1.8	-2.9	+0.5
B	-0.6	-1.5	-2.2	-3.5
C	+5.7	+1.5	+1.3	-0.2
D	+5.0	+1.3	0.0	-0.4
E	+4.0	+2.0	-1.5	+1.7

All values in degrees Celsius.

Positive differences mean temperatures are warmer than climatology and dew point depressions are drier than climatology.

2.6 Richardson Numbers

An investigation was made of the gradient Richardson number at different levels in each zone. In pressure coordinates,

$$\text{Ri (gradient Richardson number)} = -\frac{1}{\rho\Theta}\frac{\partial\Theta}{\partial p} \Big/ \left(\frac{\partial|\overline{V}|}{\partial p}\right)^2 \qquad (1)$$

where ρ = density,

p = pressure,

Θ = potential temperature, and

$|\overline{V}|$ = horizontal wind speed on a constant pressure surface.

Since the static stability parameter, $\sigma = -\frac{1}{\rho\Theta}\frac{\partial\Theta}{\partial p}$, equation (1) can be written as

$$\text{Ri} = \sigma \Big/ \left(\frac{\partial|\overline{V}|}{\partial p}\right)^2 \qquad (2)$$

Thus, the Richardson number is simply the ratio of static stability to the square of the vertical shear. The larger the vertical shear, the greater the likelihood of turbulent eddy formation; while the more stable the lapse rate, the more turbulence is suppressed (Hess, 1959; p. 290). Note that $\text{Ri} \rightarrow \infty$ as $\frac{\partial|\overline{V}|}{\partial p} \rightarrow 0$; i.e., in conditions of zero vertical shear. Thus the Richardson number will become large where the wind shear is small. It will also become large in regions where the static stability is high, such as within as inversion.

Composite averaging tends to smooth the vertical shear values of Ri so that this number will be much larger than it might ordinarily be for any individual sounding. As the values of Ri may range over as much as four or five orders

of magnitude, it is useful to look at the natural logarithm of Ri (ln Ri) when making comparisons. Bosart and Garcia (1974), in a study of clear-air turbulence accompanying the mid-tropospheric front, noted that the natural logarithm operator tends to smooth the differences between large numbers without distorting the small scale variations between small numbers. Mullen (1979) calculated the bulk Richardson number for a composite of 22 comma clouds associated with polar lows. McGinley and Sasaki (1975) calculated Richardson numbers for several dryline cases in order to study the role of symmetric instability on thunderstorm development. This will be discussed further in the next chapter.

To construct the profiles given in Figures 29 and 30, winds at significant levels were interpolated to the nearest 25 mb pressure level. Heights of the pressure surfaces were computed via the hypsometric equation:

$$Z_2 = Z_1 + \frac{R}{g}\int_{P_2}^{P_1} \overline{T}\ d\ \ln p$$

where $\overline{T} = [T(P_1) + T\ (P_2)]/2$ and the station elevation is taken to be the bottom boundary condition for Z_1. The value of Ri was calculated by taking 100 mb differences when calculating σ and $\frac{\partial|\overline{V}|}{\partial p}$ for levels at or above 800 mb, and 50 mb differences below that level. This was done to demonstrate the maximum in ln Ri which occurs in all of the zones between 800 and 900 mb. This maximum is a consequence of both the large static stabilities present within the low level inversion

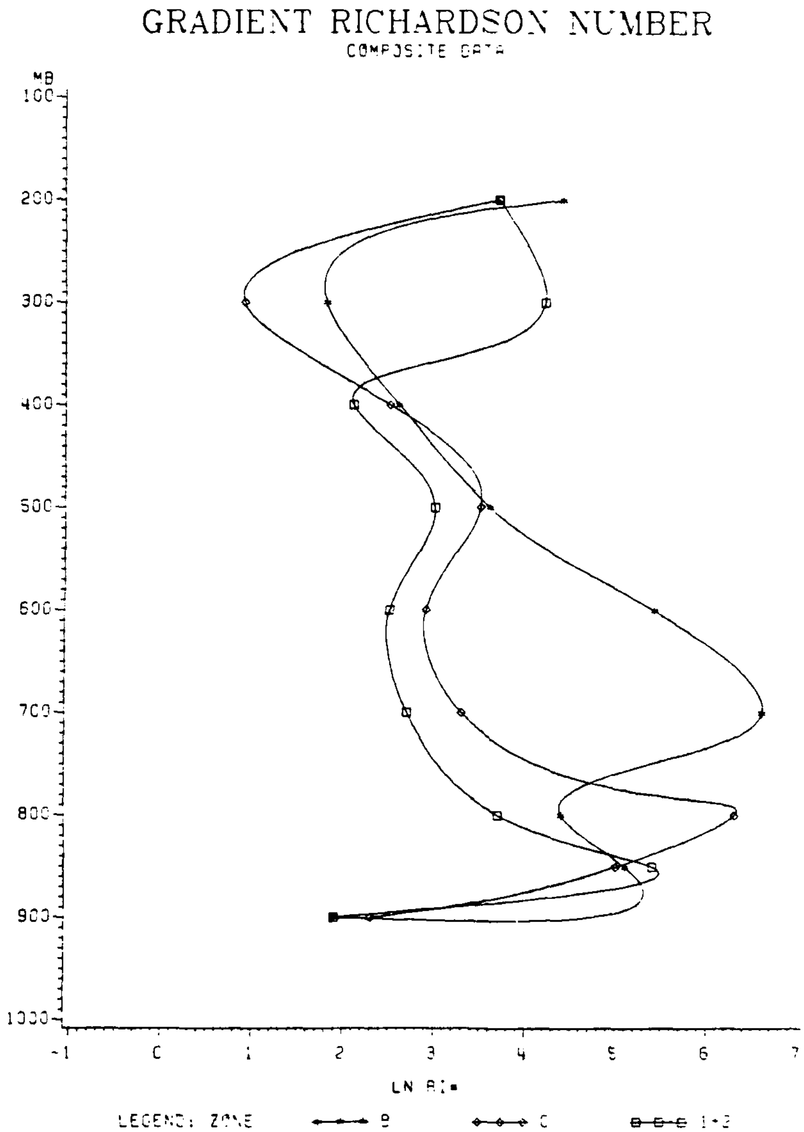

FIGURE 29: Natural logarithm of the gradient Richardson number versus pressure for zones 1+2, B and C.

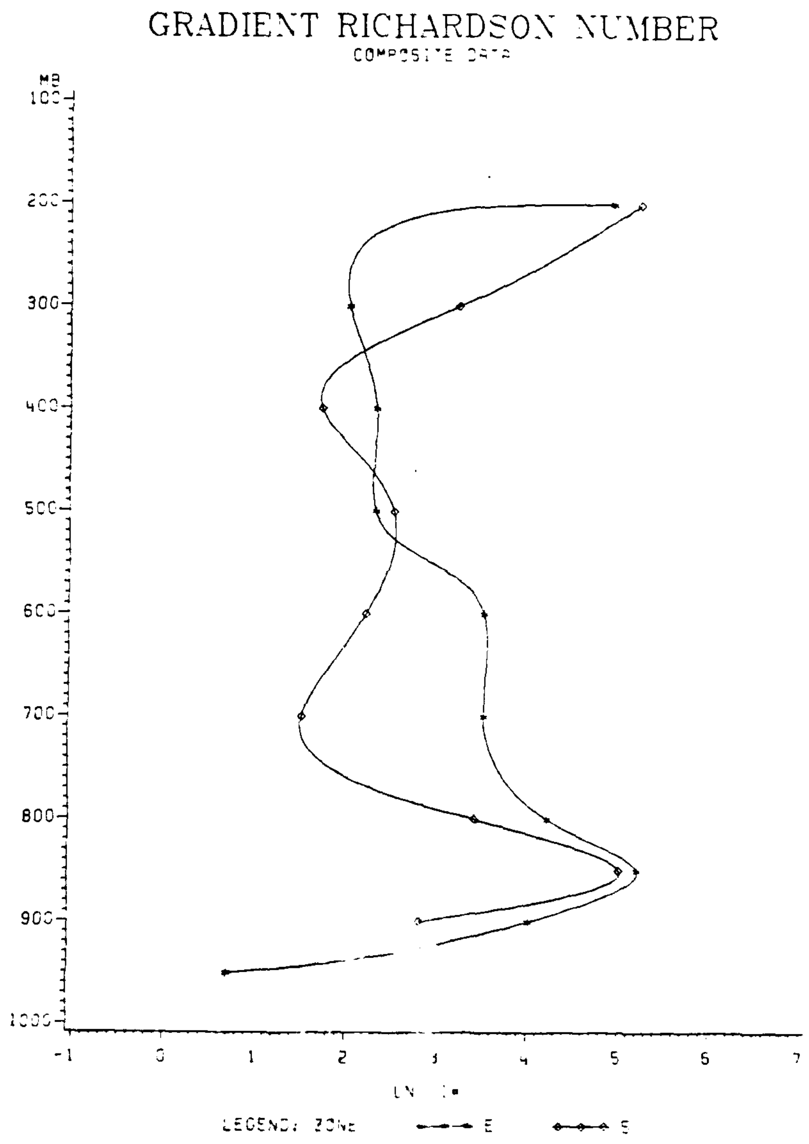

FIGURE 30: Natural logarithm of the gradient Richardson number versus pressure for zones 5 and E.

layer and the minimum in vertical shear at the top of the boundary layer. Figures 29 and 30 may be compared with profiles of static stability (Figs. 31 and 32) and with the wind speed profiles (Figs. 33 and 34).

Figure 29 shows differences between zones 1 and 2 (averaged together), zone B and zone C. Averaged over the depth of the troposphere, ln Ri is large in zone B because of both the low shear and high static stabilities. This zone is characteristically cold and moist over an appreciable depth. The profiles also show zones 1 and 2 have lower ln Ri values in the lower and middle troposphere than zone C does, even though zone C represents the warm, moist sector.

Figure 30 shows differences between zones 5 and E, across the southern end of the comma tail. Again, Richardson numbers are lowest in the boundary layer, increasing up to 850 mb where there is a relative maximum. With a composite Ri of about 2, it may be concluded that the Richardson number in zone E is often less than 1 near the surface. This is due, principally, to the very low static stabilities there. Averaged over the tropospheric column, however, the Richardson number is lower in zone 5 than in E.

In conclusion, the Richardson numbers are generally smaller in the clear zones and turbulent mixing is more likely over a larger depth. This is true because of both the larger vertical wind shear and lower static stability values in the dry air. Values of Ri in the boundary layer are small

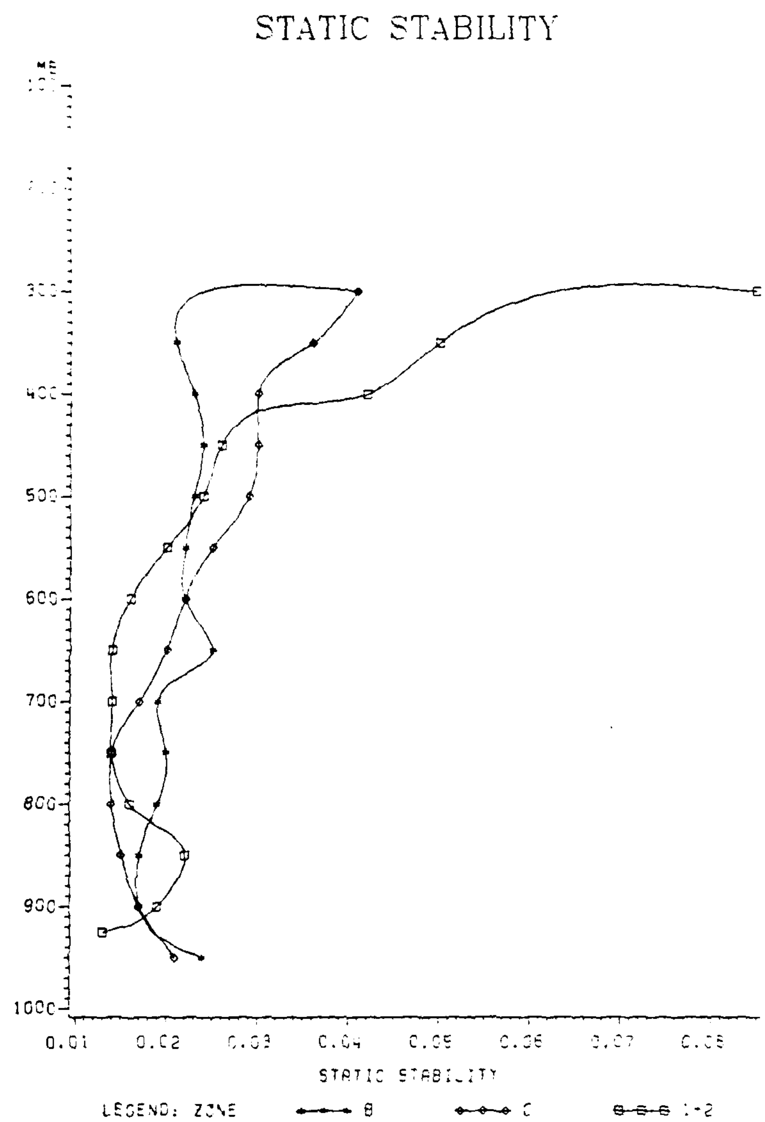

FIGURE 31: Static stability profiles for zones 1+2, B and C. Units are $m^2 sec/mb^2$.

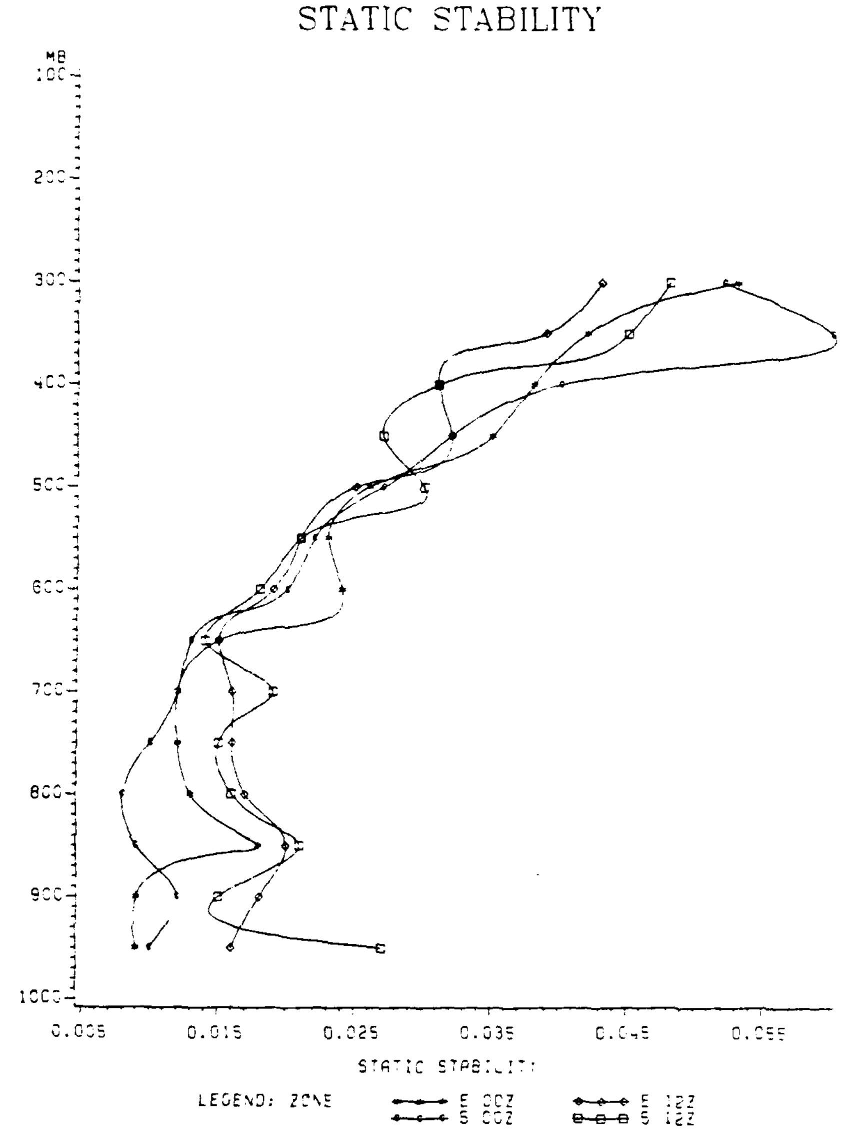

FIGURE 32: Static stability profiles for zones 5 and E at 0000 and 1200 GMT. Units are m^2 sec/mb^2.

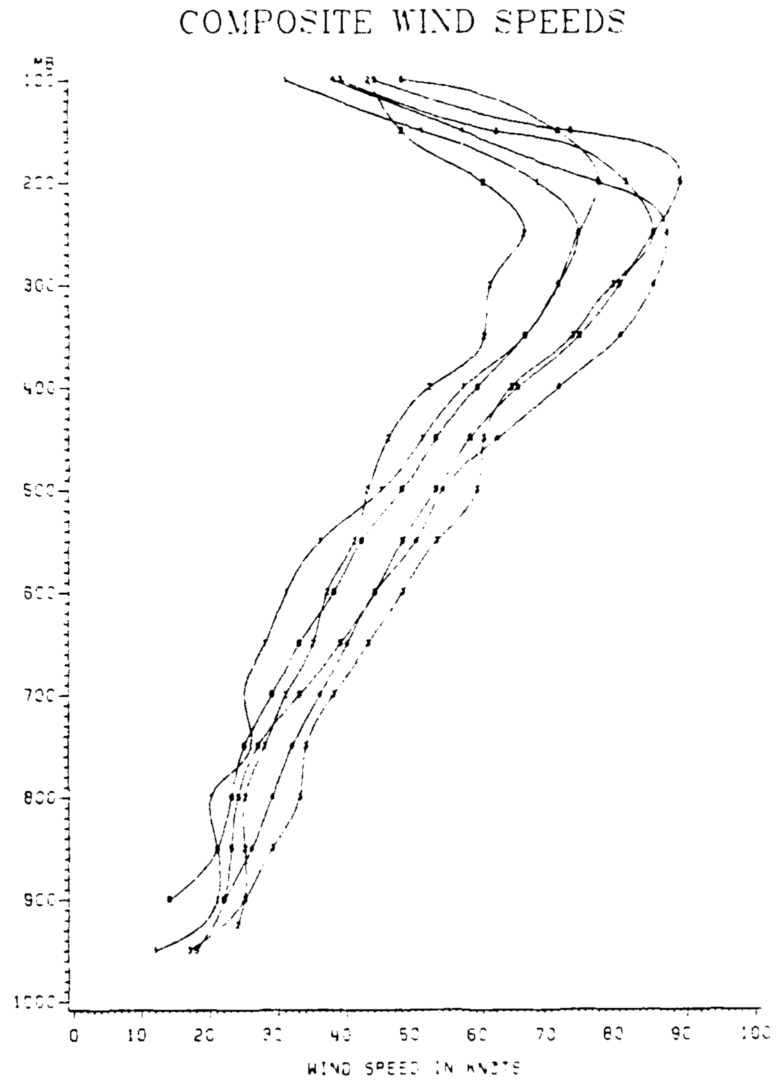

FIGURE 33: Composite wind speeds, in knots, for zones 1-6.

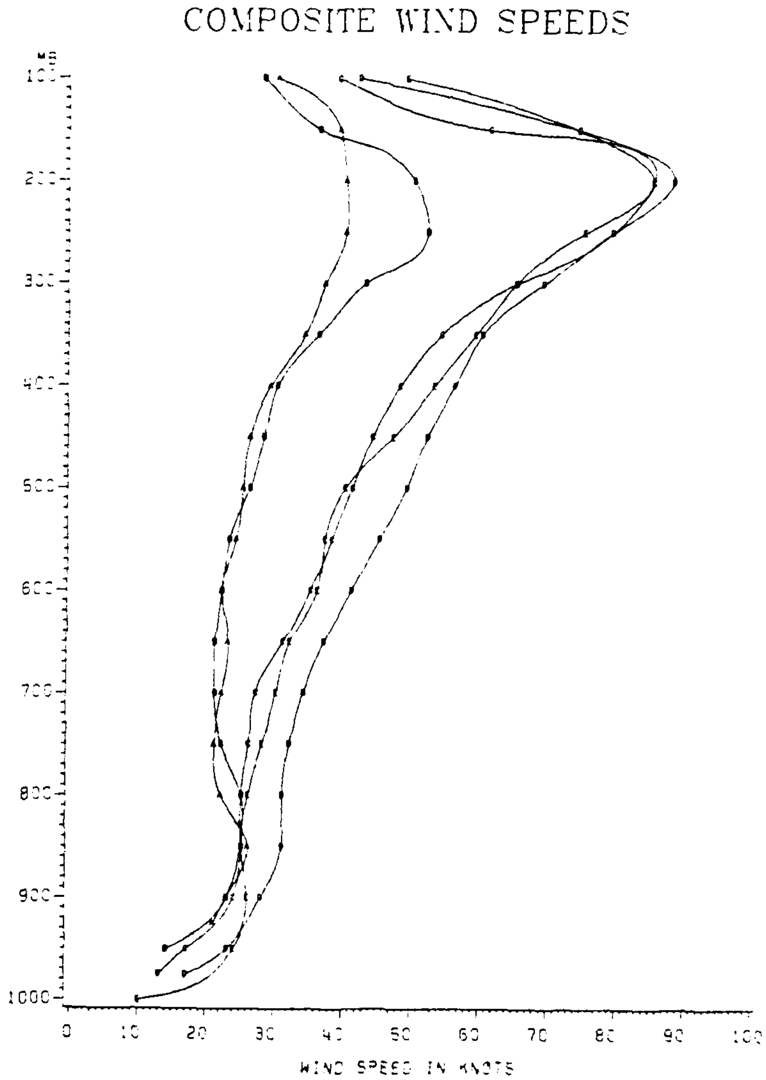

FIGURE 34: Composite wind speeds, in knots, for zones A-E.

due to large shear, but increase rapidly as the shear decreases and stability increases in the presence of a low-level inversion. Above this level, the shear again increases so that the Richardson number usually decreases. At the level of maximum winds, the shear decreases again and the Richardson number increases. Usually, static stabilities above the tropopause are so large as to overwhelm any increases in the magnitude of the wind shear. Thus the value of Ri remains high throughout the stratosphere.

2.7 Severe Weather Activity

Table 2 gives the number of severe weather events for the two 4-month periods, by zone, for all comma clouds included in the composite. Severe weather is defined here as tornados, funnel clouds, hail $\geq$ 19 mm. and winds $\geq$ 26 m/sec. Reports of severe weather were taken from NOAA Storm Data and compared with the satellite picture taken closest to the time of occurrence in order to determine which zone the event occurred in. Eighty percent of all severe events were reported in zones C-E. Severe weather in zone A was generally along the eastern edge of the comma head, and most of the reports were of hail or "cold air funnels." Within the dry intrusion, the most frequent reports were of large hail. The wet-bulb zero (WBZ) height is 1600 meters which is at the lower limit of the range given by Miller (1972) for the occurrence of hail.

TABLE 2

NUMBER OF SEVERE WEATHER EVENTS OCCURRING IN EACH ZONE

FOR CASES INCLUDED IN THE COMPOSITE

Zone	Hail	Funnels	Tornados	Winds	% by zone
A	19	10	15	9	9
B	2	1	3	2	1
C	47	11	32	47	23
D	70	26	73	49	37
E	52	27	24	13	20
1	22	5	6	3	6
2	1	2	0	3	1
3	7	2	1	1	2
Events	220	84	154	127	585

Miller's (1972) severe thunderstorm criteria are not normally met in zone A, although severe weather is often present there. Miller and McGinley (1978) found that the winds usually back with height and surface dew points are marginal in this area. The zone A composite sounding (Fig. 8) confirms these findings. However, this is also the region of coldest air aloft. As this colder air moves over zone 2, where surface temperatures are usually warmer and where low-level moisture remains plentiful, the potential instability increases. Thunderstorm activity then develops in the afternoon along the eastern edge of the comma head as surface temperatures increase and the potential instability is released. If cyclonic vorticity advection in this area is strong as well, a small comma cloud may form with thunderstorms developing along its tail. This is in the region south of the upper level low center and well behind the principal cold front.

Most of the severe weather occurs in zones C-E. The strongest thunderstorm activity in the northern portion is along the back edge of the comma tail, with the cold front. Further south, the region of severe activity moves out ahead of the cold front and is embedded in the middle or eastern half of the cloud band. Severe thunderstorms also frequently develop in zone C.

The definition of the Severe Weather Threat (SWEAT) index is given in Miller (1972) as:

$$I = 12D + 20(T-49) + 2f8 + f5 + 125(S + .2)$$

where D = 850 mb dew point in °C,

T = "Total Totals" index,

$f8$ = speed of the 850 mb wind in knots,

$f5$ = speed of the 500 mb wind in knots, and

S = sin (500 mb - 850 mb wind direction).

The index is useful because it measures a combination of factors which have been shown to be related to severe weather. The first term on the right hand side is a measure of the low-level moisture present. The second term is a measure of the atmospheric stability. The third and fourth terms are environmental wind speeds, and the last term is a measure of the vertical shear.

Values from the 0000 and 1200 GMT composites are used to compute the SWEAT indices for each zone. These are shown in Table 4. The contribution of each term in determining the SWEAT values is also shown. The highest SWEAT index values are located in the comma tail (zones C, D and E) at both time periods. This corresponds to the 80% of all severe weather events occurring in these zones (Table 3). Note that, in the morning, the largest contribution to the SWEAT value in these zones is the presence of strong winds at both 850 mb and 500 mb. By afternoon, however, the contributions of shear and low-level moisture have become just as large. Miller gives 300 as a threshold value for severe thunderstorms. None of the indices, computed from composite data, are as

TABLE 3

SEVERE WEATHER THREAT (SWEAT) INDEX

SWEAT INDEX VALUES 12Z SOUNDINGS

	1	2	3	4	5	6	A	B	C	D	E
500 mb T	-17.0	-20.6	-15.5	-18.6	-14.1	-16.0	-20.5	-18.9	-15.8	-13.7	-12.5
850 mb T	6.6	6.9	10.4	7.7	12.2	9.5	4.2	3.8	9.0	12.3	13.8
850 mb TD	2.7	0.3	-0.8	-2.8	-3.6	-6.4	0.9	-0.2	1.7	4.4	6.3
850 mb V	2318	2212	2626	2924	2820	3217	3514	1116	2118	2228	2425
500 mb V	2244	2237	2455	2647	2547	2743	3207	1914	2339	2446	2534
Total Totals	43.3	48.4	40.6	42.1	36.8	35.1	46.1	41.4	42.3	41.1	45.1
SWEAT INDEX	112	92	107	95	87	77	46	46	169	210	202
Shear part	-	27	-	-	-	-	-	-	74	55	42
Dynamic part	80	61	107	95	87	77	35	46	75	102	84
Low-level moisture part	32	4	-	-	-	-	11	-	20	53	76
Stability part	-	-	-	-	-	-	-	-	-	-	-

SWEAT INDEX VALUES 00Z SOUNDINGS

	1	2	3	4	5	6	A	B	C	D	E
500 mb T	-18.7	-21.1	-13.7	-18.2	-13.0	-14.6	-18.2	-18.6	-14.2	-12.1	-10.9
850 mb T	8.6	8.0	13.4	12.4	16.7	15.7	5.5	3.9	11.6	13.5	16.4
850 mb TD	-0.9	1.4	3.1	-5.7	-3.1	-3.6	2.6	1.4	6.4	7.9	7.2
850 mb V	1717	1720	2419	2820	2617	2917	0112	0920	1920	2025	2220
500 mb V	2139	2138	2453	2647	2550	2746	2804	1719	2338	2445	2441
Total Totals	45.1	51.6	43.9	43.1	39.6	41.3	44.5	42.5	46.4	45.6	45.4
SWEAT INDEX	73	266	128	87	84	80	59	76	264	287	245
Shear part	-	119	-	-	-	-	-	-	109	97	78
Dynamic part	73	78	91	87	84	80	28	59	78	95	81
Low-level moisture part	-	17	37	-	-	-	31	17	77	95	86
Stability part	-	52	-	-	-	-	-	-	-	-	-

large as this, but the value of 287 for the afternoon sounding in zone D indicates this threshold must often be exceeded in individual cases. The value in zone 2 could be artificially large because of the small sample (only six soundings at 0000).

2.8 Other Composites

Certain subsets of all the comma cloud cases were composited in order to examine seasonal and diurnal differences. Cases were composited by month and also by sounding time. Some of the more important diurnal differences have been discussed previously. Late spring (May, June) cyclones were centered further north and were smaller in size. This reflects the northward shift of the polar jet. The critical wavelength for baroclinic instability is inversely related to the Coriolis parameter (Holton, 1979; p. 220). Therefore, the fact that smaller disturbances are observed in May and June is also related to their formation at higher latitudes. Temperature gradients were weaker and winds lighter at all levels. The circulations also tended to be shallower in later months.

Ten of the most visually impressive cloud patterns were composited to ascertain what kinematic or thermodynamic differences might account for the more distinctive comma patterns and sharper cloud boundaries. All ten cyclones were in the well-occluded stage and had very little tilt

with height. Temperature gradients and wind speeds were stronger at all levels in comparison to the 4-month mean composite quantities.

CHAPTER III

CASE STUDY: 21-22 MARCH 1981

3.1 Background

A vivid example of the rapid growth of thunderstorms within the dry intrusion occurred on the afternoon of March 21, 1981. Further investigation of this case was motivated by the inability to explain why deep convection should occur within the so-called "dry" region. A survey of the satellite data for comma cloud cases in 1980 and 1981 showed that this phenomenon occurred on other occasions, but never so centered in the middle of the dry intrusion as in this case. Danielsen (1974) studied a similar situation and attributed the presence of clouds in the dry air to vertical mixing induced by strong surface heating and shearing instability aloft. In the present case there are several other conditions present which favor the onset of these thunderstorms.

Cyclogenesis in the lee of the Rocky Mountains began March 20th, accompanied by the eastward progression of an upper level trough. By 1200 GMT on the 21st, the surface low had begun to move out of Colorado with a cold front

trailing south across western Texas. Figure 35 shows the 1000 and 500 mb heights for 1200 GMT. The system is only slightly tilted to the west with height. A jet lies upstream from the trough axis with 64 m/sec winds at 300 mb reported at both Oakland, California and Tuscon, Arizona. At this time, there is also very cold air (-27° C) upstream from the trough at 500 mb (Fig. 36).

Satellite photographs show an increased organization of the cloud pattern on the morning of the 21st. There is a northward penetration of the dry slot and a rapid decrease in cloud material behind the frontal cloud band as subsidence increases. The 1902 GMT photograph (Fig. 37) shows the dry intrusion wrapped almost once around the low center. A sharply defined cloud edge along the Oklahoma-Arkansas border marks the separation of dry and moist air at upper levels. Cumulus clouds in eastern Oklahoma reveal the presence of low-level moist air. The western edge of these clouds coincides with the surface position of a dryline. A large area of dust can be seen throughout western and north central Texas. As late as 2000 GMT, IR imagery (Fig. 38) shows no deep convection has as yet formed. Two hours later (Fig. 39), a line of thunderstorms developed very near the surface dryline. New cells then continued to form further south along this boundary as the whole line moved east (Fig. 40). Three-quarter inch hail was reported in eastern Arkansas with this line of thunderstorms at about 0130 GMT. The 0000 GMT plots

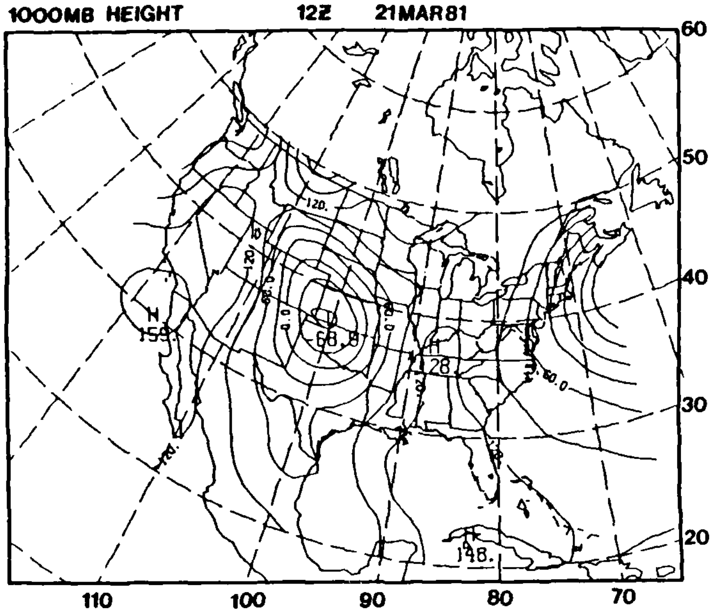

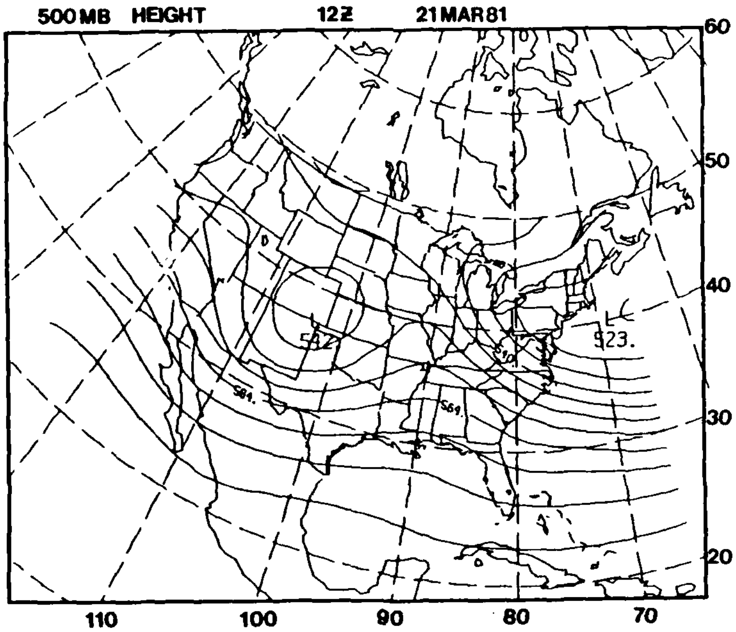

FIGURE 35: 1000 and 500 mb height fields for 1200 GMT March 21, 1981. Values of the 1000 mb surface are in meters; values of the 500 mb surface are in decameters.

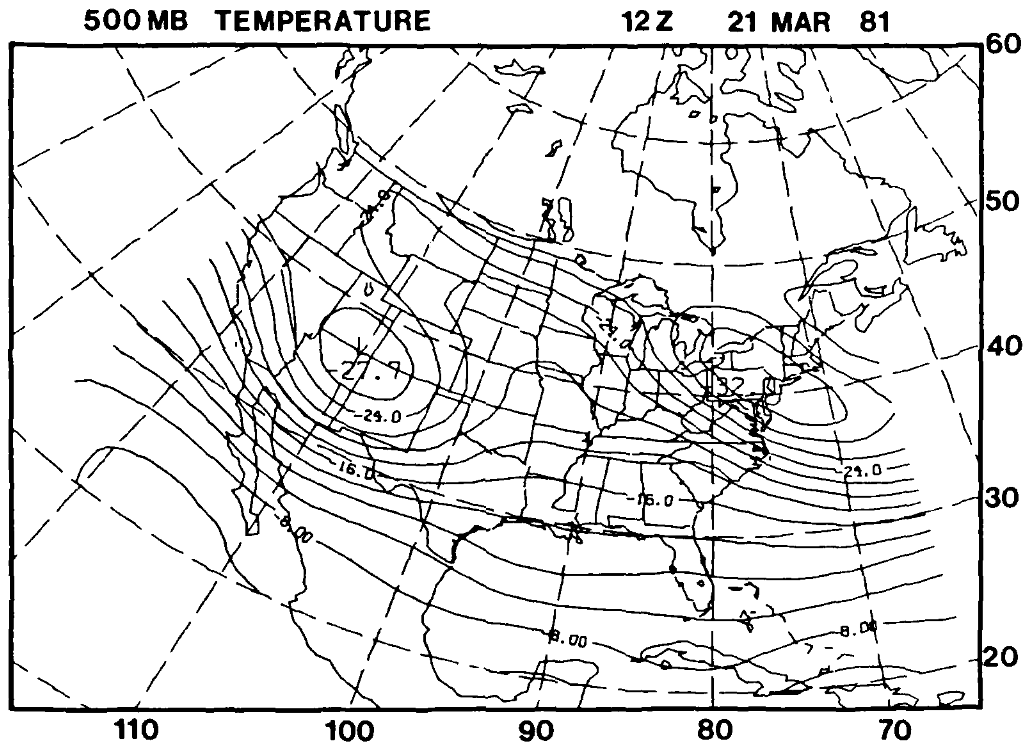

FIGURE 36: 500 mb temperature field for 1200 GMT March 21, 1981. Temperatures are in degrees Celsius.

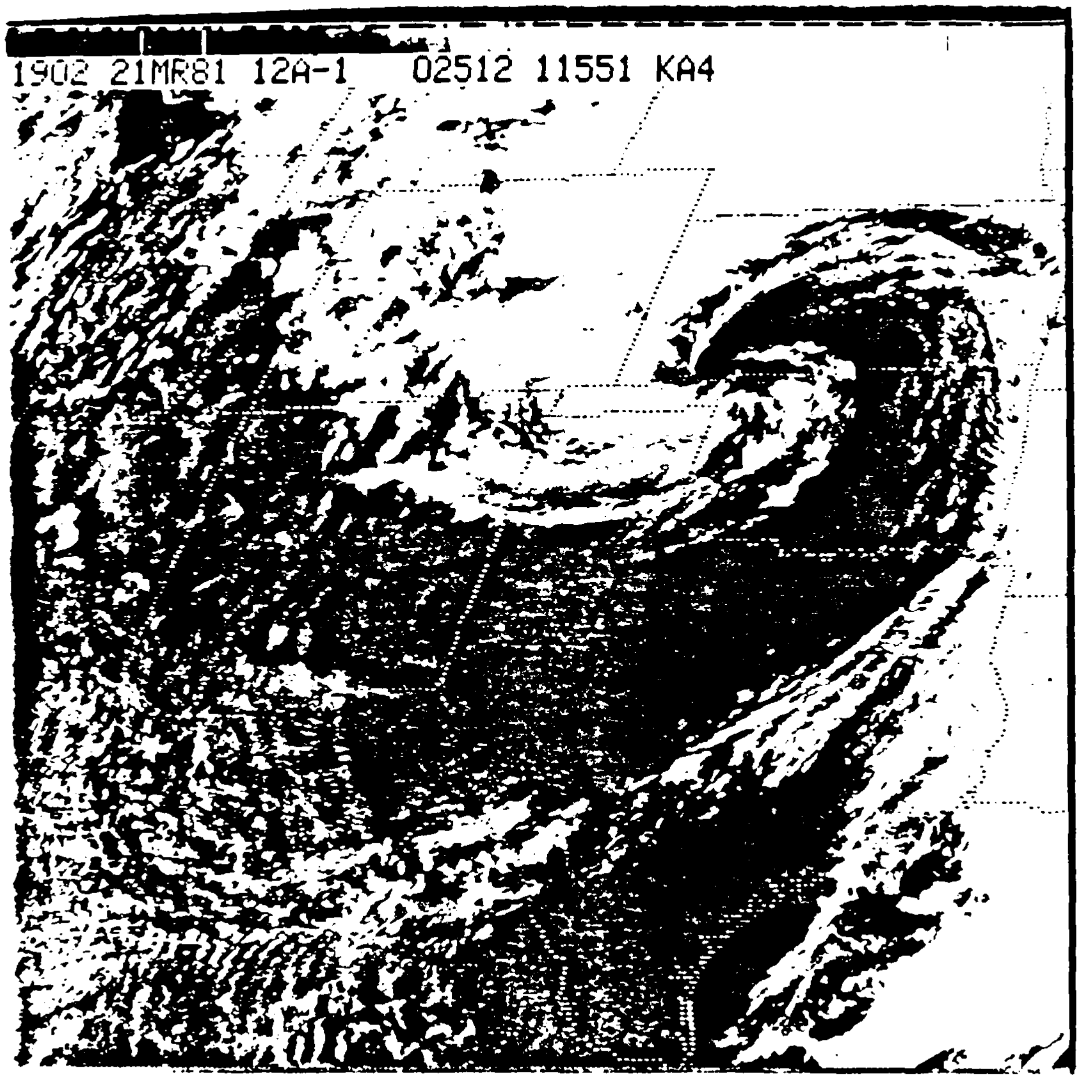

FIGURE 37: 1902 GMT March 21, 1981 GOES-East visible imagery.

FIGURE 38: 2000 GMT March 21, 1981 GOES-East infrared imagery.

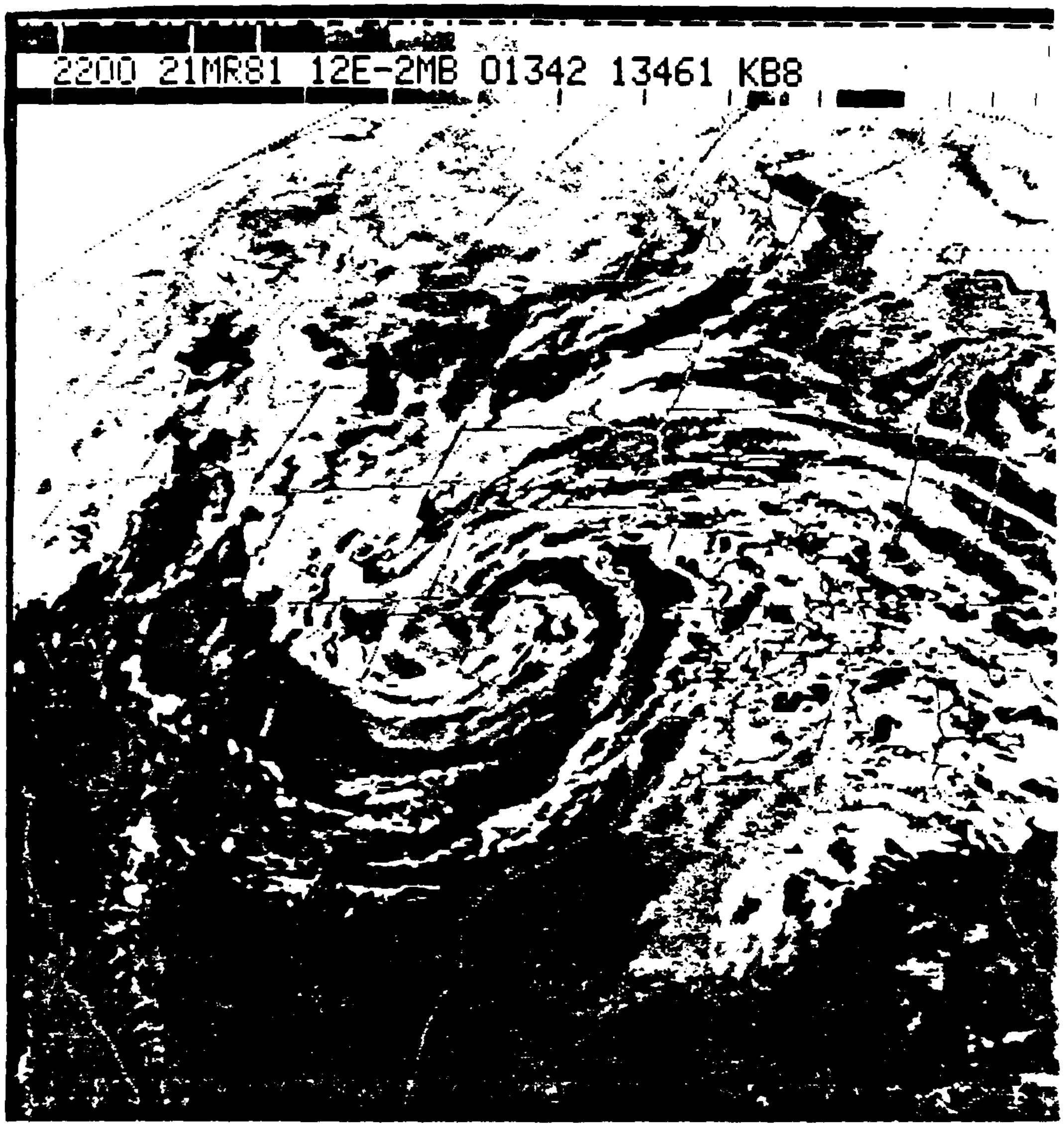

FIGURE 39: 2200 GMT March 21, 1981 GOES-East infrared imagery.

FIGURE 40: 2330 GMT March 21, 1981 GOES-East visible imagery.

of 1000 and 500 mb heights (Fig. 41) show the system has become vertically aligned and the low has started to fill while moving to the southeast. The cold air at 500 mb has moved rapidly to the east, with the coldest temperatures now located in the base of the trough over central Texas (Fig. 42).

3.2 Surface Analysis

With the initiation of thunderstorm growth between 2000 and 2200 GMT, it is instructive to examine the 2100 GMT surface map. Unfortunately, the NMC surface chart (Fig. 43) has some obvious analysis errors. The well-marked dryline is shown as an occluded front in eastern Oklahoma and as a cold front in eastern Texas. However, temperatures to the west are 6-7° C warmer than to the east of this line. Dew points are 10-11° C lower behind the dryline. A re-analysis is presented in Figure 44. Earlier maps show a cold front in western Texas. Continuity suggests that the dryline at 2100 GMT is all that remains of this earlier front. With clear skies behind the front, radiational warming of air near the ground has destroyed the surface characteristics of this cold front. However, there is still strong cold air advection aloft, as indicated by the 500 mb temperature maps. The pressure trough in western Texas has been re-analyzed as a cold front. Temperature differences of up

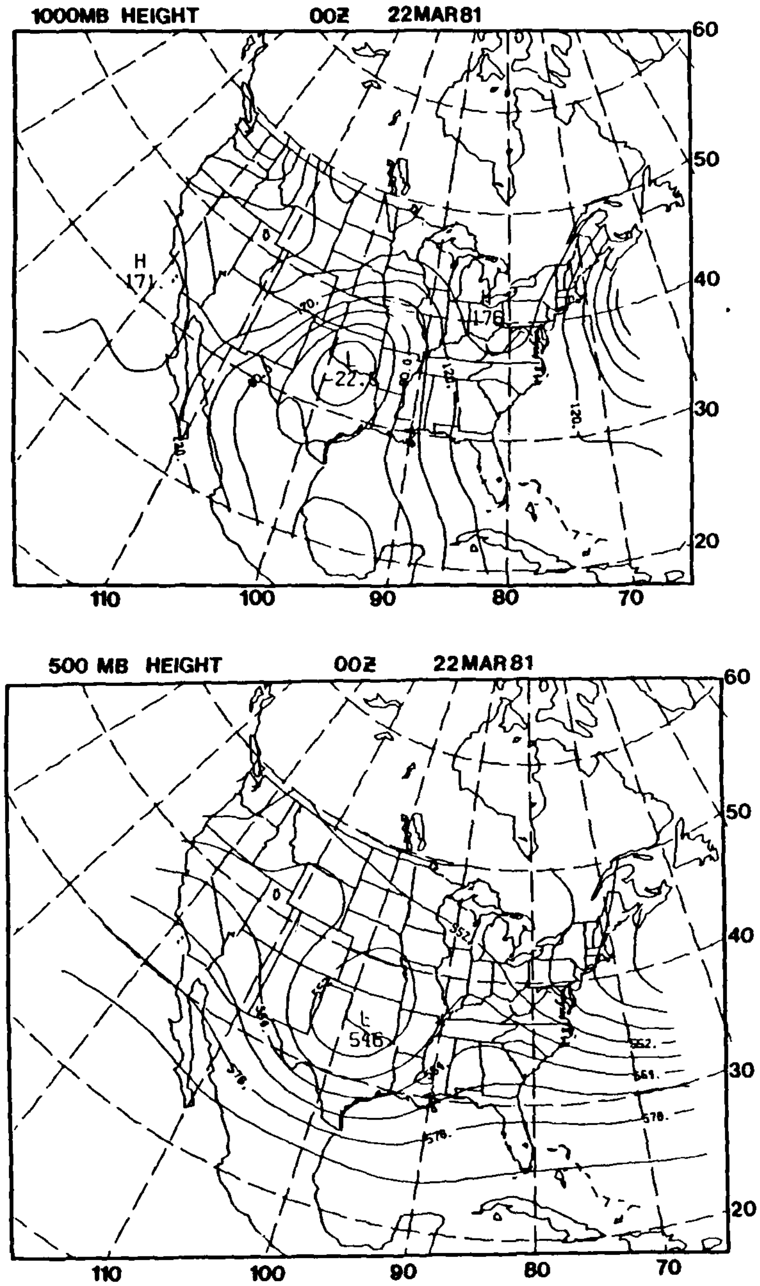

FIGURE 41: 1000 and 500 mb height fields for 0000 GMT March 22, 1981. Values of the 1000 mb surface are in meters; values of the 500 mb surface are in decameters.

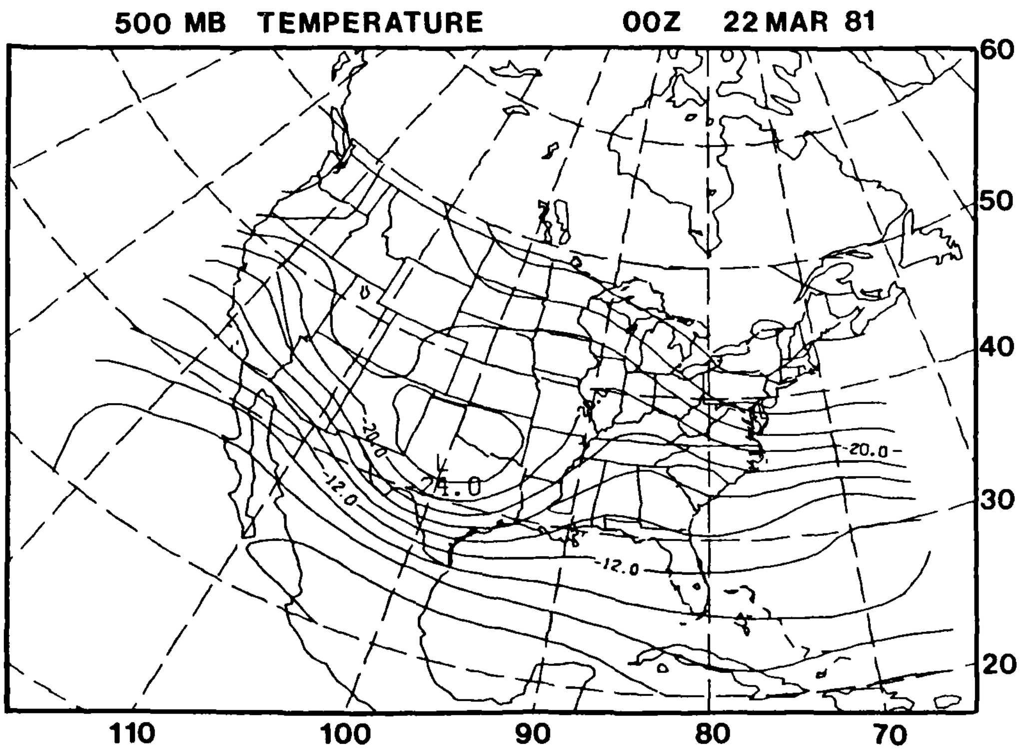

FIGURE 42: 500 mb temperature field for 0000 GMT March 22, 1981. Temperatures are in degrees Celsius.

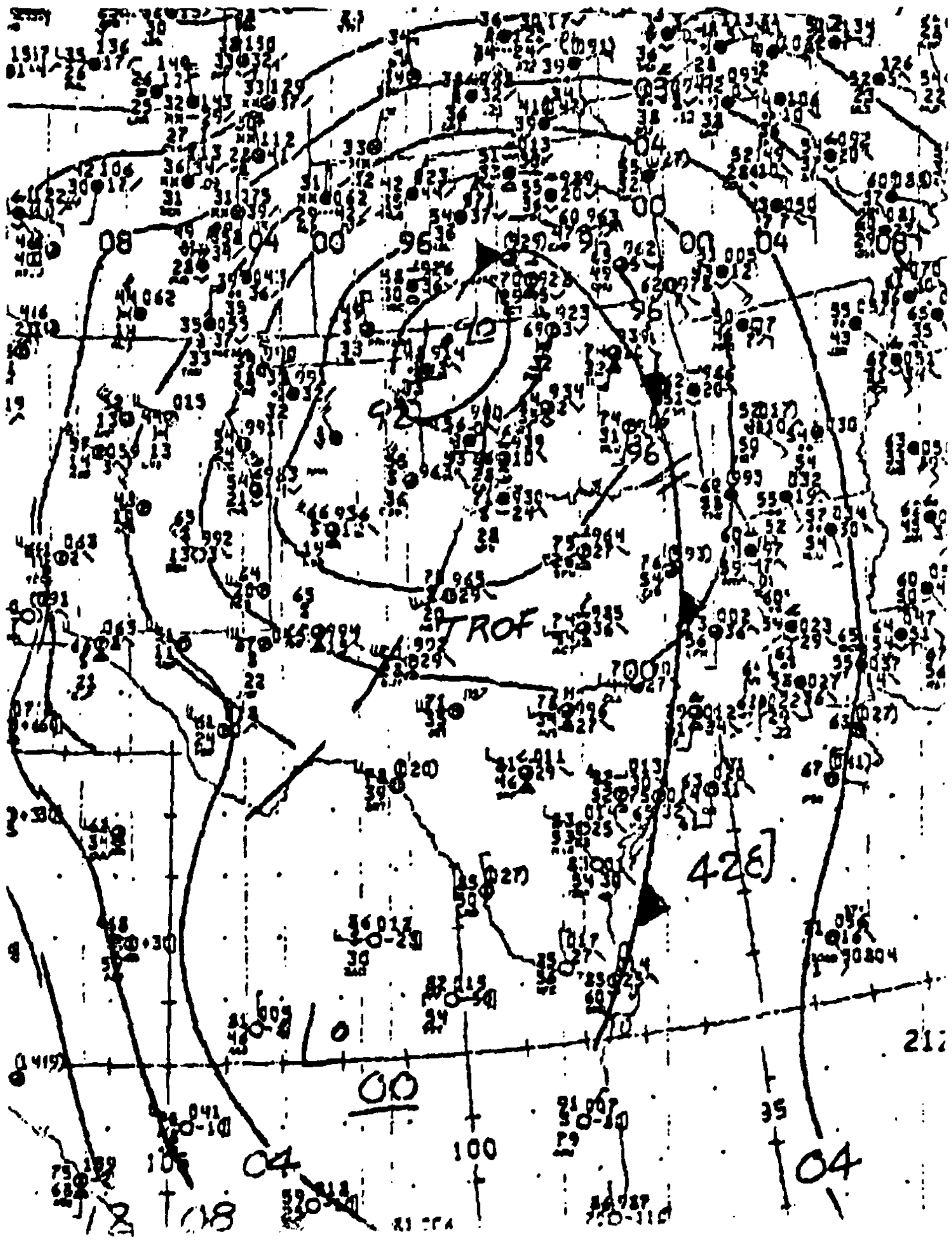

FIGURE 43: NMC surface analysis for 2100 GMT March, 21 1981.

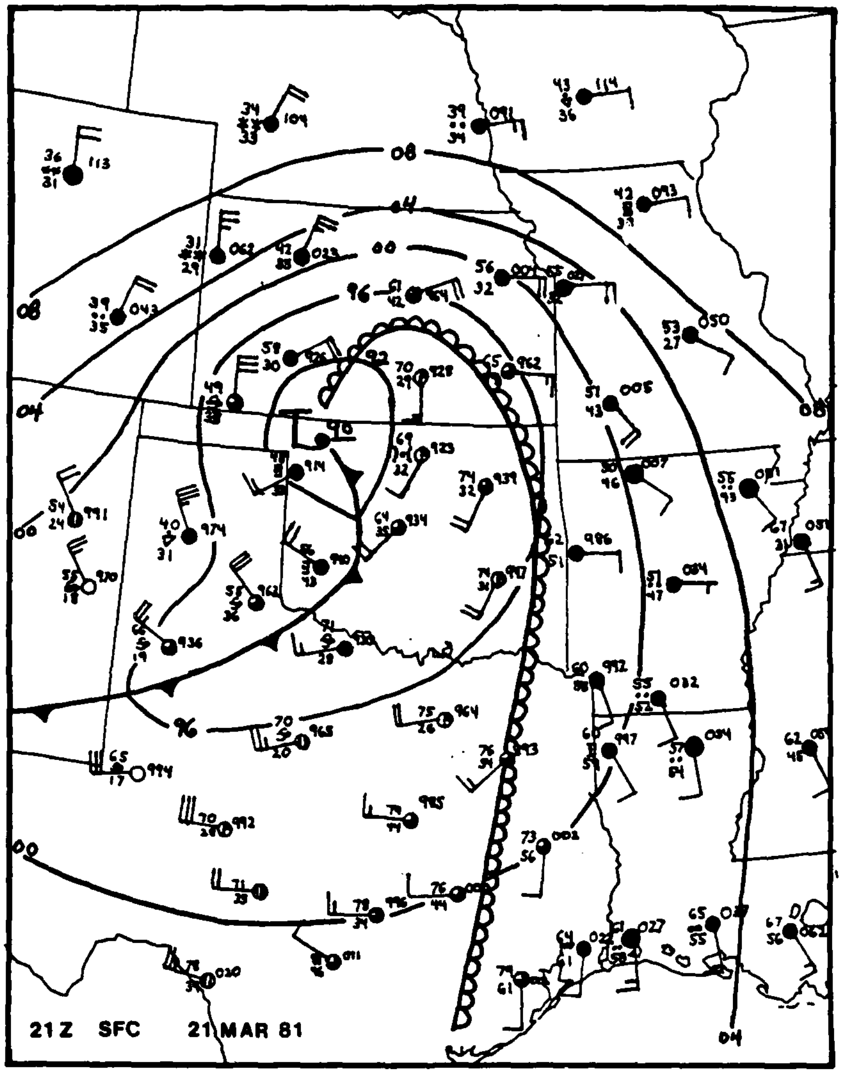

FIGURE 44: Re-analysis of the surface data for 2100 GMT March 21, 1981.

indicates position of surface dryline.

indicates position of surface cold front.

to 12° C exists across the northern portion of this front. Satellite pictures indicate this front coincides with the southern edge of a new comma cloud (cf. Figs. 40 and 44).

3.3 Temperature and Moisture Profiles

Soundings (Figs. 45-47) taken at 0000 GMT at Oklahoma City, Monett and Little Rock correspond to zones A, 1 and C, respectively. Taken within the dry intrusion, the Monett sounding shows the air to be much drier in the layer between 820 and 400 mb than at either Oklahoma City or Little Rock. But, as previously seen in the composite study, the air below 850 mb is still very moist. Warm advection in the surface to 500 mb layer is indicated by the veering wind profiles at both Monett and Little Rock. West of Monett, the low level inversion has been eliminated by radiational warming in the cloud-free skies. Skies were still overcast at Monett until late in the afternoon, however, and there is still a significant low level inversion present between 900 and 790 mb. Consequently, the 0000 GMT Lifted Index is +2.

Monett lies east of the surface dryline at 0000 GMT and there is no sounding available from behind the dry line this far north. Thus it is impossible to get a truly representative cross-section across the dryline in the region where the rapid growth of thunderstorms occurred. One means of examining the changes which occur across the dryline is illustrated in Figure 48. The 1200 GMT temperature profile

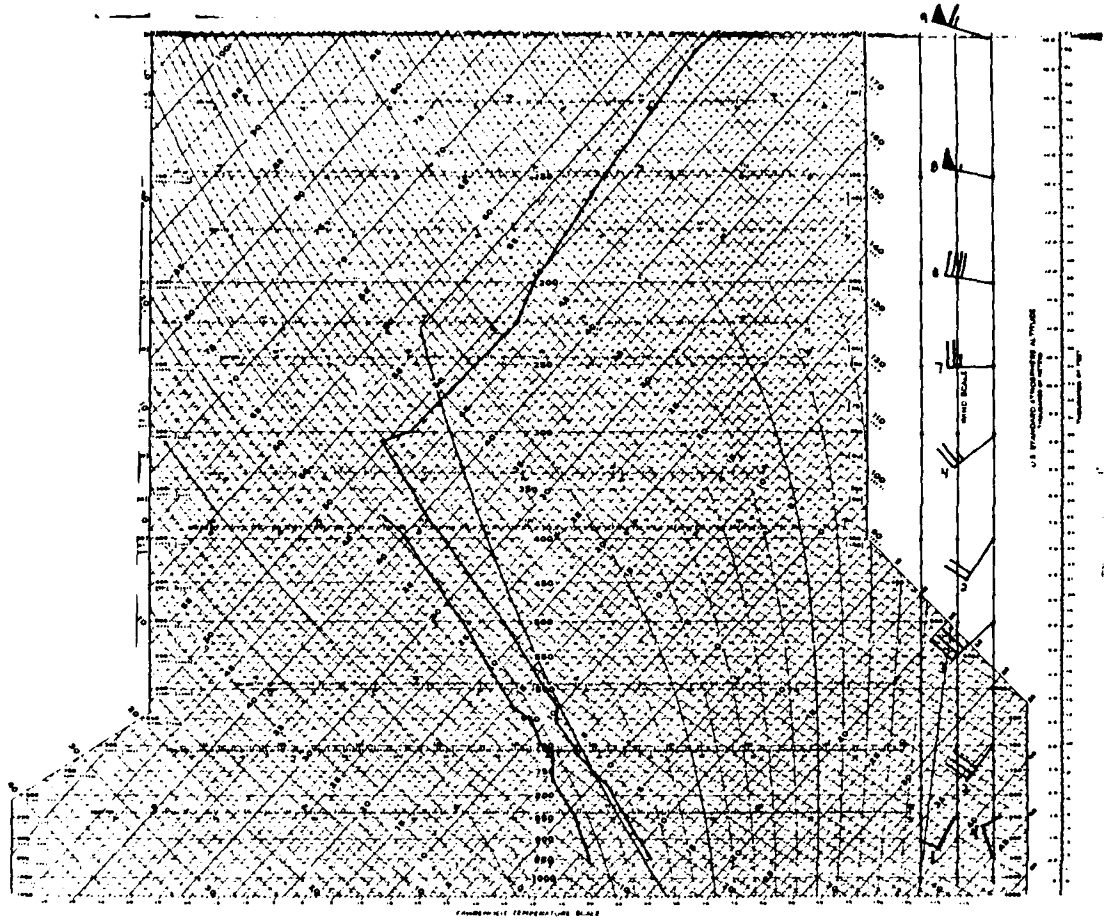

FIGURE 45: Skew-T log-p diagram for Oklahoma City, Oklahoma (zone A) at 0000 GMT March 22, 1981.

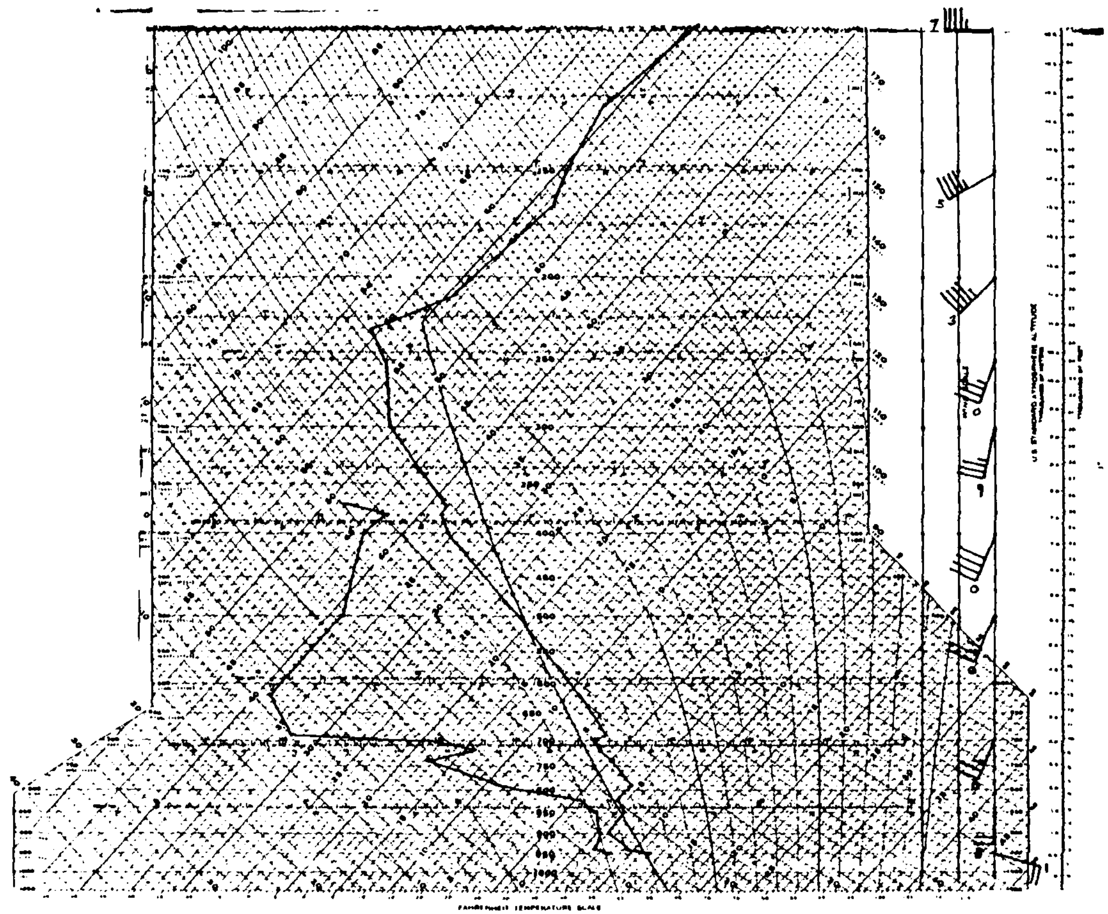

FIGURE 46: Skew-T log-p diagram for Monett, Missouri (zone 1) at 0000 GMT March 22, 1981.

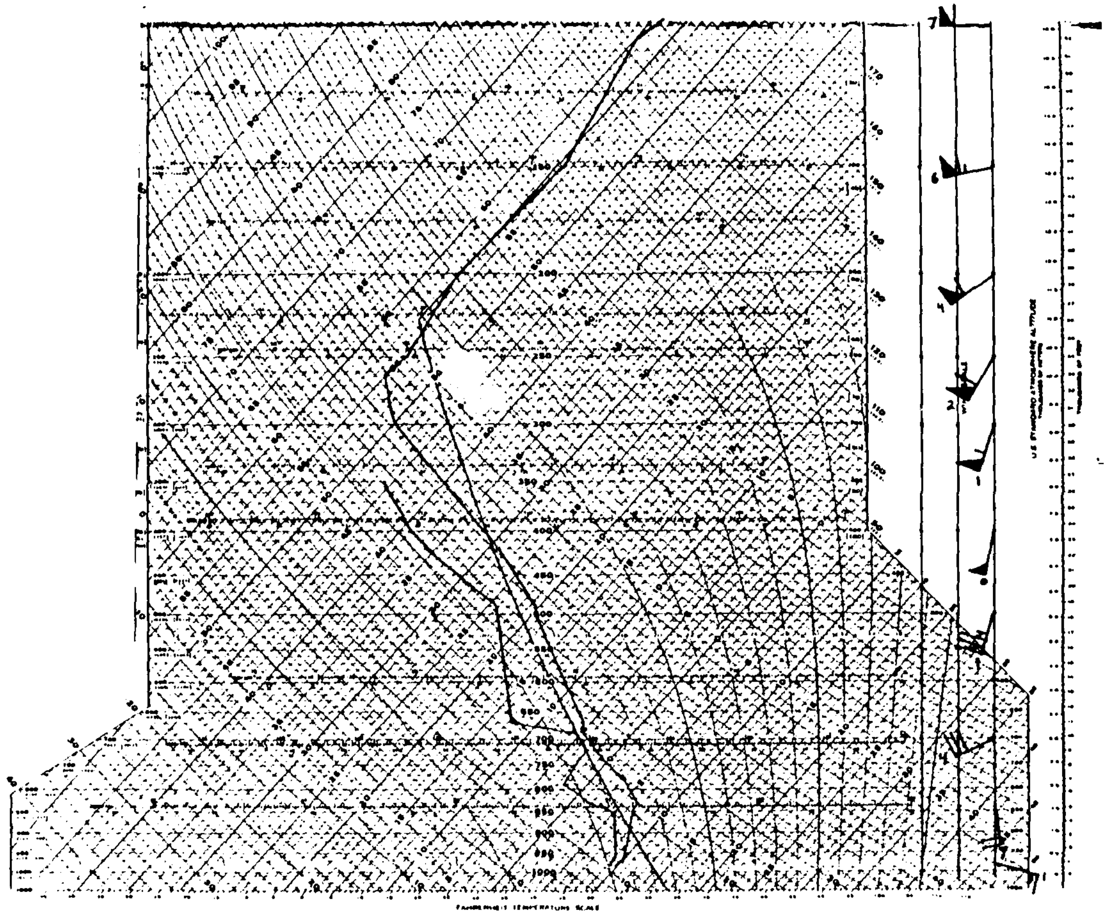

FIGURE 47: Skew-T log-p diagram for Little Rock, Arizona (zone C) at 0000 GMT March 22, 1981.

for Oklahoma City has been plotted and is assumed to represent conditions aloft over Tulsa. There is a 23 mb deep inversion present, beginning at 904 mb. A time history of the surface temperatures for Tulsa are also plotted, showing the elimination of the stable boundary layer at some time between 1800 and 2100 GMT when the dryline must have passed. If the lapse rate at Tulsa was dry adiabatic, as shown, then the well-mixed layer behind the dryline would extend up to 700 mb. Sun and Ogura (1979) found that differential surface heating across a dryline creates a deeper mixed layer on the dry air side. Vertical eddy heat transport then drives a sea-breeze type circulation with winds at the surface blowing across the dryline from cooler to warmer air. Low level convergence along the dryline is intensified by this circulation and moist air is forced upward, triggering deep convection along the line. Strong surface convergence is also present in this case (Fig. 44). At 2100 GMT, surface winds in eastern Kansas and western Arkansas are blowing nearly perpendicular to the isobars.

The Stephensville, Texas sounding for 0000 GMT (Fig. 49), further south in the dry region, is dry at the surface and represents conditions behind the dryline. The lapse rate is nearly dry adiabatic from the surface to 550 mb (the potential temperature changes only 3° C). Strong winds have mixed down from aloft and are 23 m/sec at 700 mb. The tropopause occurs at 360 mb, which is unusually low. By

AD-A119 654 AIR FORCE INST OF TECH WRIGHT-PATTERSON AFB OH F/G 4/2
A COMPOSITE STUDY OF COMMA CLOUDS AND THEIR ASSOCIATION WITH SE--ETC(U)
1982 J P MILLARD
UNCLASSIFIED AFIT/CI/NR/82-57T NL

2 OF 2
ADA
119 654

END
DATE
FILMED
10-82
DTIC

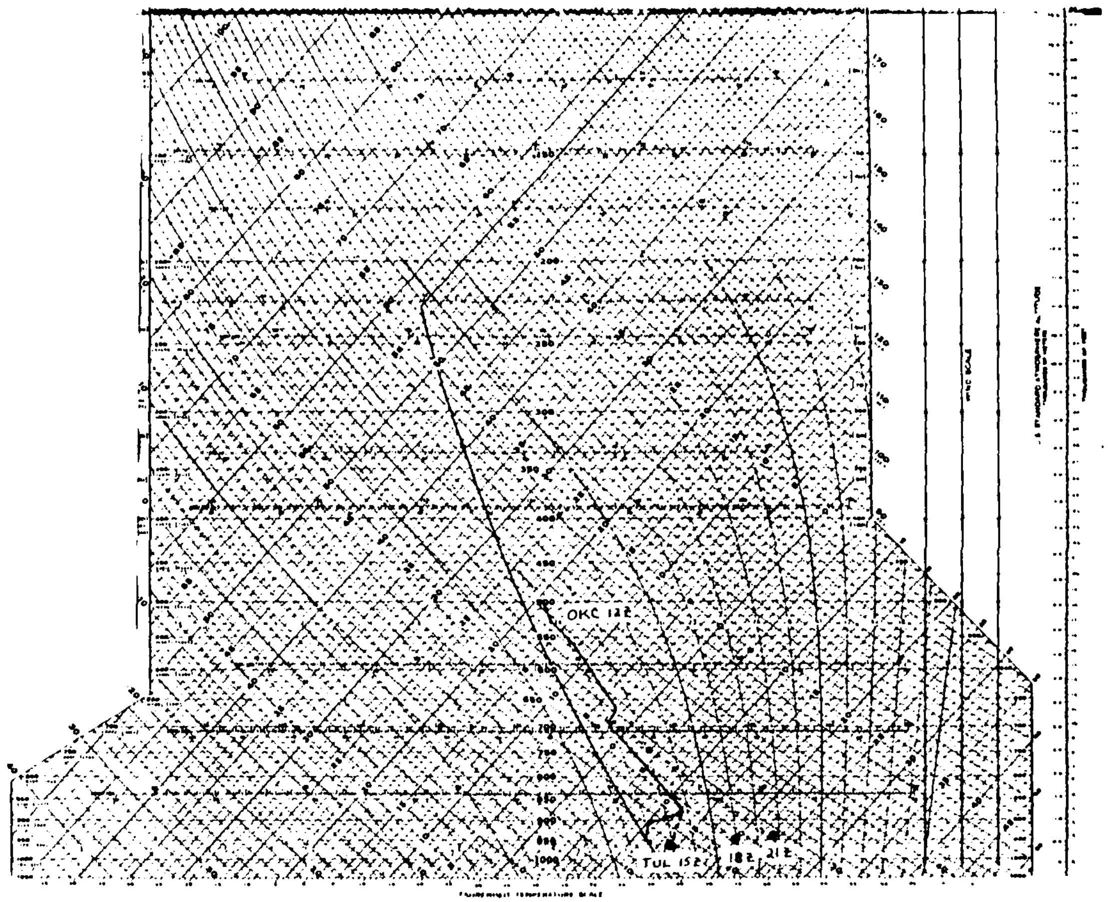

FIGURE 48: Temperature profile for Oklahoma City, Oklahoma at 1200 GMT March 21, 1981. Surface temperatures and assumed lapse rates at Tulsa, Oklahoma are superimposed for 1500, 1800 and 2100 GMT.

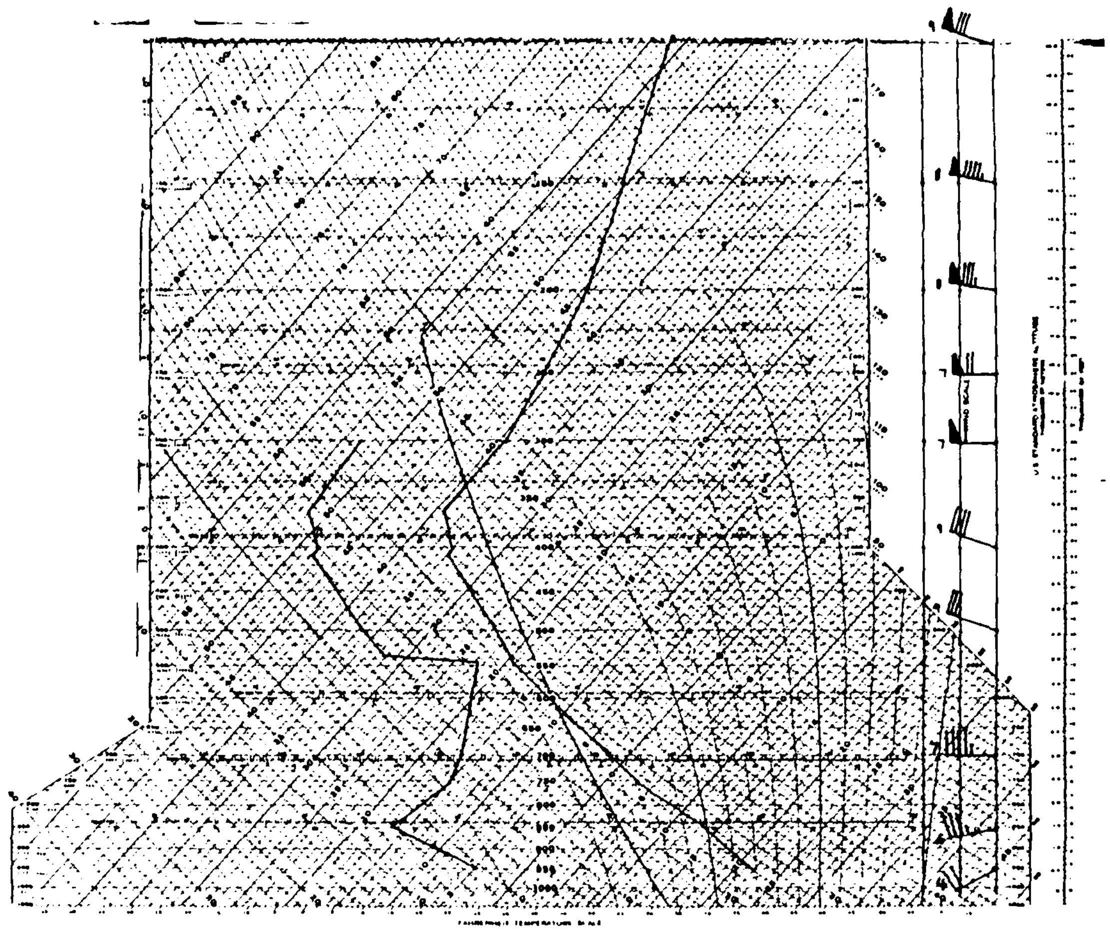

FIGURE 49: Skew-T log-p diagram for Stephensville, Texas (zone 4) at 0000 GMT March 22, 1981.

contrast, the sounding (Fig. 50) taken at Longview, Texas (zone 3) shows high dew point temperatures between the surface and 790 mb with drier air aloft. The 2230 GMT satellite picture shows both Monett and Longview are in the eastern half of the dry intrusion where dry air aloft has dissipated middle and upper level cloud cover, but still to the east of the surface dryline. The cold air advection aloft has greatly increased the potential instability across Oklahoma and northern Texas. The 400 mb temperature at Longview decreased 5.2° C between 1200 GMT and 0000 GMT, while the 850 mb temperature rose 2.2° C. Wind speeds decreased during the period and there is only slight directional shear (Fig. 50). The Lifted Index changed from +2 to -8. The SWEAT index for Longview increased from 237 to 463. Figure 51 is the sounding for Lake Charles, Louisiana (zone D), which is under the thick cloud cover of the comma tail. It is a more stable sounding, overall, than Longview's.

Figure 52 is a relative humidity cross-section between Amarillo and Lake Charles at 0000 GMT. Two separate moist areas can be seen, which represent the comma head and tail, with the dry intrusion in between them. The low-level dry air over Stephensville is separated from drier air aloft by a layer of relative humidities in excess of 50 percent at about 550 mb. This moist layer can also be seen on the Stephensville sounding (Fig. 49). A cross-section from Del Rio, Texas to Salem, Illinois (Fig. 53) does not show the

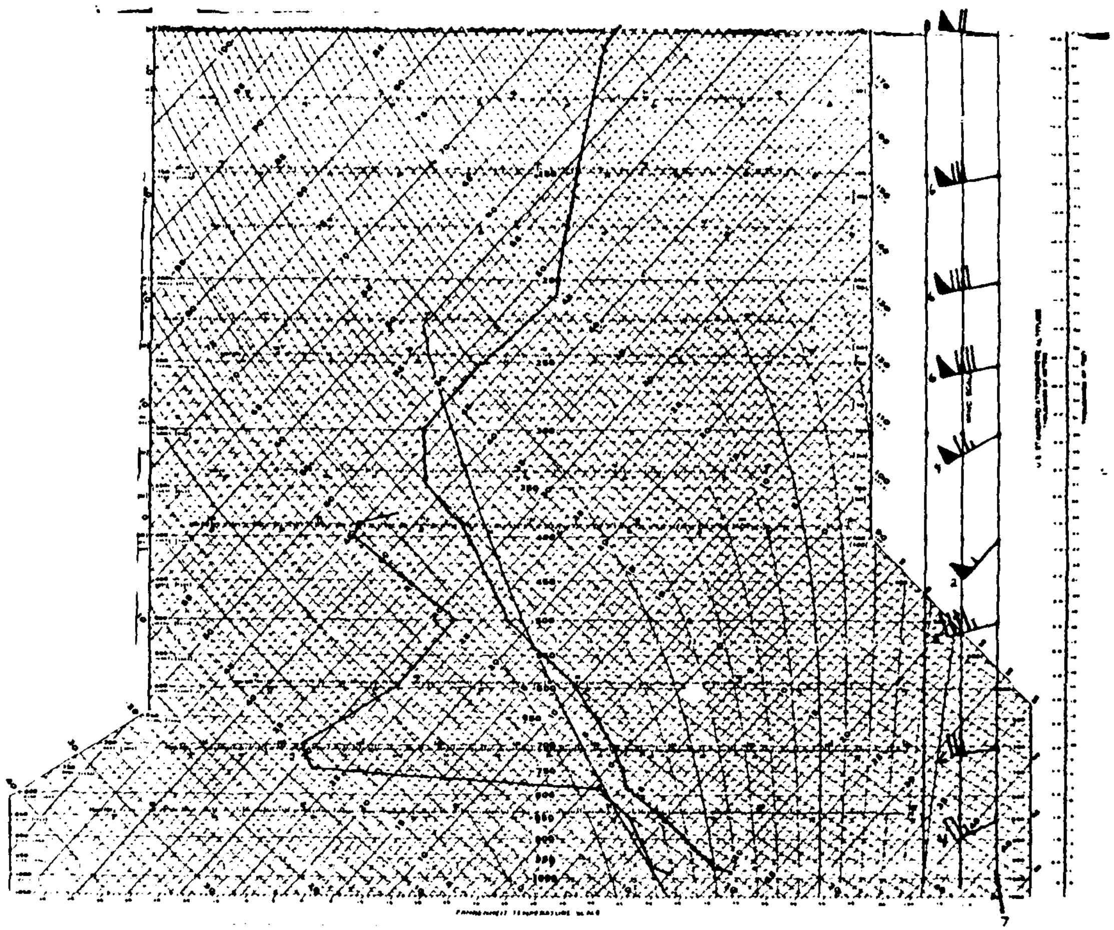

FIGURE 50: Skew-T log-p diagram for Longview, Texas (zone 3) at 0000 GMT March 22, 1981.

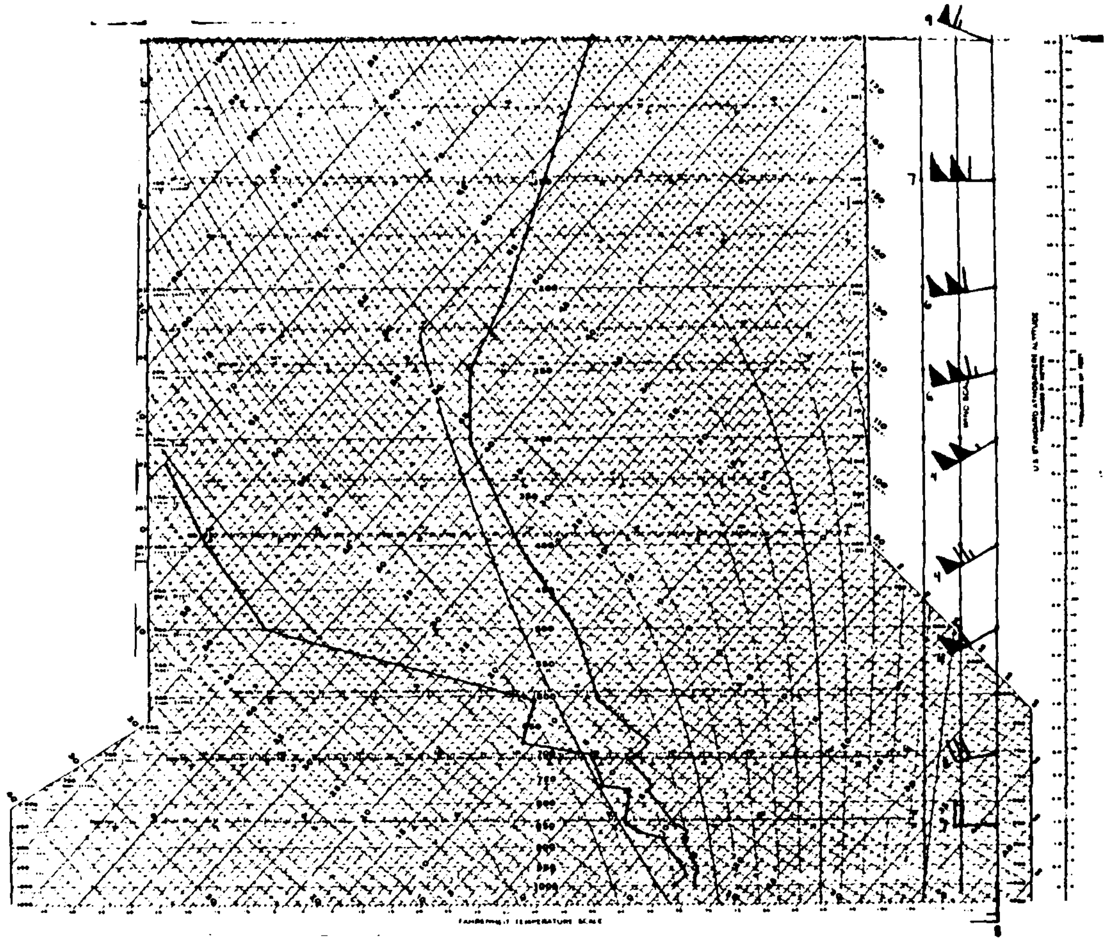

FIGURE 51: Skew-T log-p diagram for Lake Charles, Louisiana (zone D) at 0000 GMT March 22, 1981.

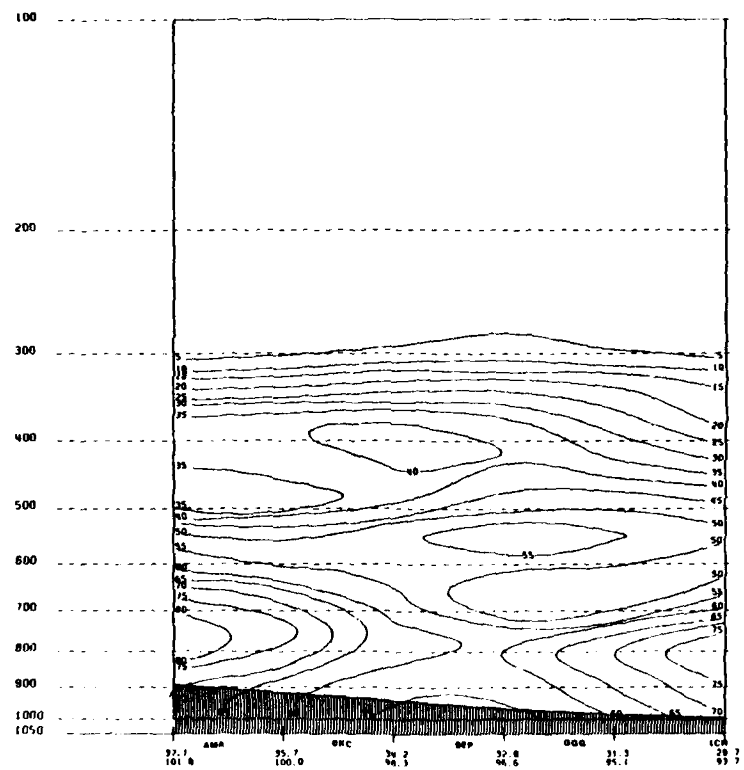

FIGURE 52: Relative humidity cross-section between Amarillo, Texas and Lake Charles, Louisiana at 0000 GMT March 22, 1981.

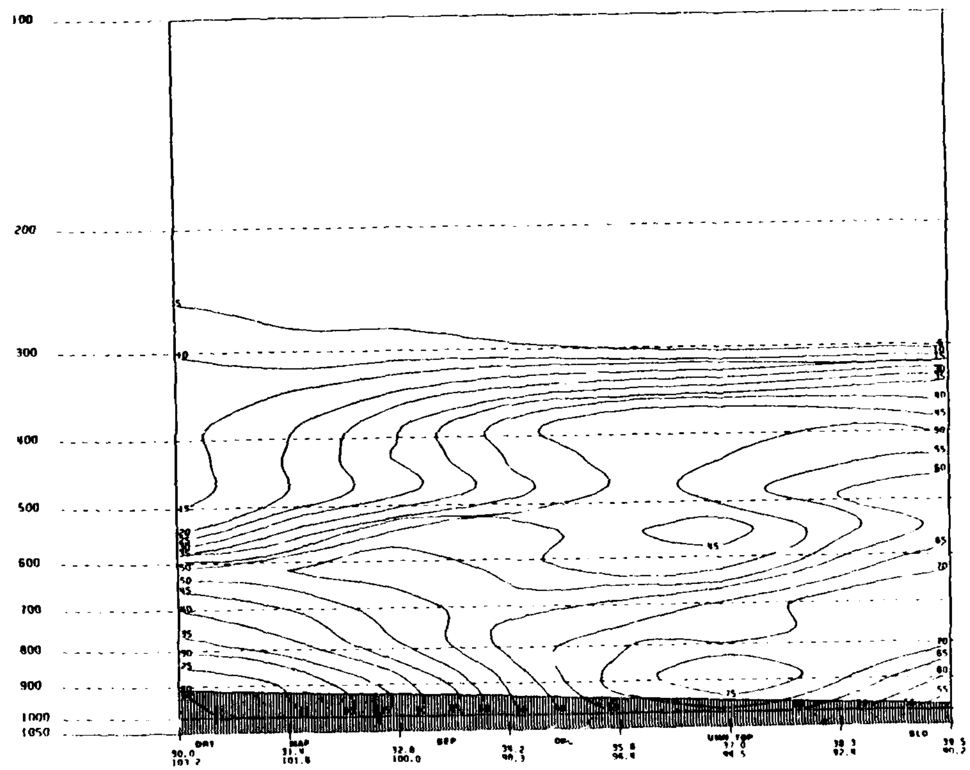

FIGURE 53: Relative humidity cross-section between Del Rio, Texas and Salem, Illinois at 0000 GMT March 22, 1981

low-level dry air between Oklahoma City and Monett, even though it intersects the dryline there. This is because there is no representative sounding available from west of the dryline in this region.

3.4 Vertical Motions

Vertical motions over the cyclone were computed by the kinematic method and by solving the quasi-geostrophic omega equation. Isentropic analyses at three levels were also constructed, and provide a third measure of vertical motions. None of these methods can be expected to show vertical motions on the scale of the line of thunderstorms in eastern Oklahoma since only synoptic-scale upper-air data were available.

Vertical motions were obtained by solving the quasi-geostrophic omega equation:

$$\left(\nabla^2 + \frac{fo^2}{\sigma} \frac{\partial^2}{\partial p^2} \right) \omega = \underbrace{\frac{fo}{\sigma} \frac{\partial}{\partial p} J \left(\Psi, \nabla^2 \Psi + f\right)}_{F1}$$

$$\underbrace{- \frac{fo}{\sigma} \nabla^2 \left[J \left(\Psi, \frac{\partial \Psi}{\partial p}\right)\right]}_{F2} \qquad (3)$$

where the Jacobian, $J(A,B) = \frac{\partial A}{\partial x} \frac{\partial B}{\partial y} - \frac{\partial A}{\partial y} \frac{\partial B}{\partial x}$. Values of stream function were computed from the geopotential height data, according to: $\Psi = gz/fo$. The heights at ten standard pressure levels were obtained from NMC gridded data tapes. The grid domain is 25°-50° N and 65°-125° W and the grid interval is

2.5°. Values of static stability σ, were calculated from temperature fields and then averaged horizontally over the domain. The effect of terrain was not included, so that the lower and upper boundary conditions were $\omega = 0$ at 1000 mb and at 50 mb. The effects of latent heating on omega were also examined. In this case, a third term on the R.H.S. of equation (3) must be added: $F_3 = -\frac{R}{c_p p} \nabla^2 (-L\omega \frac{\partial qs}{\partial p})$. Figures 54 and 55 show vertical motions which include the effects of latent heating.

At 1200 GMT the upward vertical motion pattern at 600 mb approximates the comma shape. Radar charts (not shown) at this time also portray a comma-shaped precipitation pattern with the heaviest activity in Arkansas. The maximum upward velocity is 6.8 μ bar/sec in northeastern Oklahoma. Strong subsidence is present over Arizona and New Mexico, west of the 500 mb trough (cf. Fig. 35). By 0000 GMT, the maximum in rising motion has moved to the southeast and increased in magnitude, to a value of 7.5 μ bar/sec. There is no longer any upward motion indicated north and west of the low as was seen earlier. A large area of rain and rainshowers is present in eastern Arkansas, Mississippi and Alabama; with and ahead of the maximum in rising motion. Above the dry line at 600 mb the air is still rising, but the magnitude of the ascent has decreased in eastern Oklahoma since 1200 GMT.

Each of these vertical motion fields was partitioned

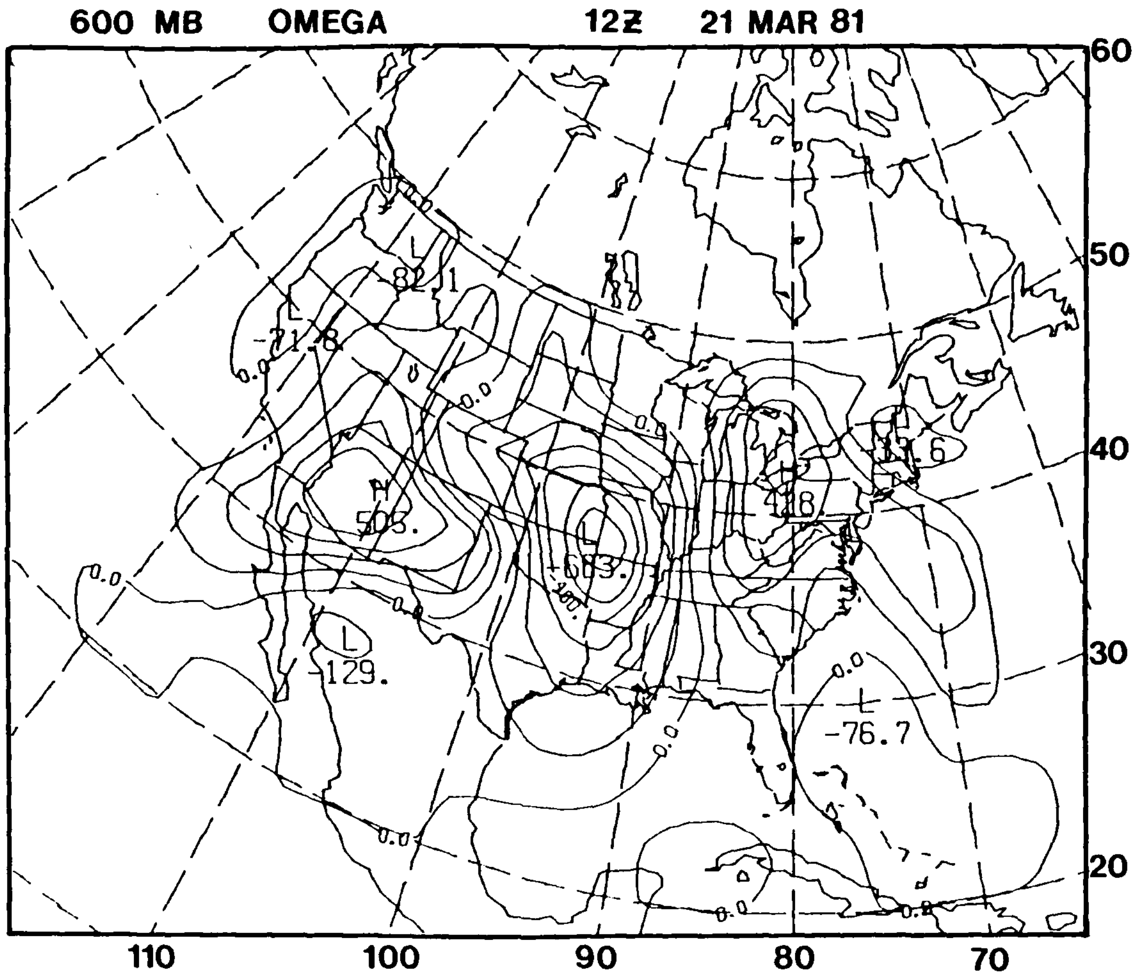

FIGURE 54: 600 mb quasi-geostrophic vertical motions for 1200 GMT March 21, 1981. Units are x 10^{-5} mb/sec.

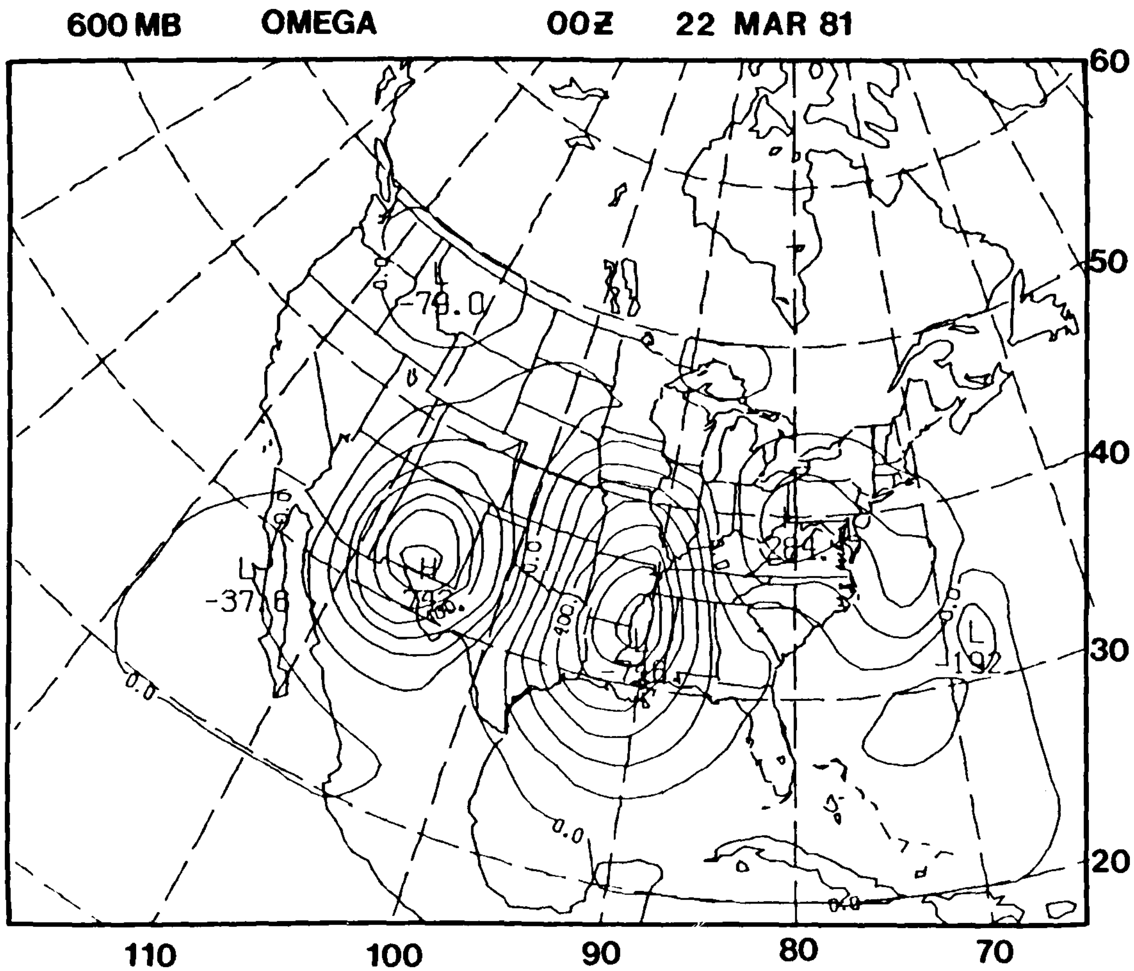

FIGURE 55: 600 mb quasi-geostrophic vertica 0000 GMT March 22, 1981.

Units are x 10^{-5} mb/sec.

in order to better understand the effects of thermal advection and differential vorticity advection. This was done by solving omega for each of the two forcing functions on the R.H.S. of equation (3) separately. Figure 56 shows the effect of differential vorticity advection (F1) at 1200 GMT and Figure 57 shows the vertical motion due to temperature advection (F2). The maximum subsidence due to vorticity advection is in Arizona, west of the 500 mb trough. Strong cold air advection in the Texas panhandle is responsible for most of the subsidence in that region where the dry intrusion has started to form. Thermal advection is also responsible for the westward extension of upward motion north and west of the low seen in Figure 54. By 0000 GMT, vertical motions due to differential vorticity advection (Fig. 58) have increased in magnitude due to the increased vorticity along the 500 mb trough axis (cf. Figs. 35 and 41). The upward vertical motion due to thermal advection (Fig. 59) has decreased in magnitude and moved southeast.

Kinematic vertical motions at 600 mb are shown in Figures 60 and 61. These are computed by solving:

$$\omega\ (P) = \omega\ (Po) - \int_{Po}^{P} \left(\frac{\partial u}{\partial x} + \frac{\partial v}{\partial y} \right)_p dp.$$

The u- and v- components of the wind are obtained from the NMC gridded data over the same domain that was used in the quasi-geostrophic calculations. The bottom boundary condition is $\omega = 0$ at 1000 mb, and values of omega are adjusted according

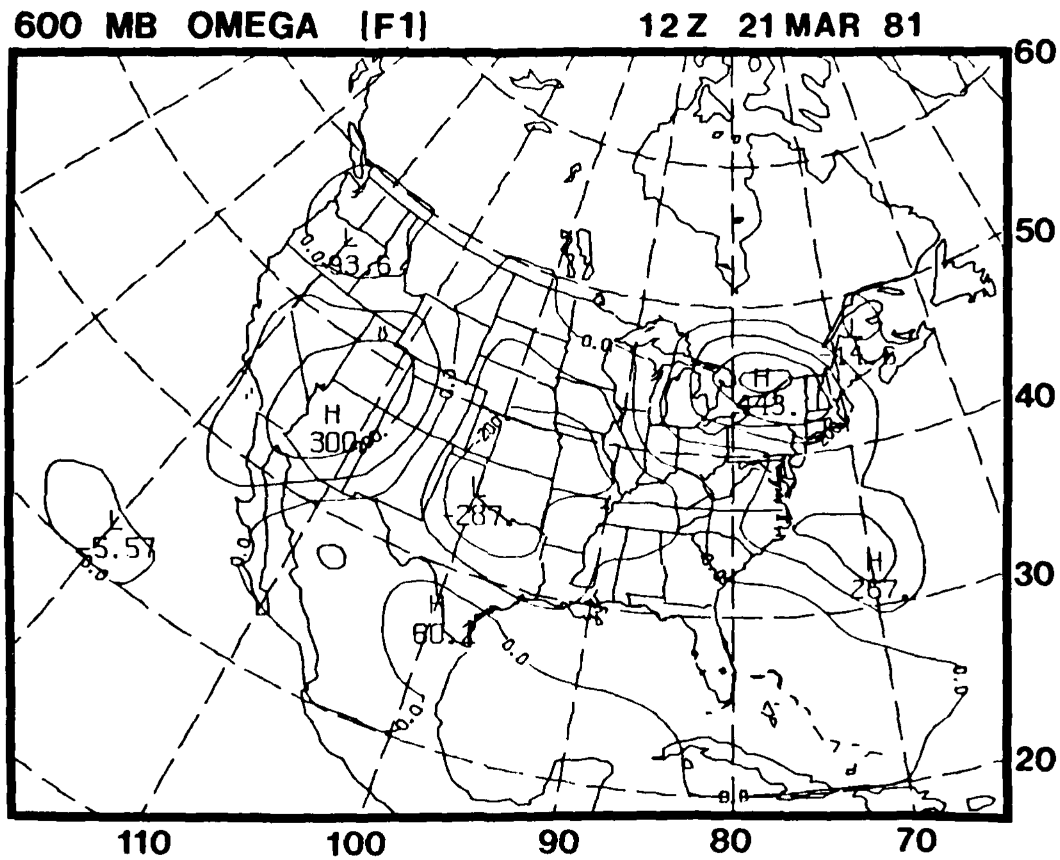

FIGURE 56: Component of the vertical motion in Figure 54 which is due to differential vorticity advection (F1).

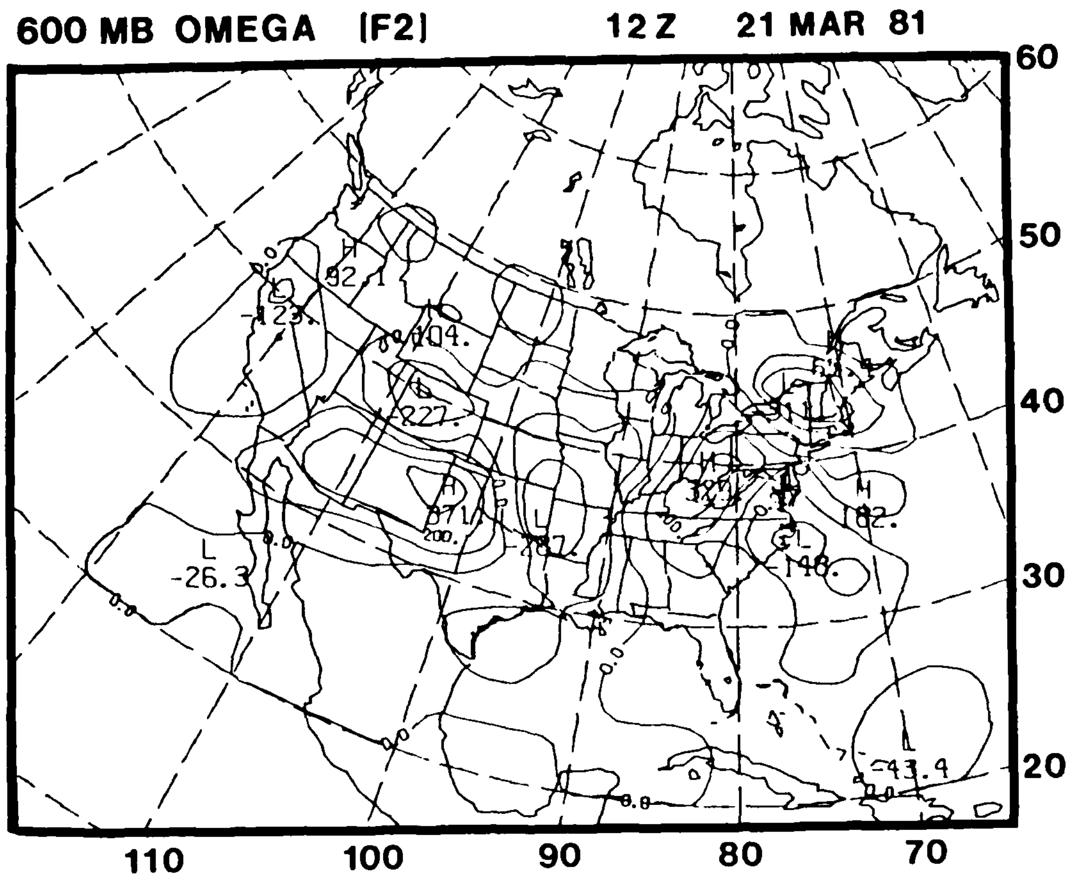

FIGURE 57: Component of the vertical motion in Figure 54 which is due to thermal advection (F2).

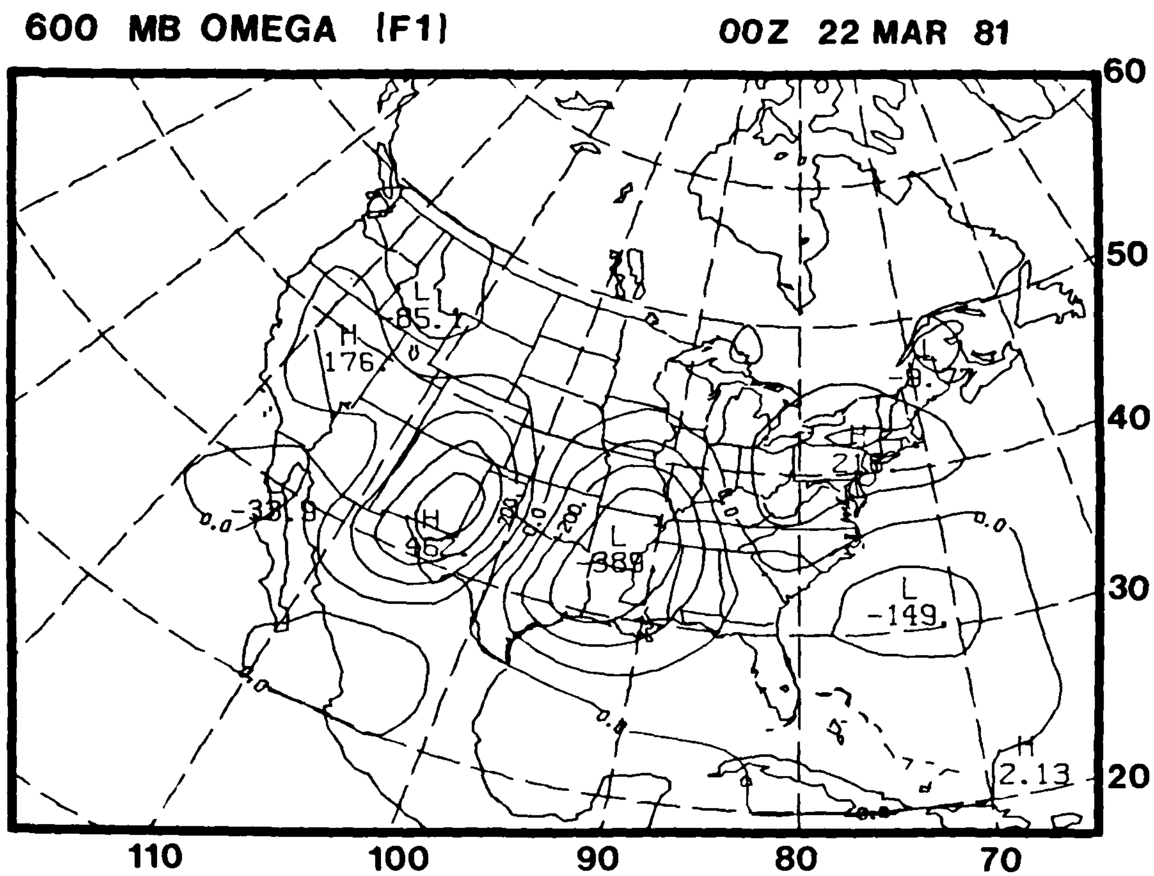

FIGURE 58: Component of the vertical motion in Figure 55 which is due to differential vorticity advection (F1).

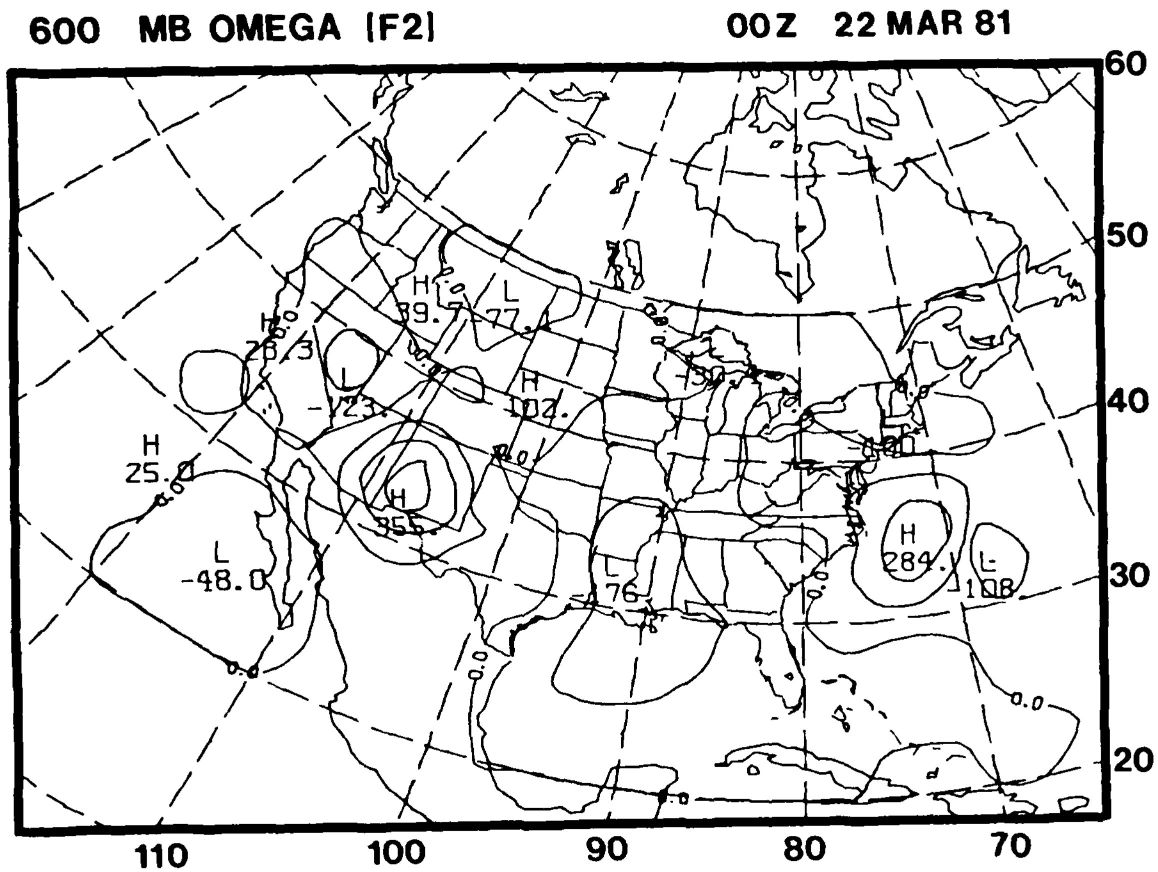

FIGURE 59: Component of the vertical motion in Figure 55 which is due to thermal advection (F2).

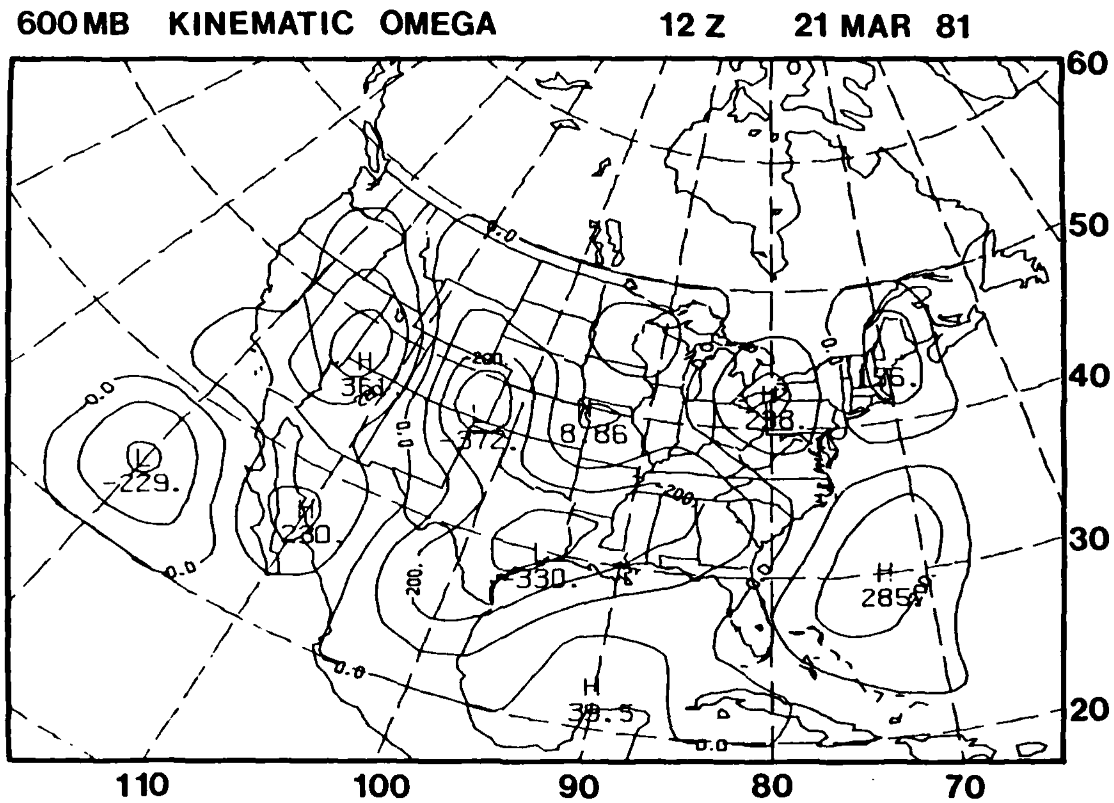

FIGURE 60: 600 mb Kinematic vertical motions for 1200 GMT March 21, 1981. Units are x 10^{-5} mb/sec.

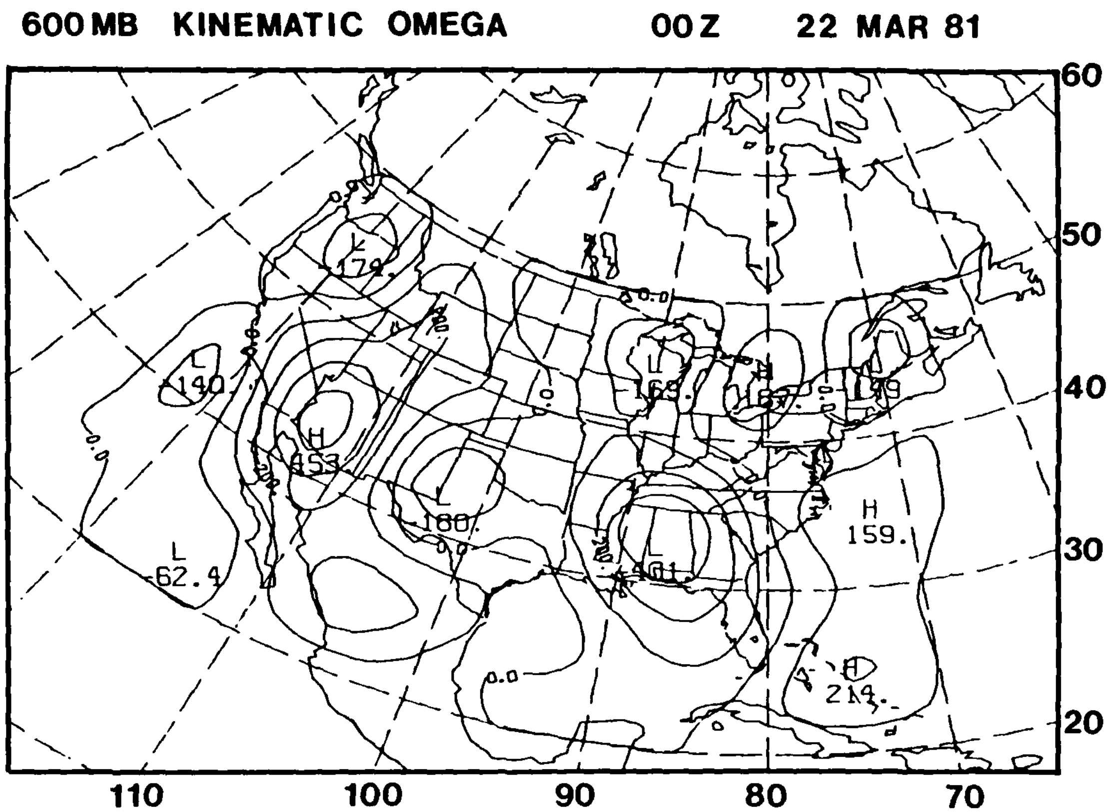

FIGURE 61: 600 mb Kinematic vertical motions for 0000 GMT March 22, 1981. Units are x 10^{-5} mb/sec.

to the method of O'Brien (1970). These kinematically-derived motion fields show some large differences when compared to the quasi-geostrophic omega fields. In the region near the surface low, low-level convergence is large and results in rising motion over the low at 600 mb. In the quasi-geostrophic calculations, the strong cold air advection results in sinking motion over the low. In the vicinity of the dryline at 0000 GMT, the kinematic calculations also show rising motion in the dry intrusion, but of a much smaller magnitude than the quasi-geostrophic value.

Isentropic analyses for 0000 GMT are given in Figures 62-64 for the 300, 310 and 320 K surfaces. Winds are shown relative to the ground; no translation vector has been subtracted. Note that the 300 K surface intersects the ground in west Texas. The pattern of rising air in the cloudy portion of the comma tail is in agreement with the composite analyses of Chapter 2. Unlike the composite, in this case the air is rising between zones 4 and 3, especially at low levels. The strongest subsidence is indicated south and east of Amarillo, behind the new cold front (Fig. 44). The only subsidence in the dry air, as indicated on the 310 and 320 K surfaces, is between Midland and Del Rio, Texas. This agrees with the quasi-geostrophic omega field (Fig. 55) which shows most of the subsidence occurring west of 100° W. Rising motion is present in eastern Okalhoma over the dry line at all three levels, but is weakest on the 310 K surface.

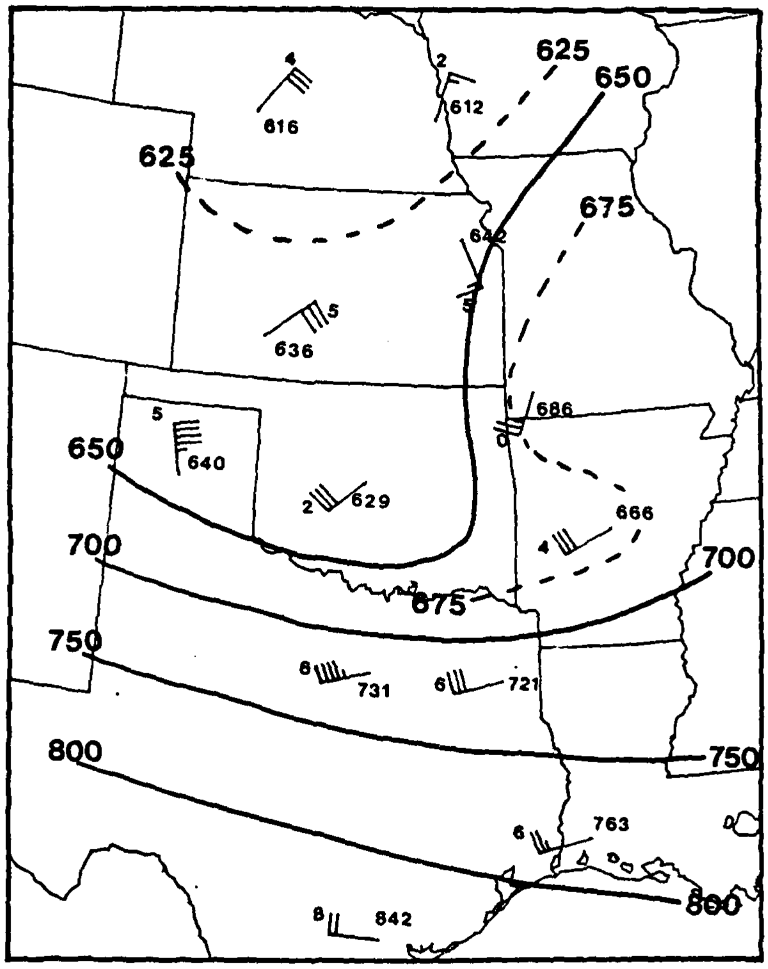

FIGURE 62: 300 K isentropic surface analysis for 0000 GMT March 22, 1981. Value to the right of the station symbol is pressure, in millibars, for this surface. Winds are in knots.

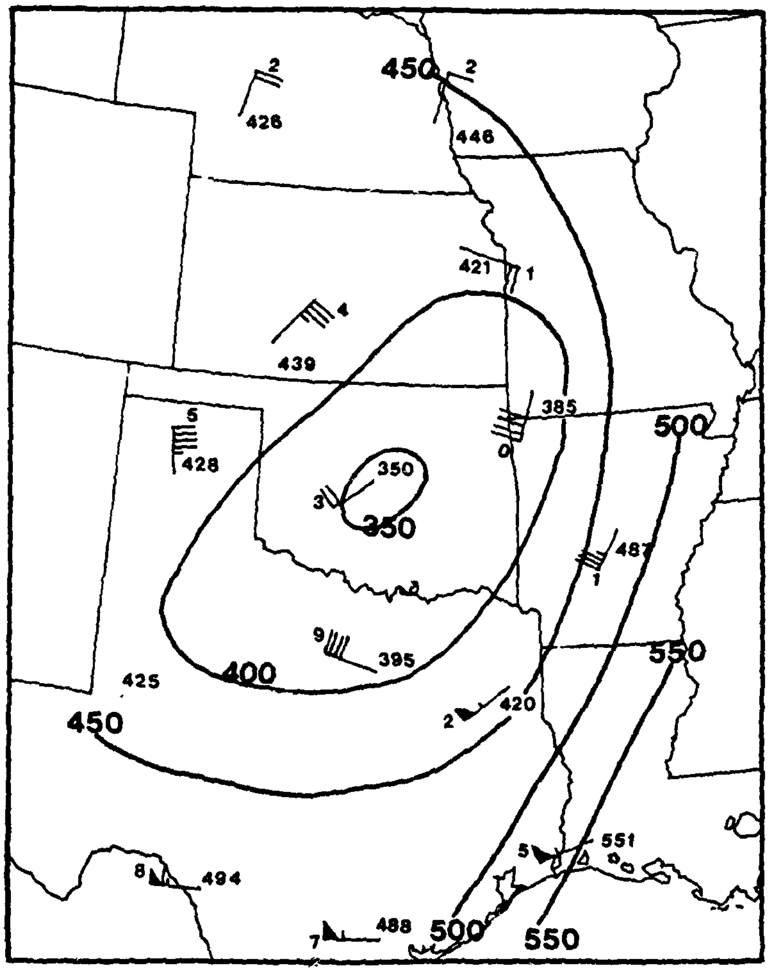

FIGURE 63: 310 K isentropic surface analysis for 0000 GMT March 22, 1981. Value to the right of the station symbol is pressure, in millibars, for this surface. Winds are in knots.

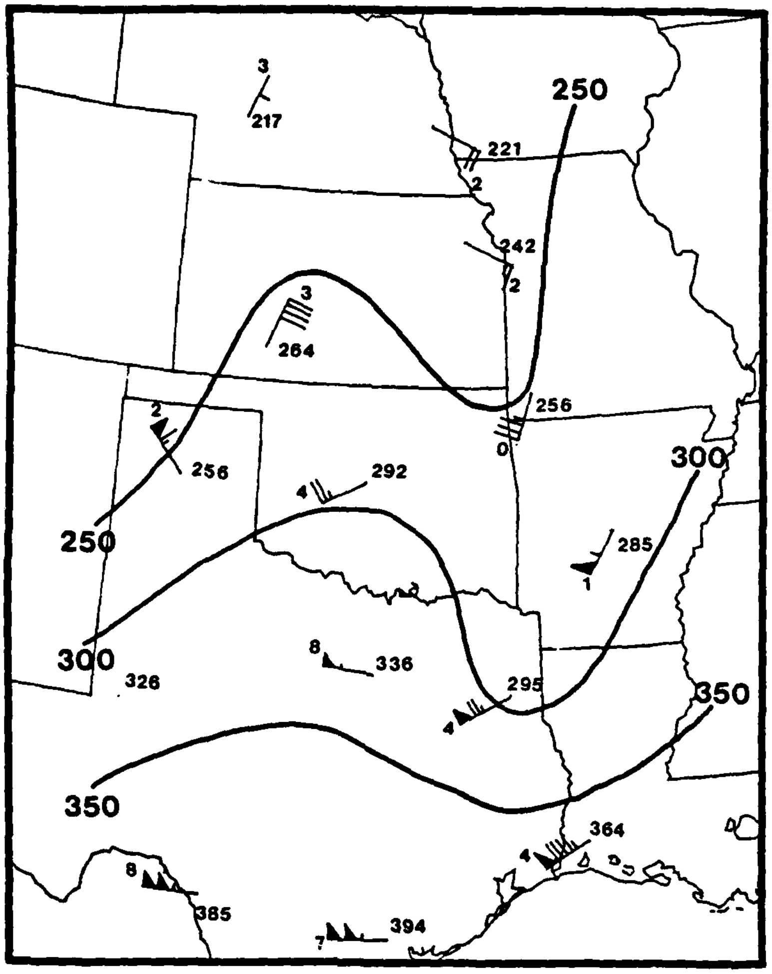

FIGURE 64: 320 K isentropic surface analysis for 0000 GMT March 22, 1981. Value to the right of the station symbol is pressure, in millibars, for this surface. Winds are in knots.

3.5 Richardson Numbers

The role of symmetric instability in connection with sub-synoptic scale wave growth on a dryline has been discussed by McGinley and Sasaki (1975). They found Richardson numbers in the range .25 to 1 over the 900 to 600 mb layer west of a dryline in 3 cases where tornado producing thunderstorms developed. At 0000 GMT in the present case, Richardson numbers at Del Rio, Texas (zone 5) ranged from .25 to 1 from the surface up to 700 mb. Figure 65 shows the Richardson number was less than 1 in the boundary layer of both zones 5 and E (Victoria, Texas). The lapse rate at Del Rio is dry adiabatic from the surface to 738 mb, and wind speeds increase from 13 m/sec at 850 mb to 25 m/sec at 700 mb. Thus, the usual sharp increase in Richardson number at low levels (Fig. 30) did not occur. Strong, turbulent mixing occurred over a deep layer in the dry air behind the dryline. Zone 5 is well west of where the dry slot convection took place, but it is impossible to judge whether conditions are the same behind the dryline in the northern sector of the dry intrusion. Although Richardson numbers in the range of .25 to 1 may be necessary for symmetric instability types of small scale wave growth (Stone, 1966; McGinley and Sasaki, 1975), it can hardly be assumed that this is a sufficient condition.

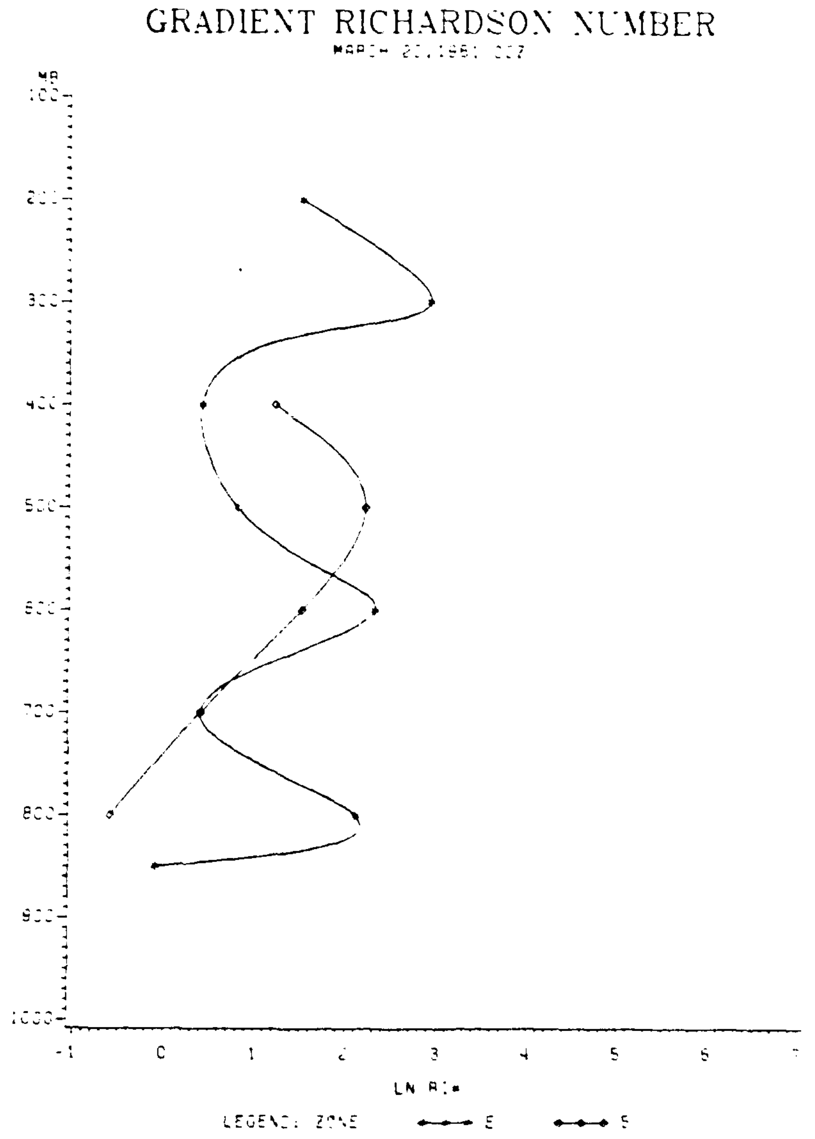

FIGURE 65: Natural logarithm of the gradient Richardson number versus pressure for Del Rio, Texas (zone 5) and Victoria, Texas (zone E) at 0000 GMT March 22, 1981.

3.6 Forecasting Dry Slot Convection

The dry intrusion cannot be dismissed as a region where severe weather will not occur. As the composite study in Chapter II indicates, synoptic-scale upward motion is normally present in this region over a large depth. High relative humidities are common at low levels. It is also potentially unstable, with cold air often advected over the region at middle levels. Since it is relatively cloud-free, surface heating during the day can increase the potential instability.

Severe weather was forecast on March 21-22, 1981 by the National Severe Storms Forecast Center at Kansas City. At 1930 GMT, a "moderate risk" of severe weather was forecast for eastern Oklahoma, eastern Texas, western and southern Arkansas, and all of Louisiana. Strong vorticity advection was forecast in the vicinity of the dryline in eastern Oklahoma. Although cyclonic vorticity advection was present, thunderstorm activity was more likely related to the increase in potential instability brought on by the advection of very cold air aloft, and by the strong low level convergence along the dryline.

Another case of rapid thunderstorm growth along a line in the northern portion of the dry intrusion occurred in eastern Iowa on March 29-30, 1981. Again, the cyclone had reached the well-occluded stage. Upper level clearing occurred in advance of a slow moving "cold front" (as

analyzed by NMC). By afternoon, surface temperatures at stations in the dry, cloud-free air had become warmer than stations ahead of the front which were still under cloudy skies. Surface dew point temperature differences were not as pronounced as on March 21-22. Cold air advection aloft lowered the 500 mb temperature 3° C during the day over the region where deep convection developed. Temperature and moisture differences across the front were larger further south, but the storms seemed to have begun closest to the low, where the surface wind (and probably the convergence) was stronger.

These observations suggest that the rapid development of thunderstorms within the dry intrusion can be forecast under certain conditions. First, the cyclone must be in a mature or occluded stage of development with a well-formed dry intrusion north of the comma head. The advection of drier air aloft must be faster than the movement of the surface cold front or dryline. If the frontal position were to be drawn on the satellite picture, it would cut across the northern portion of the dry intrusion. Second, the initiation of these thunderstorms appears to be linked to the radiational warming of air near the ground under cloud-free skies behind the front or dryline. Thus, this type of growth appears to begin in late afternoon, once the low-level inversion has been eliminated by surface heating. Third, growth is preferred where surface convergence is strongest.

Mesoscale circulations may appear later, but apparently are not necessary for initiation of these thunderstorms. A sea-breeze type circulation, such as was discussed by Sun and Ogura (1979), may assist in producing this convergence. Finally, cold air advection appears necessary in order to increase the potential instability of the atmosphere. A forecast temperature decrease of 3° C or more at 500 mb appears to be a good indicator.

CHAPTER IV

SUMMARY AND RECOMMENDATIONS FOR FUTURE RESEARCH

Quantitative information about the structure of mid-latitude cyclones has been obtained by compositing soundings taken from similar portions of their cloud patterns. Composite values allow interpretations to be made which might not otherwise have been possible.

The composite system has a closed circulation at 850 and 700 mb centered between zones A and 2. The strongest winds are found in zones 3 and 5, in the dry air immediately behind the back edge of the comma tail. Winds veer with height in response to warm air advection along the comma tail, and back with height in the head of the comma cloud. Airflow on relative-flow isentropic surfaces resembles the model of Carlson (1980). Relative to the moving storm, speed convergence takes place at upper levels along the cloud edge. Deformation is present at low levels behind the comma tail. Dew point depressions in the dry zones at 500 mb are 10-14° C drier than climatology. Richardson numbers are generally smaller in the clear zones, both because of stronger wind

shears and lower static stabilities.

This study has confirmed the findings of Leese (1962), and others, that the synoptic-scale subsidence region remains south of the comma head, and that upward vertical motion is present in the northern part of the dry intrusion. High relative humidities are present at and below 850 mb in zones 1 and 2, even though satellite pictures reveal the dissipation of high level cloudiness. High surface dew points and the coldest air at 400 mb combine to produce potentially unstable conditions in this region. A decrease with height in moist static energy is observed in zones 1 and 2.

Eighty percent of the severe weather is observed to occur in the comma tail (zones C, D and E). SWEAT indices are also highest in these zones. Diffluence is observed at 400 and 300 mb, with the flow in zones 1 and D being stronger than in zone C at these levels. A significant difference in $-\frac{\partial \Theta_E}{\partial p}$ was found between zones 5 and E, with the greatest instability in the cloudy zone.

A case study documenting the rapid _in situ_ growth of deep convection within the dry intrusion has also been discussed. Development was found to occur along a dryline where surface convergence was strong, and where cold air advection aloft increased the potential instability. Synoptic-scale vertical motions, calculated by three different methods, were upward in this portion of the dry intrusion. Other examples of squall line development within the dry intrusion

have been observed. Certain features which recur in these situations have been detailed which may aid in forecasting the onset of dry slot convection.

This research might be extended in several areas. Certainly more soundings are needed from zones 1 and 2 in order to confirm the findings of this study. There are large differences in the composite soundings for these zones when, supposedly, they represent two portions of the comma which are very close together and which should be more like one another than not. The northern portion of the dry intrusion, close to the cyclone center, is an area where interesting and important changes are occurring. Yet there are too few observations in this study to document diurnal differences in temperature and moisture within these zones. A statistical analysis should be performed on data from all of the zones. This study calculates mean quantities but no attention has been given to the variance or standard deviation of these quantities from the mean. Another interesting idea, which could not be pursued, is to composite gridded data sets for each of the comma cloud cases, rather than just the individual soungings. The major difficulty with this approach is that the comma patterns have different sizes and differently shaped dry regions. The grid has to be adjusted relative to one particular feature in all of the cloud patterns in order to obtain meaningful results. However, Mullen (1979) successfully used this method of compositing

with small comma patterns. Although several different composite studies were performed to dis' ,uish diurnal and seasonal differences, no attempt was made to stratify comma cloud patterns according to size. This would require much more data than was used in this study. Quantitative differences which might exist in storms at different stages of development could also be explored if a larger data base was available. Finally, other examples of squall line development within the dry intrusion should be studied. Future research might better examine the time history of changes in temperature and moisture at various levels across the front or dryline. It is still unclear whether the synoptic-scale conditions actually favor convective growth in this region; since little is known about the mean environment of zones 1 and 2. Ideally, any future study of dry slot convection would use surface and upper air observations of much shorter space and time scales than were used here.

APPENDICES

APPENDIX 1

LIST OF SOUNDINGS USED IN COMPOSITE

	1	2	3	4	5	6	A	B	C	D	E
3/ 4/80 12Z	UMN	DDC	OKC	AMA	SEP	MAF	DEN	OMA	SLO	LIT	GGG
3/12/80 12Z			LIT	OKC	SEP	MAF	TOP			JAN	[illegible]
3/23/80 12Z		AMA	MAF	ELP	CUU				OKC	SEP	
3/24/80 00Z			SEP	MAF	DRT		DDC	TOP		LIT	VCT
3/24/80 12Z				SEP	DRT	MAF	UMN	PIA	DAY	AHN	BVE
3/27/80 12Z			MAF	ELP			ABQ		OKC	SEP	DRT
3/28/80 00Z				MAF	DRT	ELP	DDC	LBF	LIT	GGG	VCT
3/28/80 12Z			LIT	AMA	VCT	DRT	DEN	LBF	SLO	JAN	
3/29/80 12Z			SEP	MAF	DRT	ELP	DEN	TOP	LIT	GGG	
3/30/80 00Z		UMN	GGG	SEP	VCT	DRT	DDC	OMA	SLO	JAN	
4/ 1/80 00Z			AMA	ABQ	MAF	ELP		DDC	OKC	SEP	
4/ 1/80 12Z			OKC	AMA	MAF	ELP		HON	UMN	LIT	VCT
4/ 3/80 00Z			OKC	AMA	MAF	ELP	RAP	HON		UMN	GGG
4/ 3/80 12Z	PIA		UMN	DDC	SEP	MAF	OMA	STC	GRI	SLO	JAN
4/11/80 12Z			UMN	DDC	OKC	AMA	OMA			LIT	LCH
4/13/80 12Z			VCT		BRO		SEP		GGG	LCH	
4/17/80 12Z	TOP		OKC	AMA	DRT	ELP	DDC	OMA	PIA	LIT	VCT
4/24/80 12Z				MAF		ELP	ABQ	DDC	OKC	SEP	
4/25/80 00Z	AMA		DRT	MAF			ABQ	DEN	OKC	GGG	VCT
4/25/80 12Z	SEP		DRT	CUU			MAF	DDC	OKC	VCT	
4/26/80 00Z	UMN		GGG	MAF	LCH	VCT	DDC		LIT	JAN	
5/ 1/80 00Z		AMA	SEP	MAF	CUU	ELP		DDC	LIT	LCH	VCT
5/12/80 12Z	DDC		AMA	ABQ	CUU		SLC	LBF	UMN	SEP	DRT
5/13/80 00Z			TOP	DDC	SEP	MAF		HON	PIA	LIT	LCH
5/16/80 00Z			SEP	MAF	VCT	CUU	ABQ	DDC	LIT	LCH	
5/16/80 12Z	UMN		SEP	MAF	DRT	CUU	DDC	OMA	SLO	LCH	
5/22/80 00Z				VCT			OKC		JAN	BVE	
5/22/80 12Z				LCH			LIT		CKL		
6/ 1/80 12Z				OMA			HON	INL	GRB	PIA	
6/27/80 12Z			LND				GTF			RAP	IEN
6/28/80 00Z			HON	RAP			BIS		INL	STC	

LIST OF SOUNDINGS USED IN COMPOSITE

	1	2	3	4	5	6	A	B	C	D	E
3/ 4/81 00Z			SEP	MAF	DRT	ELP	DEN	LBF	UMN	LCH	BRO
3/ 4/81 12Z	TOP	DDC	GGG	AMA		ELP	DEN	LBF	SLO	LIT	LCH
3/ 7/81 12Z				MAF	DRT	CUU	ABQ		OKC	GGG	BRO
3/15/81 12Z				SEP	DRT		OKC	UMN	LIT	LCH	BRO
3/17/81 12Z			AMA	ABQ	MAF	ELP	LND	RAP	OMA	OKC	DRT
3/18/81 00Z		LIT	LCH	VCT			DDC	TOP	BNA	JAN	
3/18/81 12Z			LCH		VCT	DRT	LIT	BNA	CKL	BVE	
3/21/81 12Z		DDC		AMA	MAF			OMA	LIT	GGG	
3/22/81 00Z	UMN		GGG	SEP	DRT	ELP	OKC	OMA	LIT	LCH	VCT
3/22/81 12Z				LCH		BRO		BNA	AHN	AQQ	
3/25/81 00Z				ABQ	ELP		DEN	LBF	DDC	AMA	MAF
3/25/81 12Z				MAF		CUU	AMA	TOP	OKC	SEP	DRT
3/29/81 00Z		DDC	SEP	MAF		CUU		OMA	UMN	GGG	VCT
3/29/81 12Z		OMA		OKC	DRT	CUU	LBF	INL	SLO	LIT	LCH
3/30/81 00Z	GRB			UMN	GGG	MAF	HON		FNT	SLO	JAN
4/ 1/81 00Z		STC	UMN	DDC	SEP	MAF		INL	GRB	SLO	LIT
4/ 4/81 00Z			OKC	AMA	MAF	ELP	LBF		UMN	GGG	VCT
4/ 4/81 12Z		GRB	PIA	OMA	SEP	MAF	STC		FNT	SLO	LIT
4/22/81 12Z			UMN	AMA			OMA		PIA	LIT	LCH
4/23/81 00Z			TOP				STC		FNT	SLO	LIT
4/23/81 12Z		GRB	SLO	TOP	UMN	DDC	STC	SSM	FNT	BNA	LIT
5/ 9/81 12Z			OKC		SEP	MAF	LBF	OMA	UMN	GGG	VCT
5/10/81 00Z		OKC	SEP	MAF	DRT	CUU	DDC	TOP	LIT	GGG	VCT
5/10/81 12Z			JAN	GGG	LCH	DRT	LIT		BNA	CKL	BVE
5/11/81 00Z			CKL	JAN	BVE	LCH	SLO	PIA	DAY	AHN	AQQ
5/14/81 12Z			LIT	OKC	GGG	MAF				BNA	CKL
5/18/81 12Z			OKC	AMA	SEP	MAF	LBF	OMA	UMN	LIT	LCH
5/19/81 00Z			LIT	AMA	GGG	MAF	TOP		BNA	JAN	LCH
5/23/81 12Z		HON	OMA	LBF	OKC	AMA	RAP	INL	PIA	LIT	LCH
5/26/81 12Z			JAN	GGG	BVE	VCT	LIT	SLO	CKL	AQQ	
6/ 1/81 00Z			LIT		SEP	MAF	UMN		BNA	JAN	LCH
6/ 1/81 12Z			LIT	OKC			PIA		BNA	CKL	BVE
6/ 2/81 00Z			LIT				PIA		BNA	JAN	LCH
6/ 2/81 12Z			LBF				RAP	BIS	STC	OMA	DDC
6/ 3/81 00Z						LBF	STC	INL	GRB	PIA	UMN
6/ 3/81 12Z			GRB		OMA		STC		SSM	PIA	UMN
6/ 6/81 00Z			LIT	OKC	LCH	VCT	UMN		BNA	CKL	BVE

APPENDIX 2

PRESERVING INVERSION LAYERS IN COMPOSITE SOUNDING DATA

It is important to understand that the compositing method described in Chapter II does not preserve the intensity of inversion layers. This is a consequence of the fact that only the mean temperature at each pressure level was computed, not the vertical derivative of temperature (i.e., lapse rate). Quantities such as the static stability parameter σ, which are computed from vertical derivatives of composite mean values, are not realistic. In order to obtain a more accurate estimate of the inversion layers in each zone, the following method was used.

First, lapse rates between each reported level were calculated from the original sounding data. Each sounding was manually searched for layers below 600 mb where the temperature increased with height ($-\frac{\partial T}{\partial p} \geq 0$). If more than one inversion layer was present, a subjective decision was made as to which layer was most representative. Usually the layer with the strongest inversion was selected. In cases where two inversion layers were spaced close together,

the uppermost layer was generally chosen. Finally, the arithmetic means of the pressure and temperature at the top of the inversion and the average depth of the inversion were calculated for each zone. Only those soundings which had inversions were included in the calculation of the mean. The average lapse rates within the inversion layer and in the 100 mb layer above the top of the inversion were also calculated.

Values of static stability in and above the inversion were calculated using the following equations:

$$\sigma \text{ inversion layer} = \frac{R\,T_t}{P_t\,\Theta_t}\left(\frac{\Theta_t - \Theta_b}{P_t - P_b}\right)$$

where the subscript, t, means quantities calculated at the top of the inversion and the subscript, b, means quantities at the bottom. The potential temperature at the bottom of the inversion, Θ_b, is obtained from Poisson's equation:

$$\Theta_b = T_b \left(\frac{1000}{P}\right) R/c_p; \quad T_b = T_t + (\Gamma \Delta p)$$

and $\Gamma = -\frac{\partial T}{\partial P}$ averaged over the inversion depth, Δp.

$$\sigma \text{ above inversion} = \frac{R\,T_a}{P_a\,\Theta_a}\left(\frac{\Theta_a - \Theta_t}{100}\right)$$

where a, means quantities calculated at the level 100 mb above the top of the inversion layer.

The results are summarized in Table 4. Static stability values in the inversion layer are 3-4 times larger than the composite mean values computed in Chapter II. The western dry zones have the fewest number of soundings with

inversions and when they do they are usually shallower. Deep inversion layers were observed in March and April compared to May and June. Morning soundings had deeper and more frequent inversion layers.

TABLE 4

INVERSION LAYER QUANTITIES

ZONE	RATIO OF STATIONS WITH INVERSIONS TO TOTAL NUMBER OF STATIONS	INVERSION TOP PRESS.	INVERSION TOP TEMP.	INVERSION DEPTH
1	8/11	860 MB	9.9 C	30 MB
2	8/14	802	5.4	33
3	39/53	831	10.7	28
4	39/58	809	7.3	26
5	36/48	827	13.2	28
6	27/46	795	8.4	24
A	32/58	804	2.8	26
B	32/44	809	3.4	29
C	48/62	860	10.4	29
D	55/67	831	12.7	28
E	40/48	809	13.8	26

ZONE	STATIC STABILITY IN INVERSION	STATIC STABILITY ABOVE INVERSION
1	.066	.022
2	.055	.012
3	.058	.015
4	.041	.013
5	.041	.021
6	.107	.015
A	.066	.017
B	.090	.016
C	.061	.015
D	.064	.013
E	.082	.015

REFERENCES

Anderson, R. K., J. P. Ashman, F. Bittner, G. R. Farr, E. W. Ferguson, V. J. Oliver, and A. H. Smith, 1969: Application of meteorological satellite data in analysis and forecasting. ESSA Technical Report NESC-51, National Environmental Satellite Center, Washington, D.C., 260 pp.

Barr, S., M. B. Lawrence, and F. Sanders, 1966: TIROS vortices and large-scale vertical motion. Mon. Wea. Rev., 94, 675-696.

Bergeron, T., 1951: A general survey in the field of cloud physics. Inter. Union Geod. Geophys. Assoc. Meterol. Brussels, 1951, Ninth Gen. Assembly Mem., 120-134.

Bosart, L. F. and O. Garcia, 1974: Gradient Richardson number profiles and changes within an intense mid-tropospheric baroclinic zone. Quart. J. Roy. Meteor. Soc., 100, 593-607.

Boucher, R. J. and R. J. Newcomb, 1962: Synoptic interpretation of some TIROS vortex patterns: A preliminary cyclone model. J. Appl. Meteor., 1, 127-136.

Carlson, T. N., 1980: Airflow through midlatitude cyclones and the comma cloud pattern. Mon. Wea. Rev., 108, 1498-1509.

Danielsen, E., 1974: The relationship between severe weather, major dust storms, and rapid large-scale cyclogenesis, part II. Subsynoptic Extratropical Weather Systems, M. Shapiro, Ed., National Center for Atmospheric Research, 226-241.

Fawcett, E. G. and H. K. Saylor, 1965: A study of the distribution of weather accompanying Colorado cyclogenesis. Mon. Wea. Rev., 93, 359-367.

Green, J. S. A., F. H. Ludlam, and J. F. R. McIlveen, 1966: Isentropic relative-flow analysis and the parcel theory. Quart. J. Roy. Meteor. Soc., 92, 210-219.

Hess, S. L., 1959: Introduction to Theoretical Meteorology. Holt, Rinehart and Winston, New York, 362 pp.

Holton, J. R., 1979: An Introduction to Dynamic Meteorology. Academic Press, New York, 391 pp.

Kreitzberg, C. W. and H. A. Brown, 1970: Mesoscale weather systems within an occlusion. J. Appl. Meteor., 9, 417-432.

Leese, J. A., 1962: The role of advection in the formation of vortex cloud patterns. Tellus, 14, 409-421.

Lowe, P. R., 1977: An approximating polynomial for the computation of saturation vapor pressure. J. Appl. Meteor., 16, 100-02.

McBride, J. L., 1981: Observational analysis of tropical cyclone formation. Part I: Basic description of data sets. J. Atmos. Sci., 38, 117-1131.

McClain, E. P. and H. J. Brodrick, 1967: Recent research on the application of meteorological satellite data to numerical weather analysis. Air Weather Service Tech. Report 196, Proceedings, Technical Exchange Conf., Monterey, California, USAF, 42-50.

McGinley, J. A. and Y. K. Sasaki, 1975: The role of symmetric instabilities in thunderstorm development on drylines. Preprints, Ninth Conf. on Severe Local Storms, Norman, Oklahoma, AMS, 173-180.

McNulty, R. P., 1978: On upper tropospheric kinematics and severe weather occurence. Mon. Wea. Rev., 106, 662-672.

Miller, R. C., 1972: Notes on analysis and severe-storm forecasting procedures of the Air Force Global Weather Central. Air Weather Service Tech. Report 200 (rev.), 190 pp.

________, and J. A. McGinley, 1978: Using satellite imagery to detect and track comma clouds and the application of the zone technique in forecasting severe storms. GE/MATSCO, Beltsville, MD, 96 pp.

Mullen, S. L., 1979: An investigation of small synoptic-scale cyclones in polar air streams. Mon. Wea. Rev., 108, 1636-1647.

O'Brien, J. J., 1970: Alternative solutions to the classical vertical velocity problem. J. Appl. Meteor., 9, 197-203.

Palmén, E. and C. W. Newton, 1969: Atmospheric Circulation Systems. Academic Press, New York, 603 pp.

Reed, R. J., 1979: Cyclogenesis in polar air streams. Mon. Wea. Rev., 108, 38-52.

Ruprecht, E. and W. M. Gray, 1976: Analysis of satellite-observed tropical cloud clusters, II. Thermal, moisture and precipitation. Tellus, 28, 414-426.

Skidmore, R. W. and J. F. W. Purdom, 1973: Application of meteorological satellite data in analysis and forecasting. Supplement #2 to ESSA Technical Report NESC-51, National Environmental Satellite Service, Washington, D.C., 53 pp.

Stone, P., 1966: On non-geostrophic baroclinic instability. J. Atmos. Sci., 27, 390-400.

Weldon, R. B., 1976: Satellite training course notes, part III. Cloud patterns of 'short wave scale' systems in the westerlies. Applications Group, NESS (NOAA), Washington, D.C., 27 pp.

________, 1979: Satellite training course notes, part IV. Cloud patterns and the upper air wind field. Applications Div., NESS (NOAA), Washington, D.C., 80 pp.

Whittaker, L. M. and L. H. Horn, 1981: Geographical and seasonal distribution of North American cyclogenesis, 1958-1977. Mon. Wea. Rev., 109, 2312-2322.

Widger, W. K., Jr., 1964: A synthesis of interpretations of extratropical vortex patterns as seen by TIROS. Mon. Wea. Rev., 92, 263-282.

________, C. W. Rogers, and P. E. Sherr, 1967: Applications of satellite observations of extratropical cloud vortices. Air Weather Service Tech. Report 196, Proceedings, Technical Exchange Conf., Monterey, California, USAF, 52-82.

Williams, K. T. and W. M. Gray, 1973: Statistical analysis of satellite-observed trade wind cloud clusters in the western North Pacific. Tellus, 25, 313-336.

ATE

LMED

-8